A Dual-Band and Dual-Polarization Feed-Multiplexer for Ku/Ka-Band Operation

by

Hendrik Albertus Thiart
B.Eng., University of Stellenbosch, 1996

A Thesis Submitted in Partial Fulfillment of the Requirements for the Degree of

MASTER OF APPLIED SCIENCE

in the Department of Electrical and Computer Engineering

Supervisor: Dr. Jens Bornemann

ABSTRACT

A feed-multiplexer for use in Ku/Ka-band satellite dish antenna systems is introduced. A circular metal waveguide loaded by a dielectric rod is used to separate the bands for correct operation. Substrate board from adjoining integrated component circuitry is used to form the Ku-band coupling structures of the feed-multiplexer. Analysis, initial design and optimization of the structure are discussed. A prototype is manufactured and related manufacturing issues are documented. Simulated results are presented along with measured results obtained from the manufactured prototype. Satisfactory performance is obtained and proof of concept achieved.

Supervisor: Dr. J. Bornemann, (Department of Electrical and Computer Engineering)

Table of Contents

List of Tables

Table of Figures

List of Acronyms

ADS®	Advanced Design System, simulation software
FEM	Finite-Element Method
HFSS®	High Frequency Structure Simulator, simulation software
IDU	Indoor Unit
LNA	Low Noise Amplifier
LNB	Low Noise Block
LRL	Line-Reflect-Line, measurement calibration procedure
ODU	Outdoor Unit
OMT	Orthomodal Transducer
PTFE	Polytetrafluoroethylene
ROU	Range of Uncertainty
SIT	Satellite Interactive Terminal
SMA	Industry standard coaxial connector type designation
VNA	Vector Network Analyzer
VSAT	Very Small Aperture Terminal
WR28	Industry standard Ka-band rectangular waveguide size designation
WR75	Industry standard Ku-band rectangular waveguide size designation

Acknowledgements

All individual achievement inevitably rests on the support of others. The author would like to thank the following individuals and organizations.

My Wife Carrie

For her unselfish nature, her encouragement and support and especially for laboring in a vocation with difficult hours and exhaustive demands, to help keep the finances going. Also, for patiently taking second place to a computer during multiple hours of personal time that should have been hers, in order for the thesis objectives to be met.

Professor Jens Bornemann my Supervisor

For taking me on as part of his research group. For always going the extra ten miles for all of his students and for being a grounded, generous and enriching human being with humble compassion and kindness, despite his many achievements and obvious abilities.

Professor W.J.R. Hoefer

For the knowledge, experience and enthusiasm shared during his courses. For his calm cultured presence that, together with that of Professor Bornemann, made the microwave group at the university a civilized and mature environment that was a joy to be part of.

Dr. Rambabu Karumudi my Friend and Colleague

For his friendship and support of my efforts. For the many discussions and humor shared while waiting for simulations and for being a top notch engineer and scientist whose acquaintance has benefited me greatly.

Friends and Colleagues from the UVic EM and Microwave Groups

For being wonderful people, rich in a tapestry of backgrounds, enriching my world and for always being interested in my work and wellbeing.

Chris Senger and Family – Friend and Mechanical Designer of the Prototype Housing

For countless hours of quality work to make the design a reality. For being willing to help his friend despite a tough personal schedule. For the patience and encouragement of his wife and family during hours that should have been theirs.

Frank Argentine of CA Tools Burnaby

For investing in my research with commitment and expert machining at much reduced rates.

Dr. Joe Fikart, Dr. Amiee Chan and Former Colleagues at Norsat Intl. Inc.

For supporting my work with encouragement and the donation of materials and the manufactured Ku-band horn.

The Members of my Committee: Dr. W.J.R. Hoefer, Dr. A.M. Rowe, Dr. B. Buckham

For being willing to make room for my work in their already demanding schedules.

The Nation of Canada

For welcoming a foreigner, giving me the opportunity to continue my studies and accepting me as an equal citizen.

Dedication

To my parents,
Henk and Toela

per slot van rekening is die totaal
die som van alle bietjies

1 Introduction

The increasing demand for broadband communication systems to enable more varied (multimedia) and faster information delivery to and retrieval from various end users is driving current development of techniques and equipment to facilitate the realization of the required infrastructure [1]. Currently, commercial market level applications for high speed two-way data exchange make use of VSAT (Very Small Aperture Terminal) technology. This is a satellite communication based infrastructure that, for the current state of technology, operates predominantly in the Ku-band frequency range. End user infrastructure equipment for this is often bulky in size and expensive to a degree beyond the reach of consumer level markets. At present, consumer level markets are predominantly serviced with cable and land line based infrastructure for the delivery of two way internet access. Due to the logistical and broadband limitations of this cable based infrastructure the opportunity arises for the use of Ku- and if possible Ka-band satellite infrastructure to deliver broadband communications to consumer level markets [2]. Specifically in the European market, where satellite television infrastructure already exists in the absence of an existing cable network, the opportunity arises for the combination of a Ka-band uplink facility with the already existing Ku-band down link that presently services the delivery of satellite television [3], [4]. This is possible through the use of SIT's (satellite interactive terminals) deployed at the end user [3]. These SIT's facilitate the reception of signals routed via satellite from the network hub earth station and in return, the transmission of signals from the end user to the hub.

The use of consumer SIT's for this particular application requires the frequency assignments outlined in Table 1 [5], [6]. Both the frequency bands are required to operate with vertical and horizontal linear polarization [7]. The polarization discrimination is used to achieve extra channel versatility. For the transmit band, the polarization of

operation is set at installation. For the receive band, however, both polarizations must be available simultaneously for processing by the rest of the SIT.

Table 1: SIT Required Frequency Specifications

	Specification	Requirement
1	Uplink from consumer to satellite	Ka-band, 29.5 GHz to 30 GHz
2	Downlink from satellite to consumer SIT	Ku-band, 10.7 GHz to 12.75 GHz
3	Polarization of operating bands	Linear, Vertical and Horizontal for both Ku- and Ka-band

In addition, the following criteria apply to the SIT equipment in order for the product to be viable for consumer market deployment:

Manufacturability/Cost: In order for the SIT to be viable for consumer level market spending ability, mass production techniques are required for the manufacturing of the SIT. The technology must lend itself to techniques such as production casting and must exhibit a high level of system sub-component integration into one physical package to minimize materials used and assembly time expended.

Size: In order for the SIT to be aesthetically acceptable to a consumer market and installation compatible with the average consumer dwelling, the size of the equipment must be kept to a minimum without sacrificing performance.

Various system parts of the SIT affect these criteria. The "front end" of the SIT can be divided into the following system components that are part of the ODU (outdoor unit) [3], as shown in Figure 1.

The *satellite dish antenna* [8], [3] includes the *waveguide feed-multiplexer* for separating the Ku-and Ka-band signals, as well as for illuminating the dish. The *LNB- (Low Noise Block) receiver* [9] amplifies and down converts the incoming signal. The *transmitter* [9]

upconverts and amplifies the signal to be transmitted to the satellite. The ODU interfaces with the IDU (indoor unit) [3] that holds the modem [9] of the SIT.

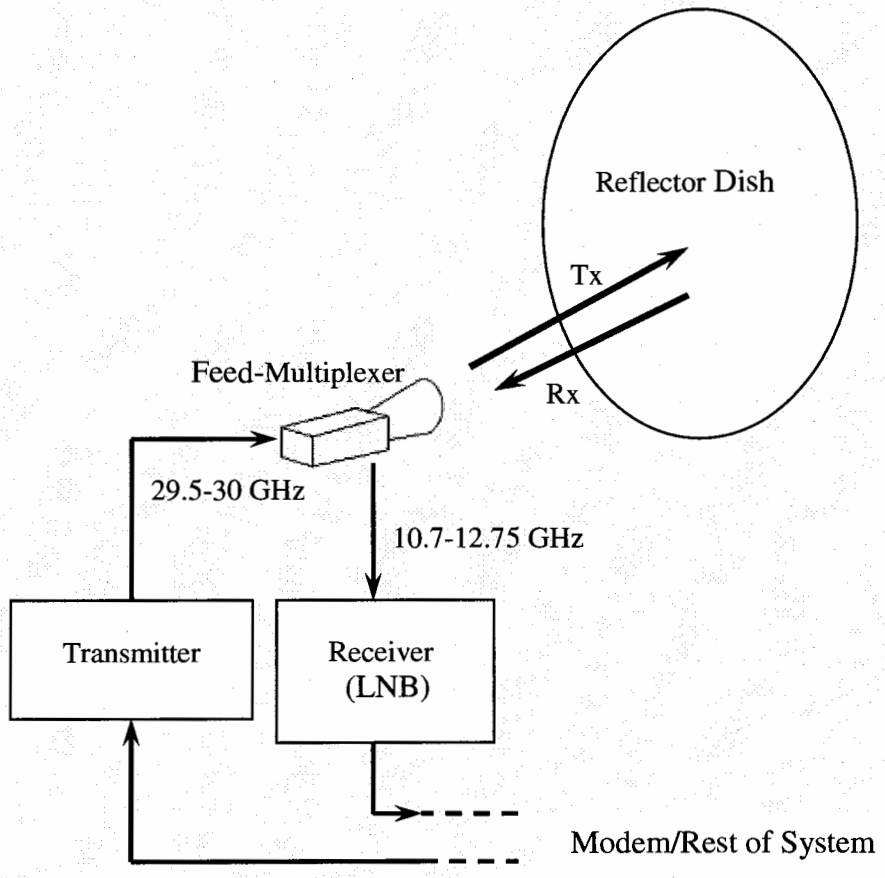

Figure 1: Satellite Interactive Terminal (SIT) Front End System Components.

In order for size and ease of manufacturability requirements to be met, a high degree of integration between the LNB (and/or transmitter) and waveguide feed-multiplexer is required. This demands certain spatial and dimensional attributes of the waveguide feed-multiplexer. It is the goal of this thesis to investigate the design of a waveguide feed-multiplexer that might better approach the abovementioned goals for the SIT than current available solutions by enabling efficient mechanical integration of the LNB and waveguide feed-multiplexer housings. Current solutions for the implementation of a feed-multiplexer for satellite dish antennas predominantly make use of elaborate waveguide

structures for the multiplexing of the Ku- and Ka-band signals in the feed-multiplexer. Although effective, these structures can be cumbersome and difficult to manufacture with inexpensive mass-production techniques, such as casting methods. Coupling waveguide structures in these applications need to be oriented orthogonal to the axis of the feed-multiplexer. The signal needs to be transferred from these waveguides to a substrate board for use in the LNB circuitry. This LNB substrate can be either parallel to the feed-multiplexer axis or orthogonal to it. In both cases, waveguide to substrate board transitions are required as well as some waveguide bends. This required mechanical orientation shift often inhibits efficient mechanical integration of the feed-multiplexer and LNB housings and consequently inhibits size and cost reduction.

In this thesis a new design solution is set out and investigated that employs etched metal probes, carried on a substrate board, as coupling structures for the Ku-band signal. The substrate board is oriented orthogonally to the feed-multiplexer axis. Such a design can make use of the already existing circuit board in the LNB to form the Ku-band coupling structures of the feed-multiplexer and thereby eliminate, the need for cumbersome waveguides orthogonal to the feed-multiplexer axis, as well as waveguide bends. Jackson [10] suggested a similar solution for an OMT (Orthomodal Transducer) in square waveguide. The result is a reduction in size, material and machining costs, when the LNB and feed-multiplexer are integrated into one physical subcomponent of the SIT. Figure 2 shows a transparent view of the proposed solution .

At the heart of the feed-multiplexer design is a coaxial waveguide structure consisting of a larger circular waveguide coaxially loaded by a smaller dielectric rod waveguide. This structure is necessary due to the large separation in frequency between the receive (Ku) and transmit (Ka) frequency bands. The Ka-band signal energy is largely contained and guided by the dielectric rod. The Ku-band signal energy propagates in the larger diameter metal waveguide loaded by the dielectric rod. The dielectric rod ends in a taper and acts as radiator for the Ka-band illumination of the antenna dish reflector of the SIT. The larger metal circular waveguide ends in a metal waveguide horn that illuminates the dish reflector for the Ku-band.

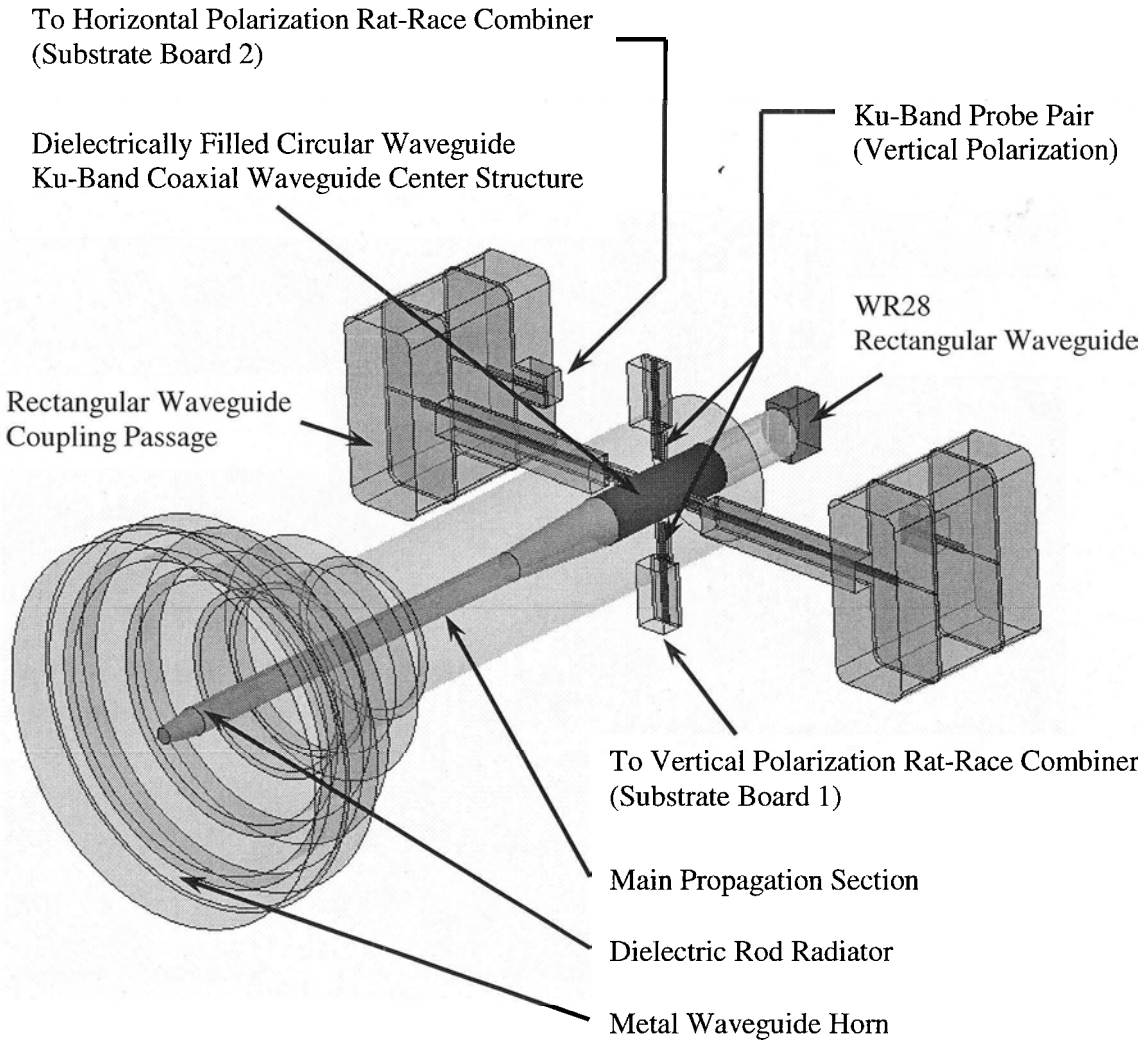

Figure 2: Dual-Band and Dual-Polarization Feed-Multiplexer, Shown Without Microstrip Rat-Race Combiners.

The use of such a coaxial structure for dual band operation was introduced in [11]. A smooth-walled metal horn loaded with a dielectric rod was used to carry two adjacent bands in the dielectric rod and two lower adjacent bands in the circular metal waveguide loaded by the rod. Symmetry was maintained by the use of four waveguide slot coupling structures in the walls of the larger metal waveguide for each of the operational bands. Good results were obtained with the lowest band (4 GHz), having a 12 % bandwidth for a return loss better than 18 dB. The paper also established that, given sufficient distance

between the dielectric rod and the surrounding circular waveguide, the dielectric rod could be designed as a stand alone antenna in the absence of the enclosure, without adversely affecting the overall structure performance.

Subsequently other authors have investigated the coaxial structure for the use in dual band waveguide antennas. Narasimhan and Sheshadri [12], designed and measured a corrugated waveguide horn for S-band (2.68 GHz), loaded with a dielectric rod for X-band (9.375 GHz). A capacitance probe with tuning screws were used for exciting the S-band in the circular waveguide. A bandwidth of 20 % for a return loss of better than 15 dB for the S-band and better than 20 dB for the X-band is reported. Lee [13] used a circular metal waveguide for the smaller inner waveguide of the coaxial structure, that ended in a tapered dielectric rod radiator inside a corrugated waveguide horn. Waveguide slot couplers were used for the coupling of both bands from the waveguide diplexer. Return loss bandwidths of 5 % were obtained for Q-band (44.5 GHz) better than 15 dB and K-band (20.7 GHz) better than 13 dB. More recently, James et al. [14], also used a metal circular waveguide center structure to carry the upper band in the vicinity of the lower band waveguide coupling slots. This was done to improve isolation between the bands. The center metal waveguide is then ended however, and continued as a dielectric rod, serving as the high band radiator inside a circular corrugated waveguide horn for the low band. For a return loss of better than 16 dB, a 20% bandwidth was obtained for Ku-band and a 24% bandwidth for C-band.

For the proposed solution in this thesis, Figure 2 shows the substrate-carried etched probes protruding into the feed-multiplexer waveguide. Symmetry of the structure is maintained to avoid moding problems that could degrade the radiation performance of the feed-multiplexer [15]. Coupling from oppositely positioned etched probes are combined by the use of a 180-degree "rat-race" combiner [10], [16] (see Figure 18, Chapter 8). Each pair of probes couples the energy in one of the two orthogonal (vertical or horizontal) polarization Ku-band channels from the feed-multiplexer structure. The dielectric rod carrying the Ka-band is transitioned into a dielectric-filled circular waveguide that forms a metal centered coaxial waveguide, for the Ku-band, towards the

end of the feed-multiplexer cavity. The Ka-band dielectric-filled waveguide continues to the rear of the structure where it joins a regular WR28 rectangular waveguide that can be rotated in either of two orthogonal positions, in order to launch a vertically or horizontally polarized Ka-band signal into the feed-multiplexer. Since the microstrip lines leading to the rat-race combiners from the four probes would have to cross, if positioned on the same board, one combiner is placed on a second substrate board. The signals from the associated pair of probes are therefore passed through a pair of rectangular waveguide coupling passages to the second substrate board that holds the rat-race combiner.

For the intended integration into a SIT dish antenna system, the performance specifications listed in Table 2 were set as design goals for the feed-multiplexer .

Table 2: Design Specifications for the Feed-Multiplexer.

	Specification	**Requirement**
1	Return Loss for Ku-band Ports	Better than 12 dB
2	Return Loss for Ka-band Ports	Better than 14 dB
3	f/d, Focal Distance over Diameter Ratio for Intended Dish Antenna	0.6
4	Ku-band and Ka-band Radiation Pattern Cross Polar Isolation	Better than 20 dB over Dish Illumination Angle
5	Ku-band and Ka-band Radiation Pattern Gain on Boresight	Better than 12 dB
6	Feed-Multiplexer Ku-band Vertical-Horizontal Polarization Isolation	Better than 20 dB
7	Transmit (Ka-band Port) to Receive(Ku-band Ports) Isolation	Better than 20 dB

The initial design of this structure was performed by analyzing the cut-off frequencies of the various types of waveguides in the design, in order to ensure the correct mode propagation for the design. To this end, existing waveguide theory was used. For the metal center coaxial waveguide, closed form expressions exist. For the dielectric rod and the dielectric rod loaded circular waveguide, the boundary conditions result in transcendental characteristic equations that have to be solved numerically. MATLAB® routines were written to solve these equations. Based on these calculations the design choices for the waveguide dimensions were made. The waveguide horn utilized in the design is an already existing component, courtesy of Norsat® Intl. Inc. The dielectric rod antenna was first designed as a stand alone antenna using a technique as set out in [17]. The Ku-band coupling probes were designed using techniques as set out in Chapter 5. Incorporating an initial design of the various parts as mentioned above, the total structure was analyzed using a full-wave solver software package (Ansoft HFSS®) based on the finite-element numerical solution technique (FEM, [18]). Proceeding with this analysis, the structure was optimized for best performance by using a parametric study approach. Finally the design dimensions were used in manufacturing a prototype that was measured to confirm the response obtained from the full-wave solver analyses. Relatively good agreement between the full-wave solver results and measured results were obtained.

This introduction presented a brief overview of the research work set out in this thesis. Following sections will expand the issues, procedures and results as set out above in more detail.

2 Dielectric Rod Design

Despite the fact that the use of the dielectrically loaded coaxial structure serves to largely separate the two operating frequency bands, complete isolation is not achieved. As a result, design choices for the correct operation of the one frequency band will inevitably affect the operation of the other frequency band. As will be apparent through the course of this thesis, this requirement of balancing the effects on the operational frequency bands can quickly become a quagmire of design choices for the designer. Consequently the design procedure sequence is equally important to the actual design technique of each individual structure in the design. After completing the research on the design, it is the view of the author that the total design is best thought of as being from the inside outwards. I.E., the Ka-band dielectric rod antenna should be designed first and the Ku-band structure added to the determined dielectric rod dimensions, with possible minor adjustments in later optimization steps during the parametric study stage of the design. The dielectric rod antenna requires a very specific diameter to operate correctly for the chosen higher frequency band. As a result, it will determine the cross section dimensions of the circular waveguide section loaded by the rod. This is the main waveguide propagation section shown in Figure 2. The design of the use of the dominant modes for both frequency bands, in this section of the feed-multiplexer, forms the foundation for the rest of the design. Hence the rod design is of paramount importance and should be conducted first.

As mentioned in the introduction, Kumazawa et al. [11] demonstrated that the design of the rod antenna can be performed as if it was a stand alone radiator in open air without detrimentally affecting its performance once combined with the larger circular waveguide and metal horn. This holds, provided that the circular metal waveguide is far enough away from the dielectric rod. Just exactly what defines "far enough" requires an analysis of the field distribution of the dielectric rod, which is shown later in this section. For the

design of the stand alone rod antenna the method as set forth in [17] was chosen and will be discussed in the following.

2.1 Stand Alone Rod Antenna

The dielectric rod antenna has a dielectrically filled circular waveguide section that serves as a feed for the dielectric rod. This is followed by a feed taper section that is mainly used for matching the feed to the dielectric rod. The main body of the antenna follows the feed taper and ends in a terminal taper as shown in Figure 3.

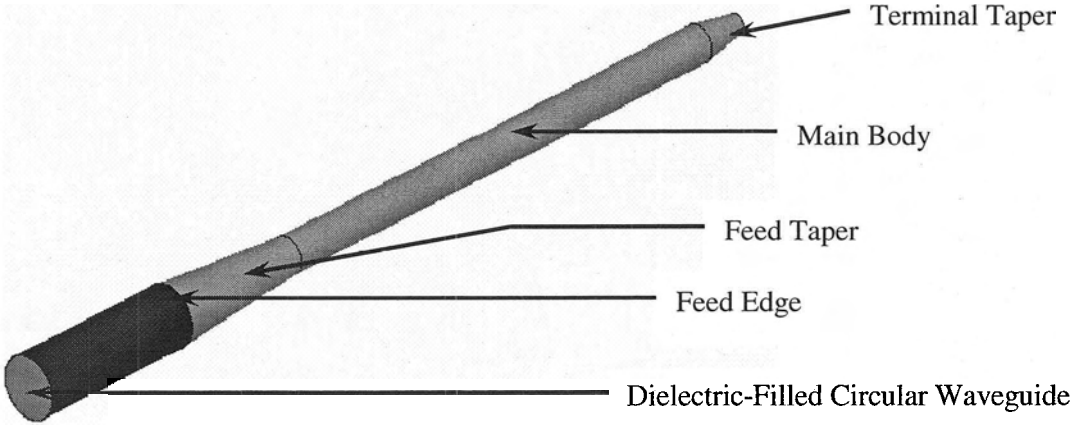

Figure 3: Stand Alone Dielectric Rod Antenna.

The design of the stand alone antenna involves the lengths and diameters of the various sections in Figure 3. As explained in [17], the phenomena that governs the operation of the antenna can be defined as two types of propagating waves. The antenna is fed by the dominant TE_{11} circular waveguide mode in the dielectrically filled section. At the feed edge discontinuity, where the metal circular waveguide ends, a hybrid mode surface wave (HE_{11}) is generated that is mostly contained by and propagates along the dielectric rod. The second propagating wave generated at the feed edge discontinuity is a radiated wave propagating through free space. The main body section of the rod is designed to support the HE_{11} mode, with the two taper sections serving to match the main body section to the

feed and also to the free space radiation termination of the HE_{11} mode at the end of the rod. The lengths of the various sections are chosen to maximize the matching effects of the structure and to have the two propagating waves in phase at the termination of the rod.

According to [17], fundamental single mode (HE_{11}) operation for the dielectric rod is guaranteed if :

$$\frac{d}{\lambda_0} < \frac{0.626}{\sqrt{\varepsilon_r}} \qquad \textbf{(2-1)}$$

with

d - the diameter of the rod

λ_0 - the free space wavelength at the frequency of operation

ε_r - the dielectric constant of the rod material

This sets an upper limit to the diameter of the main body of the dielectric rod. Adherence to this guideline at the highest frequency of operation ensures single mode operation for the entire operational band. A lower limit to the diameter of the rod is that for which the HE_{11} containment in the rod becomes negligible. Smaller diameters, for which a breakdown in mode containment occurs, result in failure of assumed hybrid surface wave operation, as explained in Section 2.2. Greater containment of the propagating energy within and around the dielectric rod is achieved for higher frequencies, given the same dielectric rod dimensions. Consequently the breakdown diameter for the lowest frequency of operation determines the lower limit of rod diameter. Using these two limits the diameter of the main body section can be chosen. For dielectric rod manufacturing a 0.001" (0.0254 mm) tolerance is achievable. Manufacturing instructions should be such that any errors will add to the rod diameter rather than subtract, since propagation of some higher order mode components will be less of a problem than operational breakdown. In order to allow for useful band separation the dielectric constant of the rod should be at least 2, but it should not be so high that excessive modal disturbance of the

TE_{11} Ka-band mode occurs [35]. In addition the commercial availability of mechanically compatible materials limits the scope of choice. A PTFE (Polytetrafluoroethylene) dielectric material with a dielectric constant of 2.55 was chosen for the design. This results in an upper radius limit of 1.96 mm, and a lower radius limit of 1.2 mm for the rod (Section 2.2, Table 3). A nominal design radius of 1.8 mm was consequently chosen, leaving ample manufacturing tolerance (> 6x 0.001") on the upper end of the range.

As explained in [17], a minimum dielectric rod length is required for the hybrid surface wave to be well established. This length is stated as being where the phase of the radiated wave in the air leads the phase of the surface wave in the rod by 120°. As a result this length can be defined as:

$$l_{\min} k_z - l_{\min} k_0 = \frac{\pi}{3} \qquad \textbf{(2-2)}$$

with

$l_{\min}$ - the minimum required length in meters

k_0 - the free space propagation constant

k_z - the propagation constant of the hybrid surface wave in the axial direction of the dielectric rod

The propagation constant of the HE_{11} mode in the axial direction of the rod plays a central role in the design of the rod antenna. This constant needs to be calculated as shown in Section 2.2. The design of the rod antenna has to be performed at the highest operating frequency in the band, since the radiation performance of the antenna starts to deteriorate rapidly above the design frequency. At 30 GHz the HE_{11} mode propagation constant for a rod of 1.8 mm in diameter was calculated to be 655.96 radians/meter, i.e. 0.656 radians/mm (Section 2.2, Table 5).

Extending the rod beyond the required minimum length serves the purpose of bringing the surface wave and the radiated wave into phase. The exact phase relation required for maximum antenna gain depends on a number of factors such as feed efficiency in

exciting the HE_{11} mode, feed taper dimensions and overall rod length. As a result the design choices for the total rod length are empirical in nature. A design equation is given in [17]:

$$\frac{\lambda_0}{\lambda_z} = 1 + \frac{\lambda_0}{pl} \qquad \textbf{(2-3)}$$

with

λ_0 - the free space wavelength

λ_z - the surface wave wavelength in the dielectric rod

p - an empirical optimization factor

l - the total length of the rod antenna

For antennas with expected lengths of between three to eight free space wavelengths, the suggested value for p is 3. Using the calculated propagation constant of the HE_{11} mode in this equation yields a total rod antenna length of 76.982 mm. With the main body diameter and total antenna length calculated, all that remains is the design of the feed and terminal tapers.

According to [17] the feed taper should be 0.2 times the total antenna length, yielding a value of 15.396 mm. The start diameter of the feed taper at the feed edge should be such that the ratio λ_0/λ_z is between 1.2 and 1.3. To determine the correct diameter that would attain a value in this range, the propagation constant of the HE_{11} mode in the rod for various diameters were calculated, as set out in Section 2.2, and used in the expression:

$$\frac{\lambda_0}{\lambda_z} = \frac{\beta}{k_0} \qquad \textbf{(2-4)}$$

with

$\beta = k_z$ - the propagation constant of the hybrid surface wave in the axial direction of the dielectric rod

A diameter of 6 mm was chosen, yielding a ratio as defined above of 1.27 (Section 2.2, Table 4). Over and above the free standing rod antenna design requirements, an overall feed-multiplexer requirement is that the dielectrically filled circular waveguide that feeds the rod, must be in cutoff for the Ku-band, but not for the Ka-band. If the Ku-band is able to propagate in the dielectrically filled circular waveguide, the formation of a coaxial waveguide section for the Ku-band will fail and so also the correct coupling of the Ku-band energy from the feed-multiplexer. The fundamental mode in circular waveguide is the TE_{11} mode with a cutoff frequency as defined by the well known analytical expression [16]:

$$f_{cutoff,TE_{11}} = \frac{1.841}{2\pi a\sqrt{\mu\varepsilon}} \qquad \textbf{(2-5)}$$

$$\mu = \mu_0\mu_r$$

$$\varepsilon = \varepsilon_0\varepsilon_r$$

with

μ_0 - permeability of free space

μ_r - relative permeability of the medium (1 for the dielectric)

ε_0 - permittivity of free space

ε_r - relative permittivity or dielectric constant of the medium (2.55 for the chosen material)

a - the radius of the circular waveguide

Using this expression the cutoff frequency for a circular metal waveguide filled with the chosen dielectric, having a diameter of 6 mm (as chosen above), is 18.336 GHz. The choice of a diameter of 6 mm for the start of the feed taper is therefore acceptable, since the Ku-band will be in cutoff but the Ka-band will be able to propagate. The next possible higher order mode in the circular waveguide is the TM_{11} mode. Since the circular waveguide is excited by the TE_{11} mode in the WR28 rectangular waveguide, the TE_{01} and TM_{01} modes in the circular waveguide will not be excited because of the incompatible modal field distributions. The cutoff frequency for the TM_{11} circular

waveguide mode in the designed dielectrically filled circular waveguide is 38.166 GHz, as calculated by equation (2-5) with the factor 1.841 replaced by 3.832 [16]. This falls outside of the Ka-band of interest and therefore presents no possible higher order mode problems.

The diameter of the dielectric rod at the end of the terminal taper should be such that the energy in the HE_{11} mode is no longer contained and radiation of the energy will occur. The best containment of energy in the rod is at the highest frequency. Consequently, this diameter should be designed at the highest frequency in the band, to ensure that containment is ended. At this diameter the propagation constant of the surface wave is approximately equal to the free space propagation constant ($\beta = k_0$), indicating a slow wave operational limit, as explained in Section 2.2.

The diameter where containment starts to break down at 30 GHz as calculated in Section 2.2 (Table 5), is 2.4 mm. A diameter of 2 mm for the end of the terminal taper was consequently chosen. Practically it is better to have a relatively flat tipped rod, since a sharp rod may poke holes in the environmentally protective sheet material that is used over the metal horn aperture in practice. The terminal taper length is suggested to be half a free space wavelength by [17], yielding a length of 4.997 mm. In [17] the total length of the rod antenna is defined as being from the feed edge to half of the length of the terminal taper. To obtain the final physical length of the rod antenna, half the length of the terminal taper must therefore be added to the total length obtained earlier, giving a final physical length of 79.480 mm. With this, the stand alone rod antenna is completely defined. The achieved design has good performance as is evident from the final results of the integrated feed-multiplexer in Chapter 12. The next section will deal with the solution of the electromagnetic problem introduced by the need for calculating the propagation constant of the HE_{11} mode in the dielectric rod, required in the design of the rod antenna. It will also deal with the computation of the electromagnetic field strengths around the dielectric rod, in order to judge whether the surrounding metal circular waveguide is far enough away from the rod to assume approximate stand alone operation.

2.2 Electromagnetic Analysis of the Dielectric Rod Surrounded by Free Space

In order to obtain the propagation constant of the surface wave along the rod, the Helmholtz wave equation needs to be solved for the geometry shown in Figure 4.

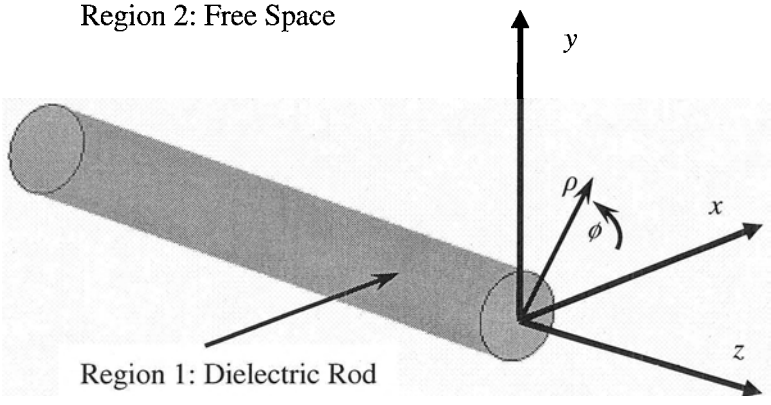

Figure 4: Dielectric Rod in Free Space.

Given the cylindrical geometry, cylindrical coordinates are used. Kajfez and Guillon [19], give an explicit account of the problem and its solution. The vector Helmholtz equations that govern the phenomena are:

$$\nabla^2 \bar{E} + k^2 \bar{E} = 0 \qquad (2\text{-}6)$$

$$\nabla^2 \bar{H} + k^2 \bar{H} = 0 \qquad (2\text{-}7)$$

with

$$k = \omega\sqrt{\mu\varepsilon} = \frac{2\pi}{\lambda} \qquad (2\text{-}8)$$

k - the wave number of the propagation medium

ω - the frequency of propagation in radians/second

μ - the permeability of the medium

ε - the permittivity of the medium

λ - the wavelength of propagation in the medium in meters

As is well known e.g. [16], [34], the total set of field components can be determined once two field components in the same direction have been solved. Consequently the scalar wave equations for E_z and H_z, contained in (2.6) and (2.7) can be solved and used to define all the other field components. In addition to the usual solving of the wave equations as just described, the geometry of the problem has two regions of differing dielectric constants. Region 1 is the inside of the dielectric rod with radius a_r and a dielectric constant of greater than unity. Region 2 is the outside of the rod, which is free space with a dielectric constant of unity. This geometry imposes a boundary condition on the problem at radius a_r, since all tangential field components across this boundary have to be continuous.

The equations resulting from the imposition of this boundary condition form a set of simultaneous equations that make up a transcendental matrix equation. This has to be solved numerically to obtain the radial wave numbers of the modes that satisfy the geometry. From the radial wave number, the propagation constant of the required mode can be calculated. The scalar wave equations for E_z and H_z in cylindrical coordinates are:

$$\frac{1}{\rho}\frac{\partial}{\partial\rho}\left(\rho\frac{\partial}{\partial\rho}E_z\right)+\frac{1}{\rho^2}\frac{\partial^2}{\partial\phi^2}E_z+\frac{\partial^2}{\partial z^2}E_z+k^2E_z=0 \qquad \textbf{(2-9)}$$

$$\frac{1}{\rho}\frac{\partial}{\partial\rho}\left(\rho\frac{\partial}{\partial\rho}H_z\right)+\frac{1}{\rho^2}\frac{\partial^2}{\partial\phi^2}H_z+\frac{\partial^2}{\partial z^2}H_z+k^2H_z=0 \qquad \textbf{(2-10)}$$

Separation of variables for the solution of differential equations dictates solutions of the form:

$$E_z(\rho,\phi,z) = P_E(\rho)F_E(\phi)Z_E(z) \quad \textbf{(2-11)}$$

$$H_z(\rho,\phi,z) = P_H(\rho)F_H(\phi)Z_H(z) \quad \textbf{(2-12)}$$

Indeed, as set out in [19], this separation can be done resulting in three differential equations for each of (2-9) and (2-10), each dependant on only one spatial coordinate:

$$\frac{1}{Z_E}\frac{d^2Z_E}{dz^2} = -\beta^2 \quad \textbf{(2-13)}$$

$$\frac{1}{Z_H}\frac{d^2Z_H}{dz^2} = -\beta^2 \quad \textbf{(2-14)}$$

with

β - a constant that represents the propagation constant in the z- direction

$$\frac{1}{F_E}\frac{d^2F_E}{d\phi^2} = -m^2 \quad \textbf{(2-15)}$$

$$\frac{1}{F_H}\frac{d^2F_H}{d\phi^2} = -m^2 \quad \textbf{(2-16)}$$

with

m - a constant

$$\rho\frac{d}{d\rho}\left(\rho\frac{d}{d\rho}P_E\right) + \left((k_\rho\rho)^2 - m^2\right)P_E = 0 \quad \textbf{(2-17)}$$

$$\rho\frac{d}{d\rho}\left(\rho\frac{d}{d\rho}P_H\right) + \left((k_\rho\rho)^2 - m^2\right)P_H = 0 \quad \textbf{(2-18)}$$

with

$$k_\rho^2 = k^2 - \beta^2 \quad \textbf{(2-19)}$$

k_ρ - the radial wave number

From the form of the differential equations and knowledge of the physics involved, solutions can be suggested for the differential equations in regions 1 and 2. Equations (2-

13) to (2-16) are harmonic functions with harmonic solutions. The ϕ dependence is chosen to satisfy the fact that the propagating electric and magnetic fields are 90^0 out of phase. The z dependence is chosen to represent a traveling wave in the z-direction. Equations (2-17) and (2-18) are Bessel equations of the mth order with Bessel functions as solutions. Region 1 inside the rod has to have finite fields at the origin. Consequently, Bessel functions of the first kind and mth order are required as solutions. In Region 2 outside the rod, however, the requirement is that the fields decay away for the edge of the rod. This is required by the fact that a solution for a surface wave is sought. Modified Bessel functions of the second kind and mth order satisfy this requirement. In summary then the solutions (2-11) and (2-12) for region 1 are:

$$E_{z1} = AJ_m\left(k_{\rho 1}\rho\right)\cos\left(m\phi\right)e^{-j\beta z} \qquad \textbf{(2-20)}$$

$$H_{z1} = BJ_m\left(k_{\rho 1}\rho\right)\sin\left(m\phi\right)e^{-j\beta z} \qquad \textbf{(2-21)}$$

with

A, B - amplitude constants

$$k_{\rho 1}^2 = k^2 - \beta^2 \qquad \textbf{(2-22)}$$

noting that for region 1, the medium is a dielectric with dielectric constant ε_r and relative permeability μ_r=1, it follows that in (2-22):

$$k = k_0\sqrt{\varepsilon_r} \qquad \textbf{(2-23)}$$

m - an integer

J_m - a Bessel function of the first kind and mth order

Solutions for region 2 are:

$$E_{z2} = CK_m\left(k_{\rho 2}\rho\right)\cos\left(m\phi\right)e^{-j\beta z} \qquad \textbf{(2-24)}$$

$$H_{z2} = DK_m\left(k_{\rho 2}\rho\right)\sin\left(m\phi\right)e^{-j\beta z} \qquad \textbf{(2-25)}$$

with,

C, D - amplitude constants

K_m - a modified Bessel function of the second kind and mth order

$$k_{\rho 2}^2 = \beta^2 - k_0^2 \qquad \textbf{(2-26)}$$

Note that the order of subtraction from equation (2-19) have been turned around. This is motivated in [19] by the fact that the argument of K_m needs to be kept real. As mentioned before, the containment of the wave within the dielectric rod at a certain frequency decreases with a decrease in rod diameter. For diameters of less than approximately a quarter of a free space wavelength, the containment of the wave within the rod is very small and the propagation constant of the wave in the rod is close to that of a wave in the surrounding free space [20]. The diameter, where the propagation constant is equal to the free space propagation constant ($\beta = k_0$), can be seen as a slow wave operational limit. For diameters larger than this, at a certain frequency, the surface wave is a slow wave i.e.:

$$\frac{\beta}{k_0} = \frac{\lambda_0}{\lambda_z} = \frac{c}{v_z} > 1 \qquad \textbf{(2-27)}$$

with

λ_z - the surface wave propagation wavelength along the rod

v_z - the phase velocity of the surface wave along the rod

c - the speed of light in free space

Slow wave operation is used in the rod antenna design since it is desired that the high frequency band be contained within the rod. Design calculation should therefore be done in this region of operation. This determines the lower limit of rod diameter to be chosen as previously mentioned in Section 2.1 . From equation (2-27) it also follows that in order to have the Bessel function argument real in region 2, the subtraction order of equation (2-26) must be used.

With z field components determined as above the other field components can be written using the z field components, as shown in [19]. The boundary continuity conditions

$$E_{z1} = E_{z2} \tag{2-28}$$

$$H_{z1} = H_{z2} \tag{2-29}$$

$$E_{\phi 1} = E_{\phi 2} \tag{2-30}$$

$$H_{\phi 1} = H_{\phi 2} \tag{2-31}$$

then lead to the set of four simultaneous equations that is used to solve for the modes and propagation constants of the surface wave along the rod. Using the following substitutions:

$$x = k_{\rho 1} a_r \tag{2-32}$$

$$y = k_{\rho 2} a_r = \sqrt{(k_0 a_r)^2 (\varepsilon_r - 1) - x^2} \tag{2-33}$$

with

$$x < k_0 a_r \sqrt{\varepsilon_r - 1} \tag{2-34}$$

in order to keep the argument of the modified Bessel function (y) real.

The set of simultaneous equations is written by [19] as :

$$\mathbf{FC} = \mathbf{0} \tag{2-35}$$

with

$$\mathbf{C} = \begin{bmatrix} A \\ B \\ C \\ D \end{bmatrix} \tag{2-36}$$

$$\mathbf{F} = \begin{bmatrix} J_m(x) & 0 & -K_m(y) & 0 \\ 0 & J_m(x) & 0 & -K_m(y) \\ \dfrac{\beta a_r m}{x^2} J_m(x) & \dfrac{\omega \mu_0 a_r}{x} J_m'(x) & \dfrac{\beta a_r m}{y^2} K_m(y) & \dfrac{\omega \mu_0 a_r}{y} K_m'(y) \\ \dfrac{\omega \varepsilon a_r}{x} J_m'(x) & \dfrac{\beta a_r m}{x^2} J_m(x) & \dfrac{\omega \varepsilon_0 a_r}{y} K_m'(y) & \dfrac{\beta a_r m}{y^2} K_m(y) \end{bmatrix} \tag{2-37}$$

a_r - the radius of the dielectric rod as shown in Figure 4

Primed Bessel functions indicate the derivative of the function with respect to the argument of the function. Since equation (2-35) is homogeneous, the only non-trivial solutions exist where the determinant of $\mathbf{F}$ is zero.

$$\det \mathbf{F} = 0 \qquad \textbf{(2-38)}$$

The values of x that satisfies equation (2-38), corresponds to the radial wave numbers (equations (2-32) and (2-33)) that define the possible modes of the rod in free space. Equation (2-38) can be evaluated numerically over x and the zero's determined. The x values at these points then lead to the radial wave numbers and, therefore, to the propagation constants along the rod of the modes of interest. Alternately, instead of evaluating the determinant, the minimum singular value [21] of matrix $\mathbf{F}$ for each x can be calculated. Where the minimum singular value equals zero, the determinant of $\mathbf{F}$ will also be zero and the x value at this point will be a solution to equation (2-38). Routines were written in MATLAB® code to perform these calculations. Figure 5 shows a high level flow diagram of the code process. The MATLAB® routines are included in Appendix 1. The main routine that calls subroutines is **KaBetaCalcFin4.m**

The second step in Figure 5 is the definition of the evaluation range for the x values. The upper maximum is set by equation (2-34). This is to keep the argument of the modified Bessel function (y) real. As already stated above, this is related to the slow wave operational limit ($\beta = k_0$) and correct surface wave containment in the rod. This is determined by the lowest β for slow wave operation as seen in equation (2-27). The lowest value for x is determined by the highest possible value for β, according to equations (2-22) and (2-32). For the same radius the lowest x occurs when β is largest but $k_{\rho 1}$ is still real. I.E. when $k_{\rho 1}$ is zero ($\beta = k$) and hence, x is zero. Technically, when $k_{\rho 1}$ is zero, radial attenuation in region 1 is zero. Consequently a starting value for x of close to zero can be taken.

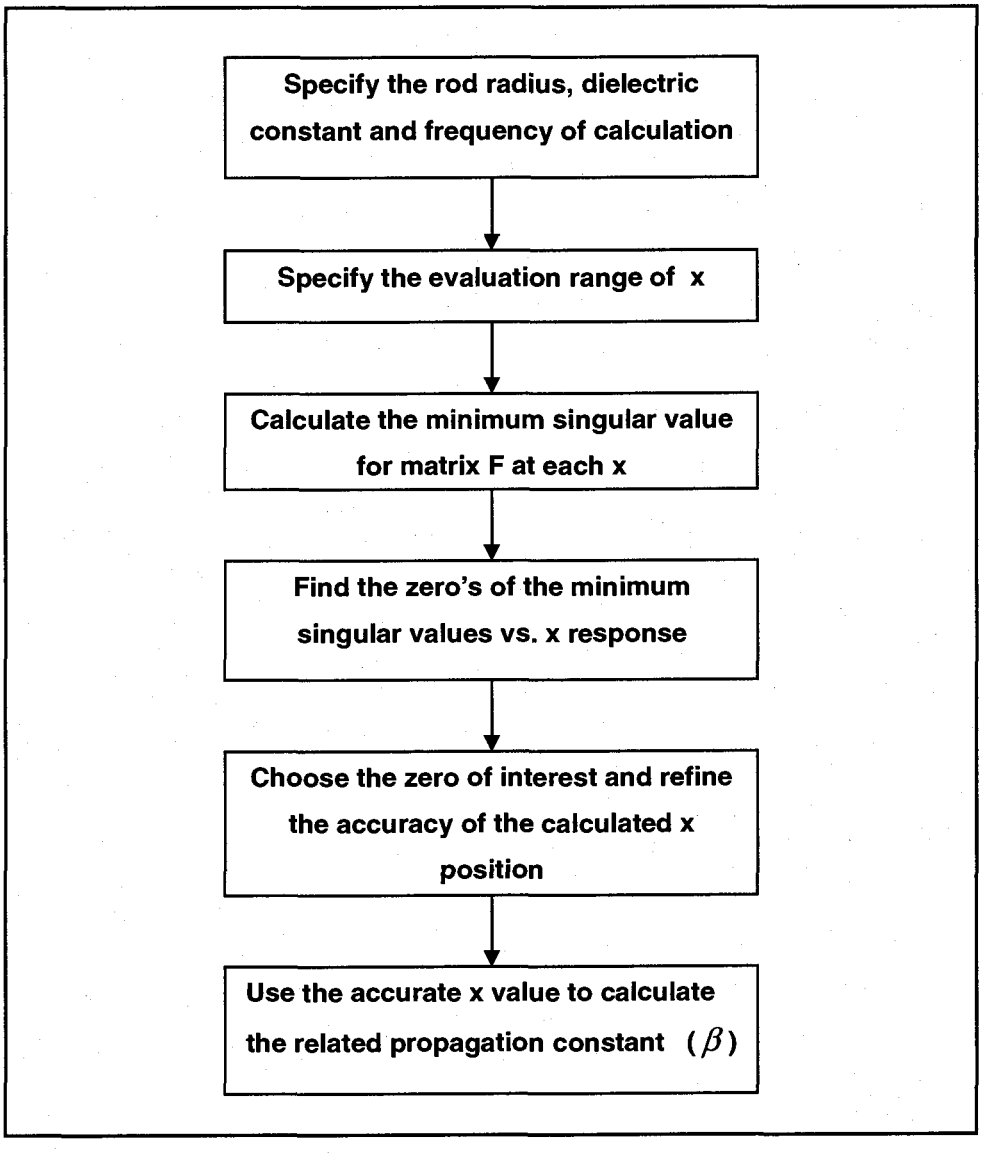

Figure 5: High Level Flow Graph for the Calculation of the Propagation Constant of the Dielectric Rod Surface Wave

The following step in Figure 5 is done by subroutine **HE1NminSing.m**. A function available in MATLAB® is used to decompose matrix **F** in order to obtain the singular values. The analytical equations used to set up **F** in the routine are those that are valid for the HE_{1N} modes of the rod. The minimum of the singular values is determined and returned to the main routine. In the main routine, the minimum singular values versus the x values response is plotted for inspection. It is then evaluated numerically at all the x

points, to determine the two slopes between three consecutive x value points. A negative slope followed by a positive slope indicates a possible zero of the response. These points are written to a matrix and represent the x values corresponding to the HE_{1N} modes. Any of the HE_{1N} mode solutions can be chosen in the main routine for further refinement. The corresponding x value is used in the subroutine **GoldKc1HE1Nsearch.m** to further refine the accuracy of the x value. The preceding and following x values, spanning the chosen x value, are used to define the span of the Range of Uncertainty (ROU) in the Golden-Section search used in the subroutine. Refinement is stopped when the ROU is small enough to yield a refined x value with a calculated minimum singular value sufficiently close to zero. The refined x value is then used in the main routine to calculate the accurate propagation constant (β) for the specified HE_{1N} mode. It is this β for the HE_{11} mode, that is used in Section 2.1 for the design of the dielectric rod antenna.

Tables 3 to 5 list values as calculated with the code described above. The ranges of radii (a_r) listed in the tables are those of interest to the design as discussed in Section 2.1. The decrease in ratio β/k_0, with a decrease in radius is evident in the listed values. The lowest radius values listed are at the very edge of slow wave operation since β/k_0 is so close to unity. These radii can therefore be taken as lower limits for slow wave operation and mode containment in the rod.

With the propagation constant known, the z-directed field components of equations (2-20), (2-21), (2-24) and (2-25) are defined, except for the excitation amplitude constants A, B, C and D. Any one of these constants can be arbitrarily chosen if a relative field strength analysis is to be performed. The other three then follows from definite relations between the constants for a specific mode as given in [19].

$$\frac{C}{A}=\frac{D}{B}=\frac{J_m(x)}{K_m(y)} \qquad \textbf{(2-39)}$$

$$\frac{B}{A}=-\frac{1}{\eta}\frac{F_3(x)}{F_2(x)} \qquad \textbf{(2-40)}$$

with

$$F_3(x) = \frac{\beta a_r m}{k_0 a_r \sqrt{\varepsilon_r}} J_m(x)\left[\frac{1}{x^2} + \frac{1}{y^2}\right] \quad \textbf{(2-41)}$$

$$F_2(x) = \frac{J_m'(x)}{x} + \frac{K_m'(y) J_m(x)}{y K_m(y)} \quad \textbf{(2-42)}$$

$$\eta = \sqrt{\frac{\mu_0}{\varepsilon_0 \varepsilon_r}} \quad \textbf{(2-43)}$$

η - the wave impedance of the dielectric medium

Table 3: Dielectric Rod Radii and HE_{11} Mode Propagation Constants at 29.5 GHz

Rod Radius (a_r) mm	Rod Diameter mm	HE_{11} Propagation Constant(β) radians/m	Ratio $\frac{\beta}{k_0}$
1.2000	2.4000	618.6929	1.0007
1.3000	2.6000	619.5514	1.0021
1.4000	2.8000	621.2876	1.0049
1.5000	3.0000	624.2414	1.0096
1.6000	3.2000	628.6705	1.0168
1.7000	3.4000	634.7129	1.0266
1.8000	3.6000	642.3763	1.0390
1.9000	3.8000	651.5477	1.0538

Table 4: Dielectric Rod Radii and HE_{11} Mode Propagation Constants at 30 GHz (2 mm to 4 mm)

Rod Radius (a_r) mm	Rod Diameter mm	HE_{11} Propagation Constant(β) radians/m	Ratio $\frac{\beta}{k_0}$
2.0000	4.0000	677.0951	1.0769
3.0000	6.0000	799.3517	1.2713
4.0000	8.0000	875.1163	1.3918

Table 5: Dielectric Rod Radii and HE_{11} Mode Propagation Constants at 30 GHz (1.2 mm to 1.9 mm)

Rod Radius (a_r) mm	Rod Diameter mm	HE_{11} Propagation Constant(β) radians/m	Ratio $\frac{\beta}{k_0}$
1.2000	2.4000	629.3025	1.0009
1.3000	2.6000	630.3517	1.0025
1.4000	2.8000	632.4071	1.0058
1.5000	3.0000	635.8169	1.0112
1.6000	3.2000	640.8275	1.0192
1.7000	3.4000	647.5501	1.0299
1.8000	3.6000	655.9552	1.0433
1.9000	3.8000	665.8876	1.0591

A can be chosen as 1 in a normalized field strength analysis and for the HE_{11} mode it then follows that :

$$A_{11} = 1 \qquad \textbf{(2-44)}$$

$$B_{11} = -\frac{1}{\eta}\frac{F_3(x_{11})}{F_2(x_{11})} \qquad \textbf{(2-45)}$$

$$C_{11} = \frac{J_1(x_{11})}{K_1(y_{11})} \tag{2-46}$$

$$D_{11} = B_{11}\frac{J_1(x_{11})}{K_1(y_{11})} \tag{2-47}$$

The electric field components in region 2 outside the dielectric rod are [19]:

$$E_{z2} = CK_m(k_{\rho 2}\rho)\cos(m\phi)e^{-j\beta z} \tag{2-48}$$

$$E_{\phi 2} = \frac{-j}{k_{\rho 2}^2}\left(\beta m\frac{C}{\rho}K_m(k_{\rho 2}\rho) + \omega\mu_0 k_{\rho 2}DK_m'(k_{\rho 2}\rho)\right)\sin(m\phi)e^{-j\beta z} \tag{2-49}$$

$$E_{\rho 2} = \frac{j}{k_{\rho 2}^2}\left(\beta k_{\rho 2}CK_m'(k_{\rho 2}\rho) + \omega\mu_0 m\frac{D}{\rho}K_m(k_{\rho 2}\rho)\right)\cos(m\phi)e^{-j\beta z} \tag{2-50}$$

Employing equations (2-46) to (2-50), the electric field strengths as functions of radial distance from the dielectric rod, normalized to the field strengths at the rod edge ($\rho = a_r$), can be evaluated. MATLAB® routines were written to do these evaluations. Files **RodE2Plot1d.m** and **const1Fe.m** are included in Appendix 1. Figure 6 shows the results.

The ϕ- and z-dependence in equations (2-48) to (2-50) were set to maximum by setting the corresponding factors equal to 1. Figure 6 therefore shows the field responses of the maximum values with the decay of the ρ dependence. These physical situations will obviously not occur at the same ϕ value for equation (2-49), as for the other two equations due to the sine and cosine dependence.

The maximum field strengths versus radius are viewed, however, to see the maximum field strength that will be interfered with at a certain radius, should a metal structure be added to the "dielectric rod in free space" scenario. Specifically the radius of 9 mm is important, as will be seen in the next section. This is the radius where the circular metal waveguide for the Ku-band was introduced in the design. Operational results for the Ka-band were still good, regardless of the extra metal boundary. Consequently, the question of how close the metal wall can be to still support the stand alone design approximation

of the Ka-band rod antenna, is answered by Figure 6. A radial distance with a maximum electric field decay level of less than -20 dB was found to be acceptable. This does not define an absolute limit, but rather a practical one that was empirically found to be satisfactory.

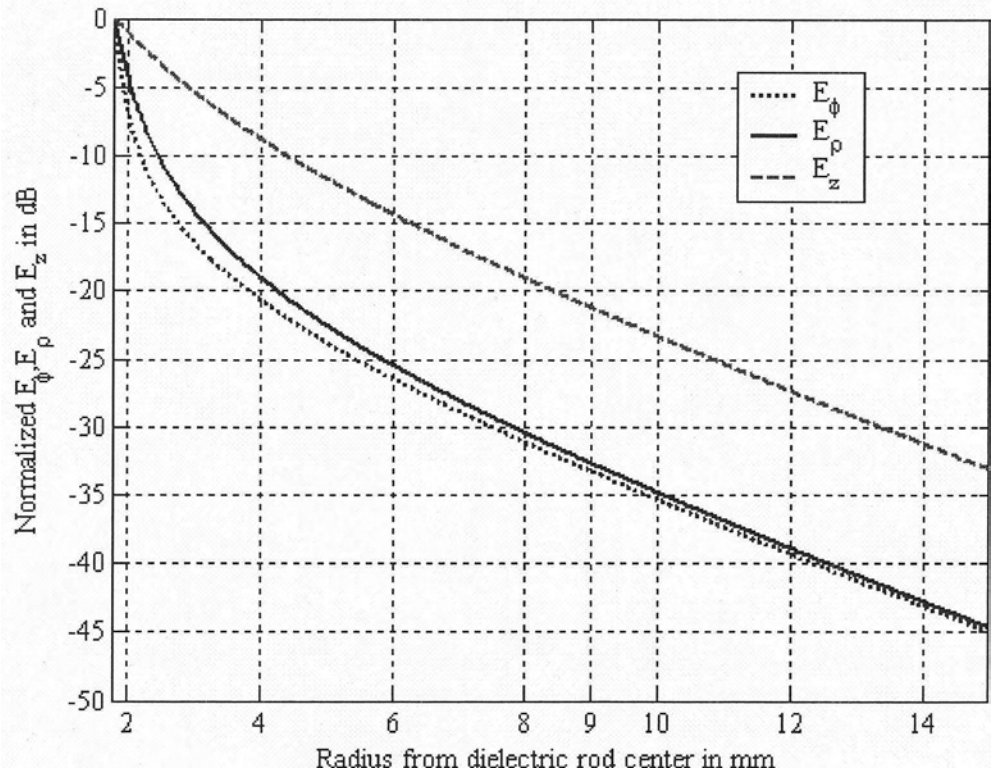

Figure 6: Normalized Electric Field Components Outside the Dielectric Rod of Radius 1.8 mm

3 Ku-band Main Propagation Section

With the dielectric rod antenna defined, the next step is the design of the cross section dimensions of the main propagation section shown in Figure 2. The diameter of the dielectric rod in this section is determined by the rod antenna design and has to stay fixed. Consequently the design of this section comes down to the diameter of the larger metal waveguide. Two issues determine design choices. Firstly, the section should allow the Ku-band TE_{11} circular waveguide mode to propagate and preferably be mono-modal in this regard. Secondly, the outer waveguide has to be far enough away from the dielectric rod to prevent major disturbance of the Ka-band HE_{11} mode in the rod.

To address the first issue, the cut-off frequencies of the modes of interest in the circular waveguide coaxially loaded by the dielectric rod need to be determined. As in section 2.2, the wave equation needs to be solved in cylindrical coordinates for the structure. Again the geometry consists of two regions. Region 1 is the dielectric rod interior. Region 2 is the region outside the rod, but now bounded by a metal boundary at a radius b_r. Figure 7 shows the problem geometry. TE_{mn} and TM_{mn} modes are of interest for the problem at Ku-band frequencies. Since the rod radius (a_r) is fixed by the Ka-band rod antenna design, only the outer radius b_r can be varied to achieve the desired Ku-band operation. At Ku-band frequencies the dielectric rod diameter is too small to support surface wave containment and as a result, only non-hybrid modes may be considered for the Ku-band operation.

Solutions for the z-directed field components, that satisfy the wave equation, need to be found. A general form for the solutions are:

$$\Psi_z = \left[AJ_m\left(k_\rho \rho\right) + BY_m\left(k_\rho \rho\right)\right]\cos\left(m\phi\right)e^{-j\beta z} \qquad \text{(3-1)}$$

$$k_\rho^2 = k^2 - \beta^2 \tag{3-2}$$

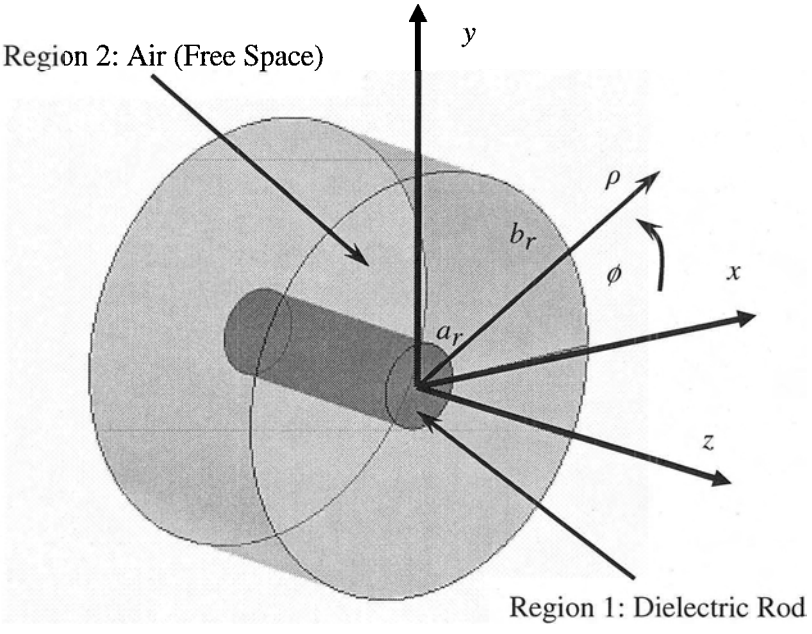

Figure 7: Problem Geometry for the Ku-Band Main Propagation Section

with

Ψ_z - the z-directed field quantity

Y_m - the Bessel function of the second kind and mth order

All other quantities follow the same definitions as in Section 2.2. Equation (3-1) can be applied directly for Region 2. For Region 1, the field quantity at the origin must be finite. The Bessel function of the second kind does not adhere to this requirement and the related term is omitted for region 1:

$$\Psi_z = AJ_m\left(k_\rho \rho\right)\cos\left(m\phi\right)e^{-j\beta z} \tag{3-3}$$

For TE_{mn} modes the z-directed electric field is zero and only the z-directed magnetic field components are valid, rendering for regions 1 and 2:

$$H_{z1} = A_1 J_m\left(k_{\rho 1}\rho\right)\cos\left(m\phi\right)e^{-j\beta z} \tag{3-4}$$

$$H_{z2} = \left[A_2 J_m\left(k_{\rho 2}\rho\right) + B_2 Y_m\left(k_{\rho 2}\rho\right)\right]\cos\left(m\phi\right)e^{-j\beta z} \tag{3-5}$$

with

$$k_{\rho 1}^2 = k_0^2\varepsilon_r - \beta^2 \tag{3-6}$$

$$k_{\rho 2}^2 = k_0^2 - \beta^2 \tag{3-7}$$

In equations (3-4) and (3-5) the three unknowns, coefficients A_1, A_2, and B_2, are present. A set of three simultaneous equations are therefore needed to solve for the three unknowns. Three equations follow from the boundary conditions that require the tangential field components to be continuous at radius a_r and that the tangential electric field component be zero at the metal wall boundary located at radius b_r.

$$E_{\phi 1} = E_{\phi 2} \tag{3-8}$$

$$H_{z1} = H_{z2} \tag{3-9}$$

at radius a_r and

$$E_{\phi 2} = 0 \tag{3-10}$$

at radius b_r.

The expressions for the electric field quantities can be derived from the z components of the magnetic field.

$$E_{\phi 1} = \frac{j\omega\mu}{k_{\rho 1}} A_1 J_m'\left(k_{\rho 1}\rho\right)\cos\left(m\phi\right)e^{-j\beta z} \tag{3-11}$$

$$E_{\phi 2} = \frac{j\omega\mu}{k_{\rho 2}}\left[A_2 J_m'\left(k_{\rho 2}\rho\right) + B_2 Y_m'\left(k_{\rho 2}\rho\right)\right]\cos\left(m\phi\right)e^{-j\beta z} \tag{3-12}$$

These expressions along with equations (3-4) and (3-5), substituted into equations (3-8) to (3-10), form the set of simultaneous equations to solve for the geometry of Figure 7. As in Section 2.2, this can be written in the form of a transcendental matrix equation that has to be evaluated numerically.

$$\mathbf{F}_{\mathrm{TE}}\mathbf{D}=\mathbf{0} \tag{3-13}$$

with

$$\mathbf{D}=\begin{bmatrix} A_1 \\ A_2 \\ B_2 \end{bmatrix} \tag{3-14}$$

$$\mathbf{F}_{\mathrm{TE}}=\begin{bmatrix} \dfrac{J_m'\left(k_{\rho 1}a_r\right)}{k_{\rho 1}} & -\dfrac{J_m'\left(k_{\rho 2}a_r\right)}{k_{\rho 2}} & -\dfrac{Y_m'\left(k_{\rho 2}a_r\right)}{k_{\rho 2}} \\ J_m\left(k_{\rho 1}a_r\right) & -J_m\left(k_{\rho 2}a_r\right) & -Y_m\left(k_{\rho 2}a_r\right) \\ 0 & J_m'\left(k_{\rho 2}b_r\right) & Y_m'\left(k_{\rho 2}b_r\right) \end{bmatrix} \tag{3-15}$$

To obtain the cutoff frequency of the structure, given a certain metal waveguide radius b_r, a similar procedure to that outlined in Section 2.2 was followed. The primary difference is that, in order to obtain the cut off frequencies, the singular values of $\mathbf{F}_{\mathrm{TE}}$ were evaluated over frequency and not over radial wavenumber as before. To achieve this, β is set to zero (the value at cut off). This forces the solution obtained, when the minimum singular value is zero, to be the one that occurs at cut off. Figure 8 shows the high level flow diagram of the routine written to perform the numerical evaluation. The MATLAB® code files used in the analysis are included in Appendix 2. Main routine and subroutine calling operations are analogous to those described in Section 2.2.

Table 6 shows the calculated results. For the 10.7 GHz to 12.75 GHz bandwidth the structure cut off for an 8 mm outer radius is too close to the operational band. The 9 mm radius cut off is well positioned, and this value was chosen for the circular waveguide radius. To ensure that higher order modes are in cut off within the operational band, the

structure with a 9 mm waveguide radius was analyzed with HFSS®. Since the excitation field distribution of the waveguide is that of an incident plane wave on the feed-multiplexer, the next possible mode with a corresponding field distribution that can be excited in the waveguide after the TE_{11} mode, is the TM_{11} mode [16]. Analysis showed that the TM_{11} mode cutoff frequency is approximately 20.15 GHz. This is well outside the band of interest.

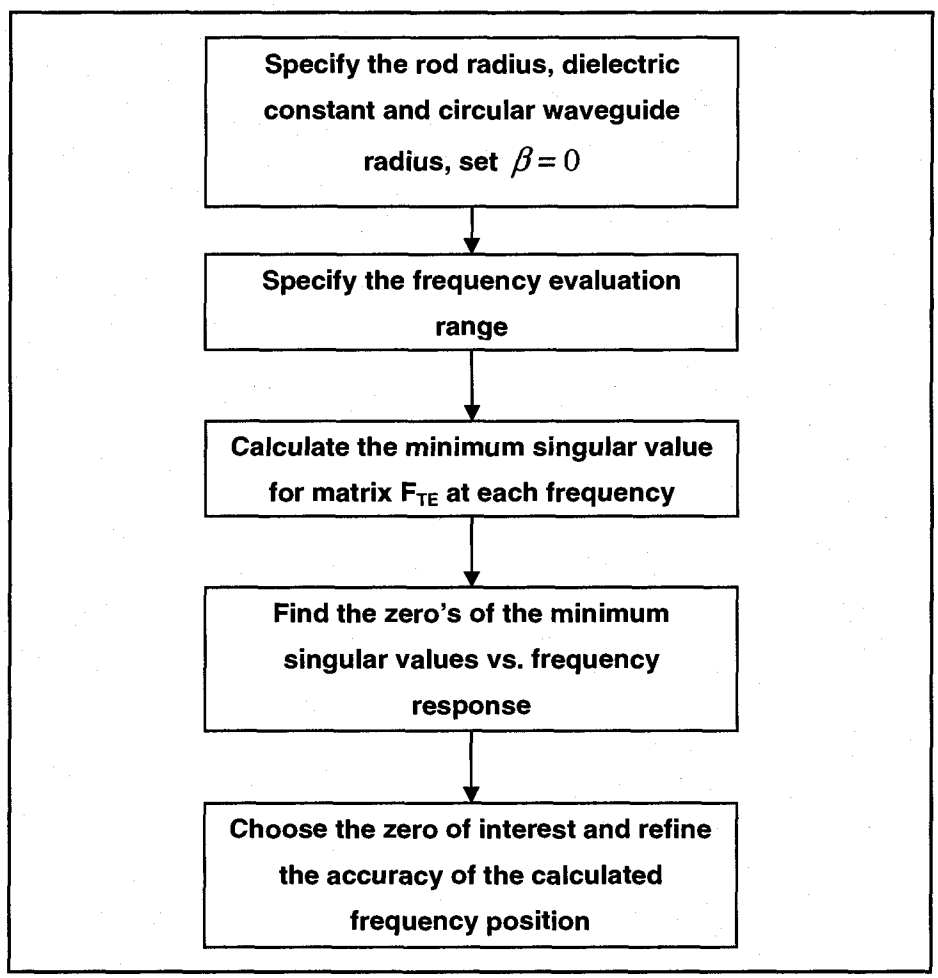

Figure 8: High Level Flow Diagram for the Evaluation of the TE_{mn} Mode Cut-Off Frequency in the Feed-Multiplexer Main Propagation Section

Table 6: TE_{11} Mode Cut-Off Frequencies of the Main Propagation Section Structure with a_r = 1.8 mm

Waveguide Radius (b_r) mm	Structure Cut-Off GHz
6.00	13.576
7.00	11.854
8.00	10.504
9.00	9.420
10.00	8.534
11.00	7.796
12.00	7.173

With the design as set out in this section, the main propagation section satisfy the first requirement of allowing the TE_{11} mode to propagate for the Ku-band, while not presenting any higher order mode problems (mono-modal). The second issue named at the beginning of this section, i.e. whether the circular waveguide wall is far enough away from the dielectric rod to prevent interference with the Ka-band surface wave, was addressed at the end of Section 2.2. A radius of 9 mm corresponds to a surface wave field decay of more than 20 dB from the value at the rod edge. The final feed-multiplexer response proved this to be sufficient.

4 Ku-Band Coaxial Waveguide Section

This section is formed by the Ku-band circular waveguide and the center structure shown in Figure 2. Figure 9 shows the coaxial waveguide section with the Ku-band probes. The center structure is a metal wrapping for the Ka-band dielectric rod, extending from the back of the feed-multiplexer that ends at the start of the rod antenna feed taper. It is an extension of the Ka-band dielectrically filled circular waveguide section that starts at the WR28 rectangular waveguide junction. The coaxial waveguide section is required to form the orthomodal transducer (OMT) [22] for the Ku-band when combined with the four probes extending into this section of the feed-multiplexer. For the Ka-band operation, the coaxial waveguide section effectively moves the feed edge (Figure 3) of the Ka-band rod antenna further out along the axis of the feed-multiplexer. Had this section not been there, the feed edge would coincide with the termination of the Ku-band circular waveguide at the back of the feed-multiplexer. If this was the case, the Ku-band probes would be operating in close proximity to an unshielded section of dielectric rod. Both the Ka-band HE_{11} mode of the dielectric rod and the Ka-band radiated wave generated at the feed edge would then be affected by the presence of the probes. By using the coaxial waveguide section, the probes are separated from the HE_{11} mode in the rod, resulting in better Ka/Ku-band isolation and operational separation. Sufficient operational separation is vital to the design of optimum performance in both the frequency bands.

Since the Ku-band propagation medium changes from a dielectrically loaded circular waveguide to a metal center structure coaxial waveguide at the feed edge, a discontinuity is introduced that will affect the propagation and, therefore, the return loss of the Ku-band. As is intuitive and from the parametric study conducted on the structure, the metal wrapping of the dielectric rod that forms the center structure needs to be as thin as

possible to minimize disturbance at the discontinuity. However, skin depth [16] needs to be considered for the induced currents on the center structure to ensure proper coaxial waveguide operation. Copper foil was chosen for the dielectric rod wrapping. Greater skin depth, requiring thicker foil, occurs at lower frequencies. Worst case design is therefore done at the lowest frequency in the band.

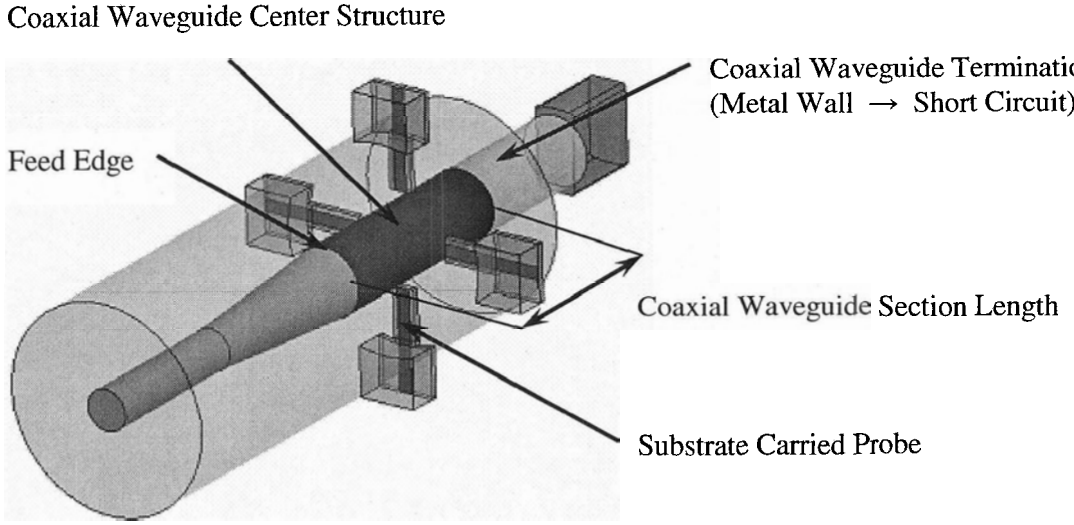

Figure 9: Ku-Band Coaxial Waveguide Section

From [16]

$$\delta_s = \sqrt{\frac{1}{\pi f \mu_0 \sigma}} \qquad (4\text{-}1)$$

with

δ_s - the skin depth

f - the frequency of operation

μ_0 - the permeability of free space

σ - the conductivity of the metal

This gives a skin depth of 0.66 μm in copper, at a frequency of 10 GHz. Adhesive backed copper foil with a thickness of 0.04 mm (more than 60 times the skin depth) was commercially available, providing ample margin for proper conduction in the center structure. Thinner adhesive copper foil was not available.

The design of the coaxial section has only the length of the section as variable since the diameters involved are determined by the rod antenna and main propagation section designs. Before this length can be designed, the coaxial structure cross section must first be investigated to ensure that the Ku-band coaxial TE_{11} mode is not in cut off. For a thorough investigation of the structure a procedure similar to those used in Section 2.2 and Chapter 3 for the analysis of the propagation constants and cut off frequencies can be followed. Since the cross section diameters are already determined by previous design considerations, a less elaborate calculation is more appropriate. In [16], equations often used in practice for an approximate coaxial waveguide design are given.

$$f_c = 1.05\frac{ck_\rho}{2\pi\sqrt{\varepsilon_r}} \tag{4-2}$$

$$k_\rho = \frac{2}{a+b} \tag{4-3}$$

with

f_c - the structure TE_{11} mode cut off frequency

c - the speed of light in free space

ε_r - the relative permittivity of waveguide material

a - the center structure radius

b - the outer waveguide radius

k_ρ - the approximate radial wavenumber of the coaxial waveguide given by equation (4-3)

Use of these equations requires an approximation safety margin. This is included by the factor of 1.05 in equation (4-2) that introduces a 5 % safety margin. Using this approach results in a cut off frequency of 9.243 GHz for the coaxial structure. The Ku-band will

therefore be out of cut off and the coaxial dimensions that resulted from the previous design considerations are acceptable.

The length of the coaxial section was designed by a parametric study of the Ka-band and Ku-band return loss response as affected by the length. Since the Ku-band probes will be positioned at a distance of approximately a quarter coaxial guide wavelength from the termination of the waveguide as set out in Chapter 5, an appropriate starting length for the parametric study of the coaxial section is half a coaxial guide wavelength. This allows coaxial waveguide length on both sides of the Ku-band probes. The probes should preferably not be too close to the end of the feed edge of the coaxial waveguide section. Close proximity of the two discontinuities may complicate optimization of the structure. Using the approximate radial wave number of equation (4-3), the wavelength of the coaxial waveguide can be calculated. This gives a half wavelength of 19.35 mm. The Ku-band response is predominantly affected by the distance of the probes to the waveguide termination. This can be set separately from the length of the coaxial section. The Ka-band return loss response is strongly affected by the length of the coaxial section due to the interaction of the radiated wave from the feed edge with the waveguide short circuit at the waveguide termination and also with the Ku-band probes protruding into the coaxial waveguide. It is, therefore, best to first determine the Ku-band probe position in relation to the waveguide termination (Chapter 5) and then, with this dimension fixed, change the coaxial section length to give a good Ka-band return loss response. Once this is obtained, the Ku-band return loss is checked again to ensure that both bands are functioning well with the determined coaxial waveguide length. Such a parametric study using HFSS® was performed and an optimum realizable coaxial waveguide length was achieved at a length of 18 mm.

5 Ku-band Coupling Probe Structures

As mentioned in the introduction the metal probes carried by dielectric substrate board are at the heart of the thesis investigation. If these structures can be used as Ku-band coupling structures and so complete a functional multiplexer, the advantages mentioned in the introduction are achieved since the same board used for the circuitry of the LNB of the SIT can be used to form the coupling probes protruding into the coaxial waveguide section of the feed-multiplexer. The success of this approach depends on whether the probes can be used without disturbing the Ka-band aperture field distribution and whether the probes can couple the TE_{11} Ku-band mode effectively from the feed-multiplexer cavity. Though the Ku-band structures are intended for reception of incoming signals, for the purpose of analysis, the mode excitation and radiation response of these structures can be investigated. Reciprocity of passive components and antennas underline that a well functioning radiator is a well functioning receiver. As a result, the transmission characteristics for the Ku-band are used to measure the performance. The radiation patterns of both the Ka-band and Ku-band of the complete feed-multiplexer and the return loss response of the feed-multiplexer in both bands are the telling results that show whether the stated goals have been achieved. Chapter 10 deals with the desired radiation characteristics for the feed-multiplexer. In short, it can be said that if the probes disturb the Ka-band modes in the feed-multiplexer sufficiently and if the probes excite undesirable modes in the Ku-band, the field distributions in the horn aperture will in turn be disturbed, and the desired radiation patterns will not be achieved. This implies that firstly the Ku-band excitation of the TE_{11} mode by the probes has to be matched with regards to return loss. Following this, the effect of the realized structures on the Ka-band and Ku-band radiation patterns need to be evaluated.

Figure 10 shows a close-up view of one of the probes. A microstrip line inside a metal walled channel is used to carry the signal to the probe from the preceding system circuitry. This line is designed to be a microstrip line of a certain width that would realize a propagation medium with a characteristic impedance of 50 ohm, given the thickness and dielectric constant of the substrate board used [23]. With a substrate board that is 20 thousands of an inch thick (0.508 mm) and has a dielectric constant of 3.38, the line width is 1.1 mm at a frequency of 11.725 GHz. The channel width is on the order of four times the 50 ohm microstrip line width to ensure that the structure operates as a microstrip line, i.e. the sidewalls have to be far enough away from the line. The channel height can be the same or slightly less. Again, care must be taken that the height is sufficient to allow regular microstrip operation [23], [24]. Failure to do so will complicate matching this section of propagation media with the microstrip in the preceding section of the system. In conjunction with these considerations, the channel can be seen as a waveguide that might allow leakage of the Ka-band signal from the feed-multiplexer cavity. The dimensions of the channel must, therefore, be such that the highest frequency in the Ka-band is in cut off inside the channel to prevent any leakage and improve Ka/Ku-band isolation. A channel with a dielectric slab having the thickness of the substrate used was analyzed with HFSS® to ensure the proper operation. A channel width of 4 mm and a height of 3 mm was found to have a fundamental mode cut off frequency of between 37 GHz and 38 GHz. This is well beyond the Ka-band frequencies in use and presents dimensions suitable for the Ku-band microstrip operation in the channel.

At the edge of the circular waveguide, the substrate board is cut away to follow the contour of the metal strip extending into the coaxial waveguide, with a slight offset due to manufacturing considerations. The ground plane metallization on the back of the substrate board is etched away behind the metal strip protruding into the coaxial waveguide. It is resumed at the circular waveguide edge to help present a proper ground plane for the microstrip in the channel, continuous with that of the rest of the substrate board circuitry.

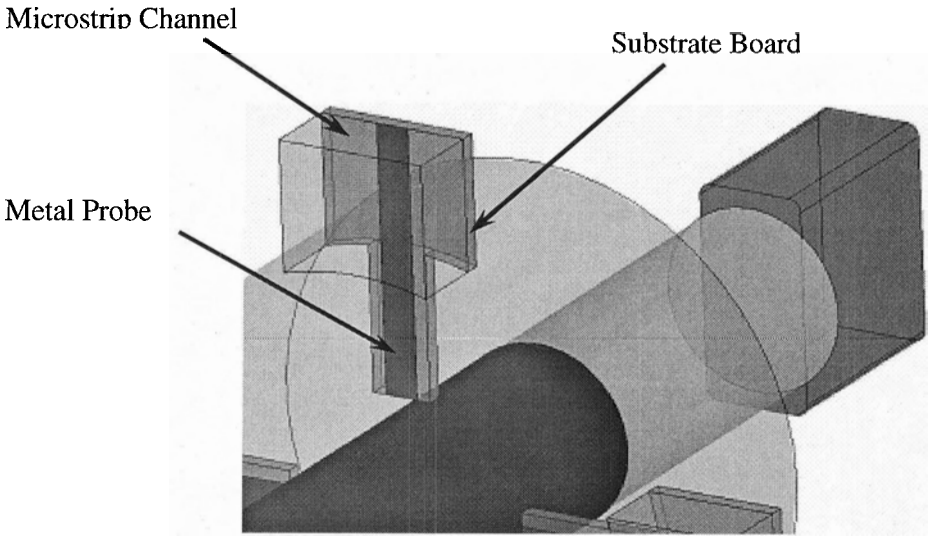

Figure 10: Substrate Carried Metal Probe

The design considerations for the probe are similar to that of a coaxial line to rectangular waveguide transition. These transitions are prolific in microwave industry. A valuable exposition is given by [25] on the design and function of this type of transition. The coaxial line is orthogonal to rectangular waveguide, and the center conductor of the coaxial line extends into the waveguide to form a probe. This probe is in close proximity to one end of the rectangular waveguide that is closed. The closed end of the rectangular waveguide forms a short circuit termination of the waveguide. The critical design dimensions to obtain a good match between the coaxial line and rectangular waveguide are the length of the probe and the distance of the probe from the termination of the waveguide. The termination of the waveguide that presents a short circuit to the signal in the waveguide is known as a "backshort", and the distance from the termination to the probe is known as the "backshort distance." These terms will be helpful in the following discussion. Analogous to the coaxial line to rectangular waveguide transition, the termination of the coaxial circular waveguide section by the closed end of the coaxial waveguide in the current design, is a short circuit for the propagating waves in the waveguide which acts as the backshort for the Ku-band probes. The distance between the probes and the termination of the waveguide is the backshort distance for the substrate carried probes.

In [25] it is explained that an optimum return loss response for the coaxial line to rectangular waveguide transition can be obtained by correctly choosing the probe length and backshort distance. The interaction between the probe structure and the backshort is used to resonate ("tune") out reactance and/or transform the real impedance value of the waveguide to that of the coaxial line. Optimum dimensions can vary depending on the bandwidth of the application and whether matching structures external to transition are used. In general, a good return loss response is obtained when the backshort distance is set to be approximately a quarter of a rectangular guide wavelength. This is somewhat intuitive since one can foresee the coupling probe to function best where the electric field strength of the standing wave inside the rectangular waveguide is a maximum. I.E. at a quarter wavelength away from the probe, the electric field is forced to be zero. Apart from a physical positioning of the probe at a standing wave maximum for the electric field in the waveguide, the impedance of the load seen by the coaxial line into the probe structure plays a predominant role in the design for a good return loss response. The behavior of this impedance needs to be studied and design choices made based on the reactance and resistance of the impedance and the rate of change of these values over frequency. The backshort distance equal to a quarter guide wavelength is, usually, a good starting point for a parametric study design that will optimize the structure for best performance.

Though the substrate carried probe fed by a microstrip line is a different propagation medium than a coaxial line, and the coaxial waveguide section in the feed-multiplexer is different from rectangular waveguide, the phenomena that govern the operation of the two transition structures are analogous. The starting value for the backshort distance in a parametric study design of the substrate probes is therefore taken as a quarter coaxial guide wavelength, as also mentioned in Chapter 4, when choosing the length of the coaxial waveguide section of the feed-multiplexer. In literature, several papers have been written about the transition from printed circuit boards to waveguide. Among those that are applicable to this thesis design are [26] and [27]. In [26], a first order design was followed by experimental optimization to achieve the best return loss for a microstrip to rectangular waveguide transition by means of a substrate carried probe. A computer

assisted design study of the same type of transition, similar to the parametric study technique used in this thesis, was performed in [27]. Two prototypes were measured to verify the results. Both these papers confirmed that with a parametric study or experimental optimization, a combination of probe dimensions and backshort distance can be readily achieved that result in a good return loss response for the transition across the entire waveguide frequency bandwidth. With these basic concepts underlined, the actual parametric design of the probe structures can now be discussed.

In order to avoid modal field distribution disturbance, it is essential that a two plane symmetry be maintained inside the feed-multiplexer. This requires that for each Ku-band polarization in the feed-multiplexer (vertical and horizontal) two oppositely positioned probes be used to couple the signal, carried in that polarization, from the feed-multiplexer. This results in the use of four probes in a symmetric cross configuration. Without this symmetry the TE_{11} mode distribution will be compromised, resulting in a non-symmetric aperture field distribution in the horn aperture and a skewed radiation pattern with a poor cross polar response. To excite the TE_{11} mode in the coaxial waveguide, each pair of opposite probes related to one of the two polarizations, have to be excited 180^0 out of phase. This is achieved by the use of a rat-race combiner, also known as a 180^0 hybrid, as discussed in Chapter 7.

The requirement of symmetry has an advantage in that it makes the analysis of the feed-multiplexer structure easier by allowing the use of electric and magnetic symmetry plane boundaries. A quarter structure can therefore be solved in the FEM software (HFSS®) instead of the full structure. This considerably reduces the solution time required for each run and speeds up the parametric design process. It must be noted though that only a magnetic symmetry boundary is allowed to bisect the microstrip channel that feeds the probe. If an electric symmetry boundary is used in the analysis, the actual microstrip mode [23] is prevented from existing since the electric field tangential to the bisecting plane perpendicular to the microstrip is forced to be zero. This scenario is only allowable if the probe channel so bisected is that of the probe pair perpendicular to the polarization being analyzed and when doing so, it must be remembered that the channel will not be

presenting the right loading to that probe due to the fact that the correct microstrip mode is not being modeled. Validity of results must be evaluated accordingly. With the above in mind, the probe design can be performed in two stages.

Firstly, a quarter structure such as shown in Figure 11, with the probe coupling to a coaxial waveguide that has no discontinuity, is analyzed and the probe length and backshort distance investigated to find the values that will result in a good return loss response for the probe input. Noticeable in Figure 11 is that the orthogonal probe to the one of interest can be omitted in the initial design stage. The orthogonal and symmetric configuration of the four probes ensures a great deal of isolation between the two polarizations and their respective probe pairs. Consequently, analysis including the orthogonal probe pair can be left as a final check of the full structure once the design is finished. Backshort distance is started at a quarter coaxial guide wavelength and gradually reduced. Probe length is started at about 0.8 times the distance between the center structure of the coaxial waveguide and the outer waveguide and gradually reduced. Reducing these lengths successively exposes the trend of response versus parameter change and allows the optimization of these values. Modern software such as HFSS® have optimization utilities that can be set up and run to optimize such parameters. This requires a great deal of experience with the software, and it is the view of the author that manual control of the iterative runs are better since the designer gains insight into the parametric response.

In the second stage of the probe design, the realized probe dimensions from the first stage are introduced to the complete feed-multiplexer quarter structure (Figure 12) and fine tuned in similar fashion as in stage one. The stage one design serves to "get the dimensions in the right ballpark" without straining the software analysis with the full solution space of the whole feed-multiplexer quarter structure. Once stage one is complete, stage two includes the impedance changes seen by the probe input due to the discontinuity at the rod feed edge, where the coaxial waveguide transfers to a dielectrically loaded circular waveguide, as well as the load presented by the rest of the

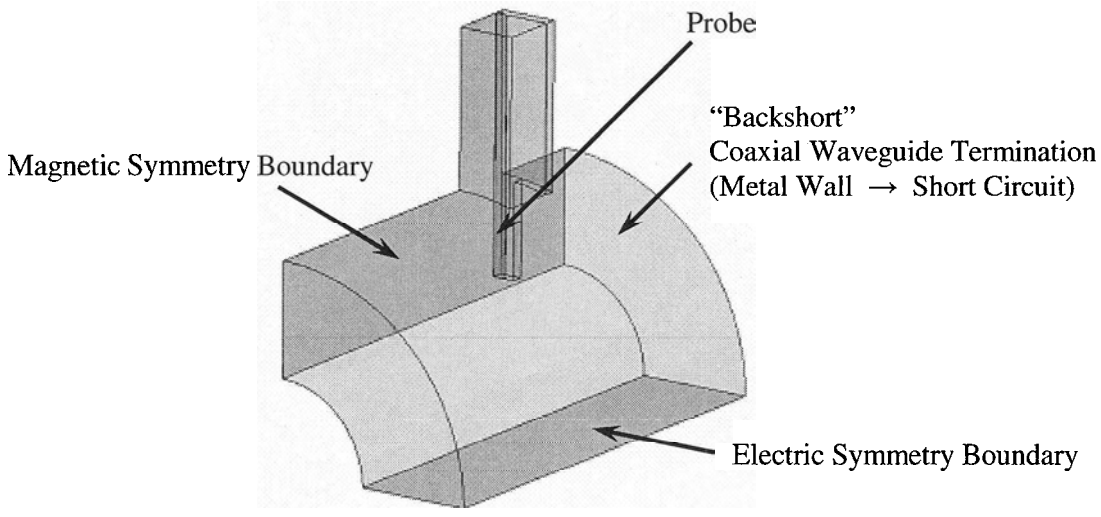

Figure 11: Probe to Coaxial Waveguide Quarter Structure

dielectrically loaded waveguide terminated in the waveguide horn. With this introduction into the complete feed-multiplexer, the length of the coaxial waveguide section will affect the response of the probe. This length should be optimized to have a good response. A return loss of better than 10 dB was obtained across the Ku-band for the return loss seen into the probe, with a probe length of 4.44 mm combined with a backshort distance of 8 mm and the coaxial waveguide section length at 18 mm as stated in Chapter 4. It must be noted here that only a quarter or half structure analysis will give the correct response for the functioning of the probe pair. If the opposite probe of the probe is included in the HFSS® analysis, it will present a load on the probe of interest and result in incorrect results. As a result of the 180^0 feeding of the pair of probes, the total structure can be seen as consisting of two half structures that can be treated as two separate feed-multiplexer structures having only one probe as input each. Indeed, if this separation is not done in HFSS®, the S-parameter analysis of the structure will load the port of the probe being analyzed with the port of its corresponding pair probe. This will give incorrect results that are incoherent with correct operation of the total feed-multiplexer. Only if the microstrip combiners are included in the structure model, giving one input to both of the probes in the probe pair, can a full structure analysis be run to ascertain the response of correct operation. Since external microstrip structures can be used to further improve the return loss, as set out in Chapter 8, return loss of better than

10 dB across the Ku-band is acceptable at the input to the probe.

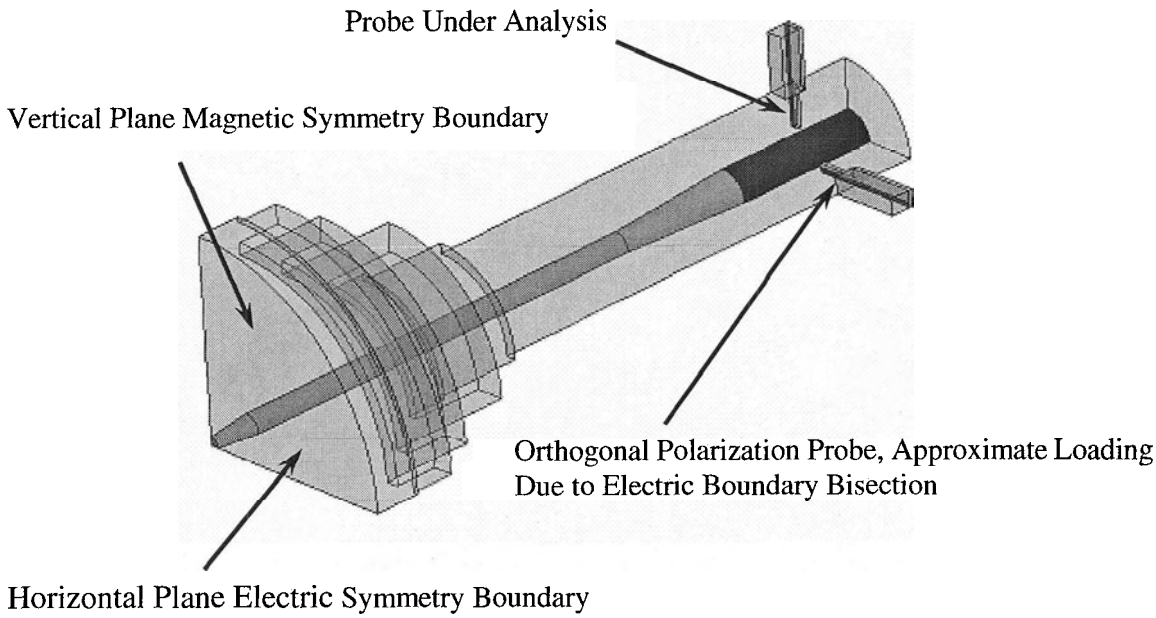

Figure 12: Ku-band Feed-Multiplexer Quarter Structure

6 Rectangular Waveguide Coupling Passages

The rectangular waveguide coupling passages are the structures, shown in Figure 2, that are connected to the horizontal Ku-Band polarization probe pair. The use of two orthogonal probe pairs etched on the same substrate board introduces a layout problem. The problem is that when the microstrip lines from the two probe pairs run to their respective combiners, two lines (one from each probe pair) inevitably will have to cross. This affects the symmetry of the microstrip line pairs that run to the combiners since a discontinuity is introduced to only one of the lines of each line pair. As a result, combiner operation will be affected detrimentally. An acceptable way of crossing can be sought or, as an alternative, the crossing of the two lines can be avoided altogether. One way of accomplishing the latter is by passing the signal of one probe pair to a second substrate board that carries the related combiner. This is the solution presented in this thesis. The passing of the signal from the first substrate board to the second, is done by the use of two rectangular waveguide passages. To do this, a microstrip to rectangular waveguide transition as described in Chapter 5 and also in [26] and [27], is used. Such a transition is employed on each of the substrate boards and the two transitions are connected by a section of rectangular waveguide. This solution is practical, since it allows for a carrier-plate to be positioned between the two substrate boards. This solves the problem of the physical mounting of the boards in the feed-multiplexer housing. The rectangular waveguides are machined through the carrier-plate.

In order to keep the feed-multiplexer fairly compact and light weight, this plate should not be too thick. It should still be thick enough to allow for proper mechanical screw fastening to be used. As a result, an arbitrary thickness of 10 mm was chosen.

Figure 13 shows a half-structure of one of the passages. The structure is designed using a similar technique as for the probe design in Chapter 5. Microstrip probe length and backshort distance are optimized from starting values by a parametric study using HFSS®, to optimize the return loss performance of the passage over the entire Ku-band.

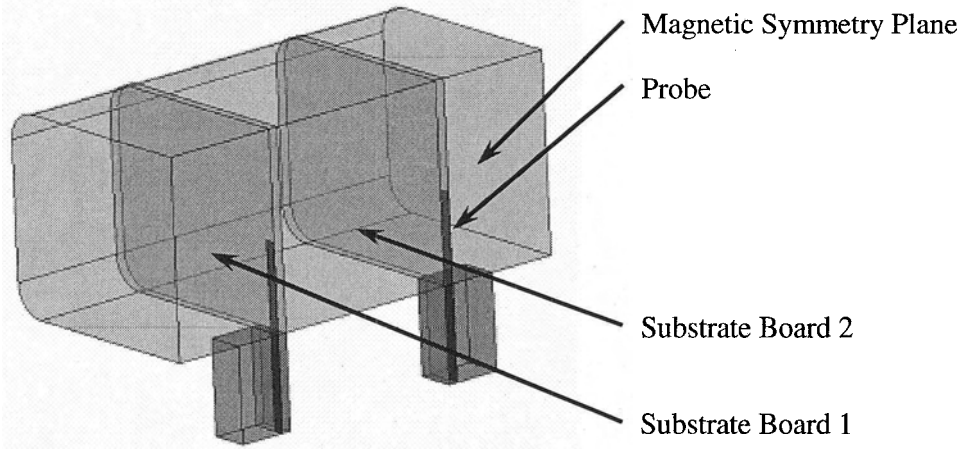

Figure 13: Ku-Band Rectangular Waveguide Coupling Passage Half Structure

Structure symmetry allows the use of a magnetic symmetry boundary that reduces the solution volume of the structure by half, as indicated in Figure 13. Machining cutter radii are included in the model, accounting for the rounded corners of the rectangular waveguide. WR75 rectangular waveguide dimensions are good starting values for the waveguide dimensions. These are industry standard dimensions for rectangular waveguide operating in the 10 GHz to 15 GHz band. Originally it was thought to make the waveguide dimensions smaller than the 19.05 mm x 9.525 mm of the WR75 waveguide. A smaller cross section would take less space and still support the Ku-band of interest (10.7 GHz to 12.75 GHz). Attempts to do this showed, however, that in order to have a good response for the passages across the entire Ku-band of interest, the frequency response of the structure needed to be scaled down. The waveguide dimensions and the probe length were scaled. The carrier-plate length and the dielectric constant and thickness of the substrate board were kept the same. Further optimization of

the dimensions from these scaled values resulted in a return loss of better than 18 dB across the entire Ku-band of interest as shown in Figure 14. This was achieved with a waveguide width of 24 mm, a waveguide height of 10.5 mm, a backshort distance of 6.3 mm and a probe length of 4.7 mm.

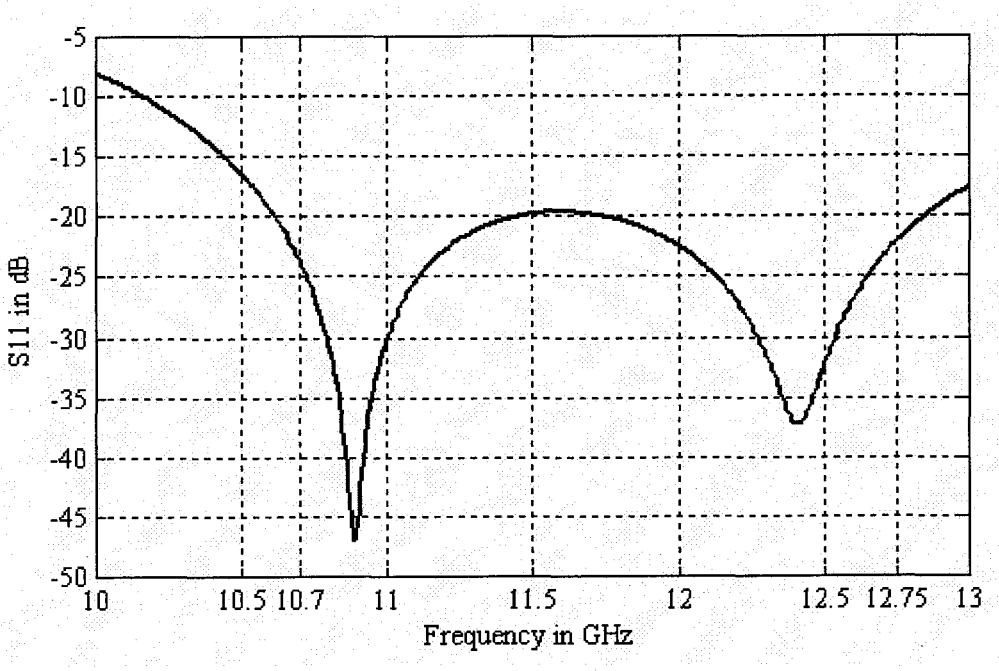

Figure 14: Coupling Passage Return Loss Results - HFSS®

Given the symmetric position of the probes the next possible higher order modes that may be excited in the rectangular waveguide after the dominant TE_{10} mode are the TE_{11} and TM_{11} modes. The cut off frequency for these modes in air filled rectangular waveguide is given by [16]:

$$f_{mn} = \frac{c}{2\pi}\sqrt{\left(\frac{m\pi}{a}\right)^2 + \left(\frac{m\pi}{b}\right)^2} \qquad \textbf{(6-1)}$$

with

f_{mn} - the modal cut off frequency

c - the speed of light in free space

a - the long edge dimension of the rectangular waveguide cross section

b - the short edge dimension of the rectangular waveguide cross section

m,n - the modal indices

For the optimized dimensions the TE_{11} and TM_{11} mode cut off is calculated from equation (6-1) to be 15.582 GHz. These dimensions, therefore, also avoid possible higher order mode problems within the operational Ku-band.

Figure 15 shows the insertion loss response of the coupling passage. The insertion loss includes the conductive losses in the microstrip as well as the dielectric losses in the substrate board material. The material has a dielectric loss tangent (tanδ) [16] of 0.0027. Silver was assigned as the metal for the microstrip conductor since the copper tracks of the substrate board are silver plated during manufacturing. Losses in the feed-multiplexer structure preceding the LNA (Low Noise Amplifier) [28] of the SIT LNB (Low Noise Block) [9] are important, since they effectively degrade the gain of the whole SIT satellite dish antenna. As a result, the signal to noise ratio [8], [9] at the output of the LNA will be detrimentally affected and system performance degraded. Figure 15 indicates that losses including reflection losses, conduction losses and dielectric losses are low enough for the coupling passage structure. This will have to be added to the losses in the microstrip circuitry and combiner in Chapters 7 and 8. For these analyses, conductive losses in the waveguide walls are considered negligible.

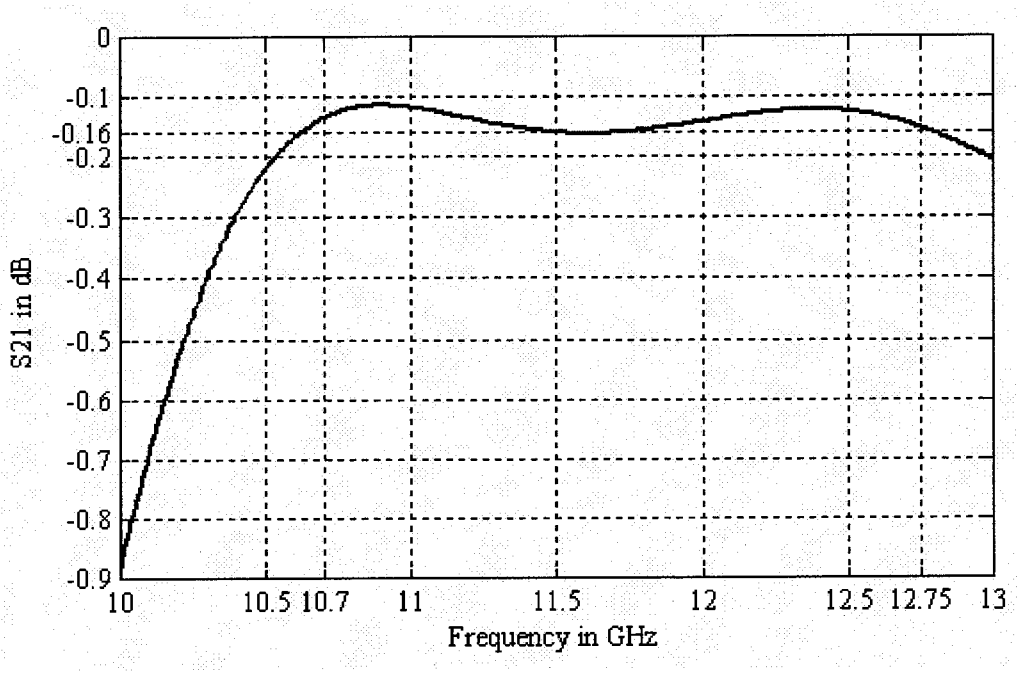

Figure 15: Coupling Passage Insertion Loss Results - HFSS®

7 Rat-Race Combiners

Figure 16 shows the rat-race combiner microstrip structure. As mentioned in the introduction, the combiner is used to combine the two signals from two opposite probes of the feed-multiplexer. Rat-race combiners are also known as 180^0-hybrids. This nomenclature suggests the reason for their use in the current design. As mentioned in Chapter 5, the two opposite probes of each probe pair need to be excited 180^0 out of phase, in order to excite the TE_{11} circular coaxial waveguide mode in the feed-multiplexer structure. By reason of the reciprocal property of passive circuits and since the Ku-band structures will be used for the receive channels, the combiner used to combine the two output signals from the probes, will have to constructively add the two signals despite the 180^0 phase difference. The rat-race combiner readily performs this task, as can be seen from the scattering matrix of an ideal (lossless) rat-race combiner [16].

$$\mathbf{S} = \frac{-j}{\sqrt{2}} \begin{bmatrix} 0 & 1 & 1 & 0 \\ 1 & 0 & 0 & -1 \\ 1 & 0 & 0 & 1 \\ 0 & -1 & 1 & 0 \end{bmatrix} \tag{7-1}$$

For the port assignments as indicated in Figure 16, the entries of interest are S_{42}, S_{43}, S_{12} and S_{13}. The structure is used to combine the inputs at port 2 and 3 and have the sum as the output at port 4. S_{12} and S_{13} are both 1, meaning that if the signal at port 2 is 180^0 out of phase with the signal at port 3, a resultant null will be formed at port 1 and none of the signal energy will we directed to port 1. On the other hand, S_{42} and S_{43} are of opposite sign, resulting in the 180^0 out of phase signals from ports 2 and 3 adding constructively at port 4 and combining the signal energy of the two signals. Port 1 is terminated with a 50 ohm resistor, as is usually done with rat-race combiners, to dissipate the energy incident

on port 1 due to phase cancellation mismatch, that occurs as the operational frequency varies from the design frequency.

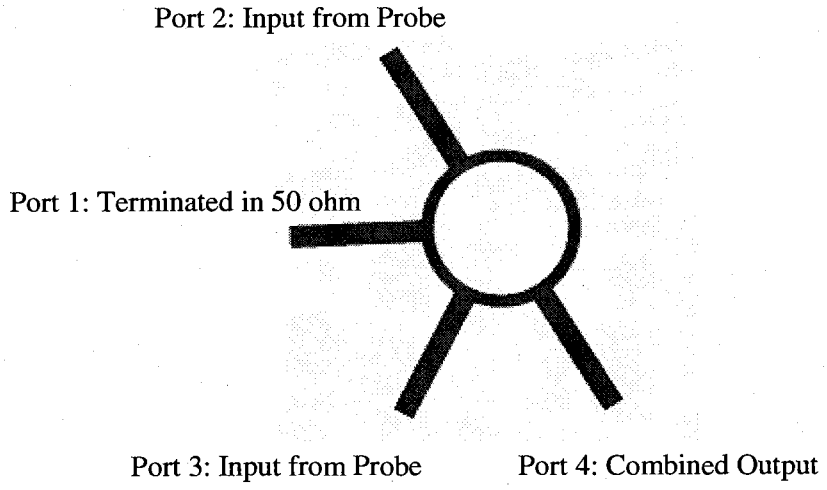

Figure 16: Rat-Race Combiner Microstrip Structure

The design of the rat-race combiner was performed by setting the characteristic impedance of the rat-race microstrip line to $\sqrt{2}$ times that of the microstrip lines feeding the combiner [16]. This structure was modeled in HFSS® and further optimized to center the response of the combiner across the operational Ku-band. Figure 17 shows the HFSS® results. Variation between S_{42} and S_{43} across the band of operation is less than 0.3 dB, which is acceptable in order to support the required power combining.

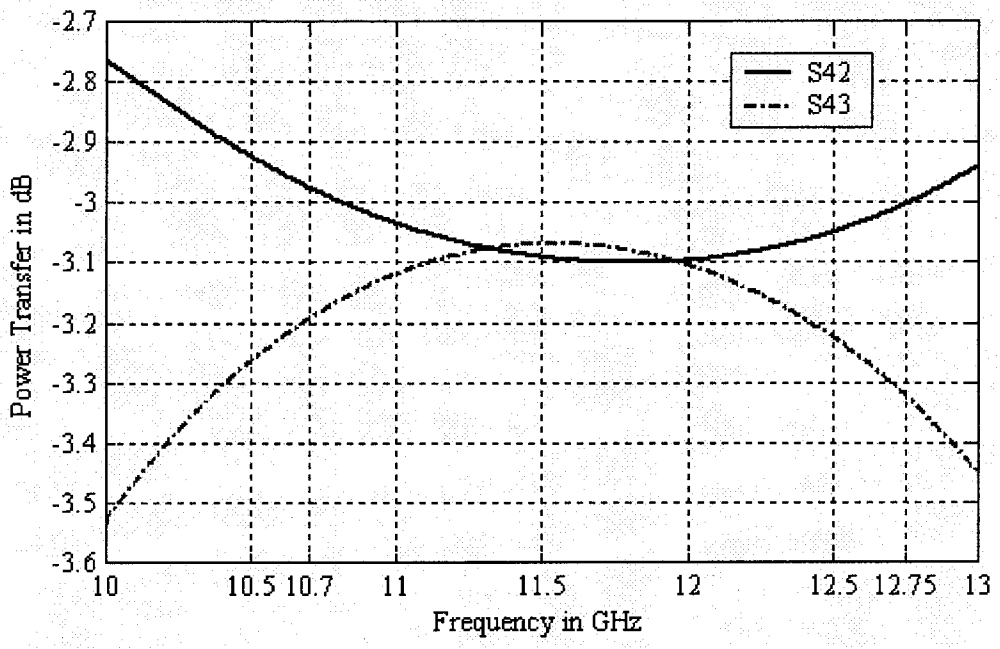

Figure 17: Rat-Race Combiner Power Splitting/Combining Response - HFSS®

8 Microstrip Connection and Matching Circuitry

Figure 18 shows a transparent view of the feed-multiplexer as in Figure 2, but with the microstrip structures added (only the metal tracks are shown, substrate boards are omitted). The rat-race combiners were discussed in the previous chapter; all that remains is to note that the combiners are centered on the respective symmetry axes of the feed-multiplexer, in order to have the microstrip circuitry that feeds the combiner from the respective probe pairs, symmetric. Apart from the microstrip combiners, the rest of the microstrip circuitry are impedance matching sections and 50 ohm lines that connect the probe outputs with the combiners, and the combiner outputs with the feed-multiplexer coaxial connectors [29]. Three matching sections are employed. One to improve the impedance match of the vertical polarization probe(s) to the 50 ohm connecting line(s), another to improve the impedance match of the horizontal polarization probe(s) to the waveguide coupling passage(s) and a final section for the optimization of the impedance match seen by the feed-multiplexer connectors. The ultimate component integration goal is for the feed-multiplexer to supply the two Ku-band polarization signals to the LNB circuitry located on the same substrate boards. The first stage of the LNB (Low Noise Block) is an LNA (Low Noise Amplifier) [28] and as such, matching done between the feed-multiplexer and the LNA will be to realize an optimum noise match for the LNA. An optimum noise match is most often very different from, and in conflict with, an optimum return loss match. Nonetheless, for the purposes of the thesis study, the matching circuits were designed to demonstrate the achievement of an acceptable return loss response that could be, if required, altered for a noise match.

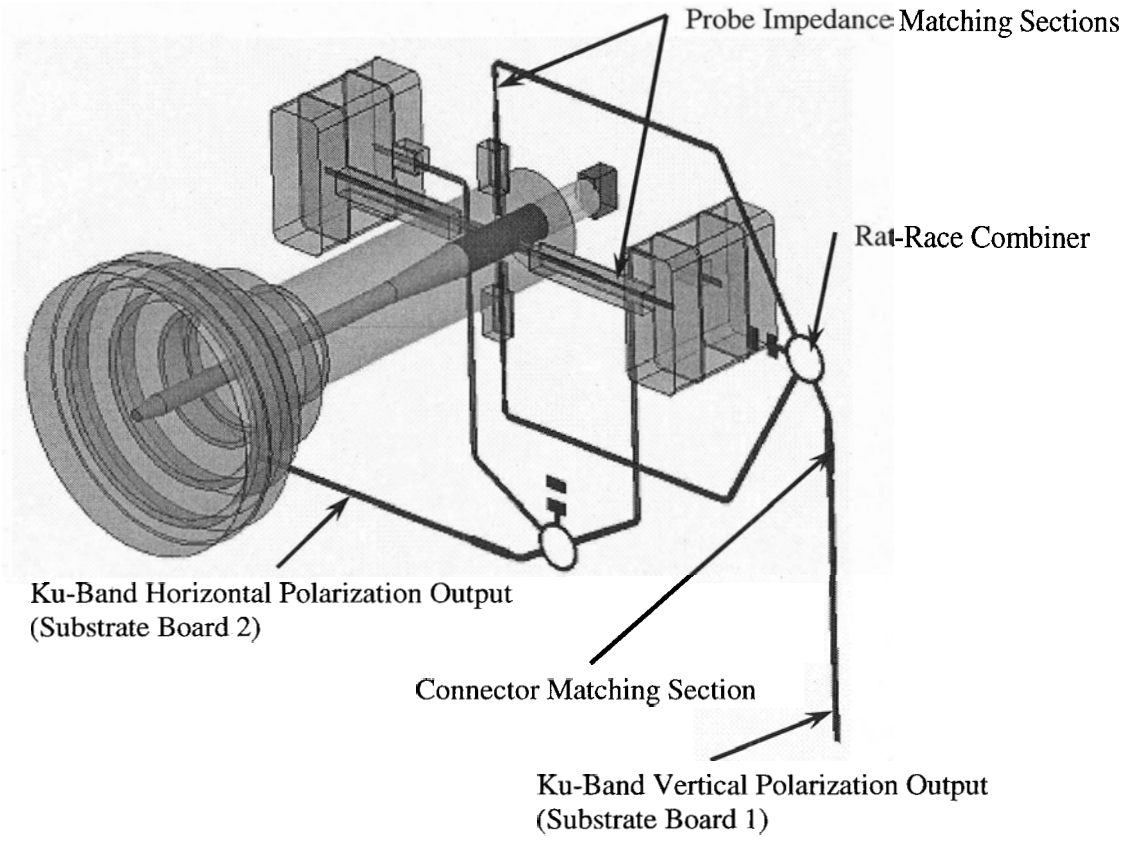

Figure 18: Feed-Multiplexer with Microstrip Structures

The matching section design was done by taking the s-parameter data from the HFSS® analyses of the feed-multiplexer, coupling passage and rat-race combiner and using these s-parameter files in the ADS (Advanced Design System)® circuit design software by Agilent®. Since the variation of the probe input impedance is over a wide frequency band (10.7 GHz to 12.75 GHz), an optimizer is required to perform a matching improvement over the entire band. ADS® has such an optimizer utility. Simple line section width and length variation [29], yielded the best wide band results. These sections are more than just quarter wavelength transformers, since both real and imaginary part impedance matching are required over the wide bandwidth. Matching sections similar to the probe impedance matching sections are employed for the connector matching sections. Figures 19 and 20 show the microstrip layouts for the two substrate boards of the feed-multiplexer. Figures 21 and 22 show the input return loss responses for the vertical and

horizontal polarization Ku-band outputs of the feed-multiplexer, as optimized and predicted by the ADS® software. Both have a response of better than 16 dB over the frequency band of interest.

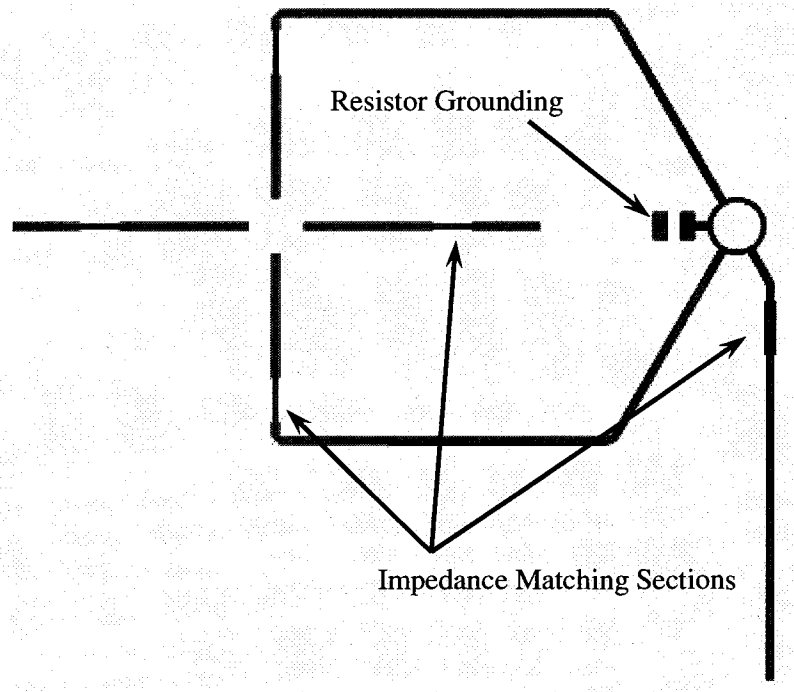

Figure 19: Substrate Board 1 Microstrip Circuitry

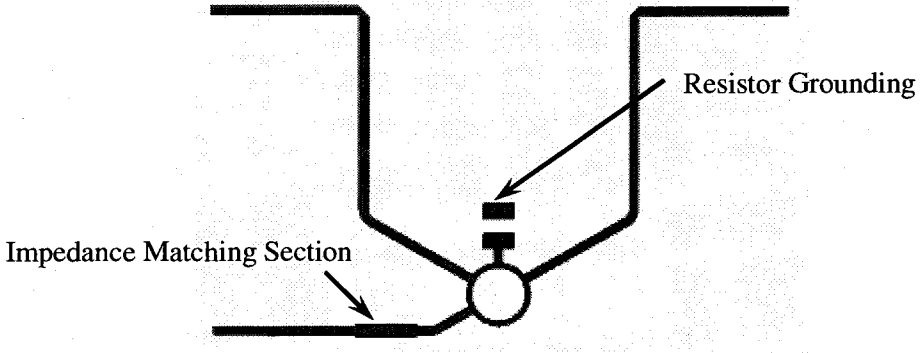

Figure 20: Substrate Board 2 Microstrip Circuitry

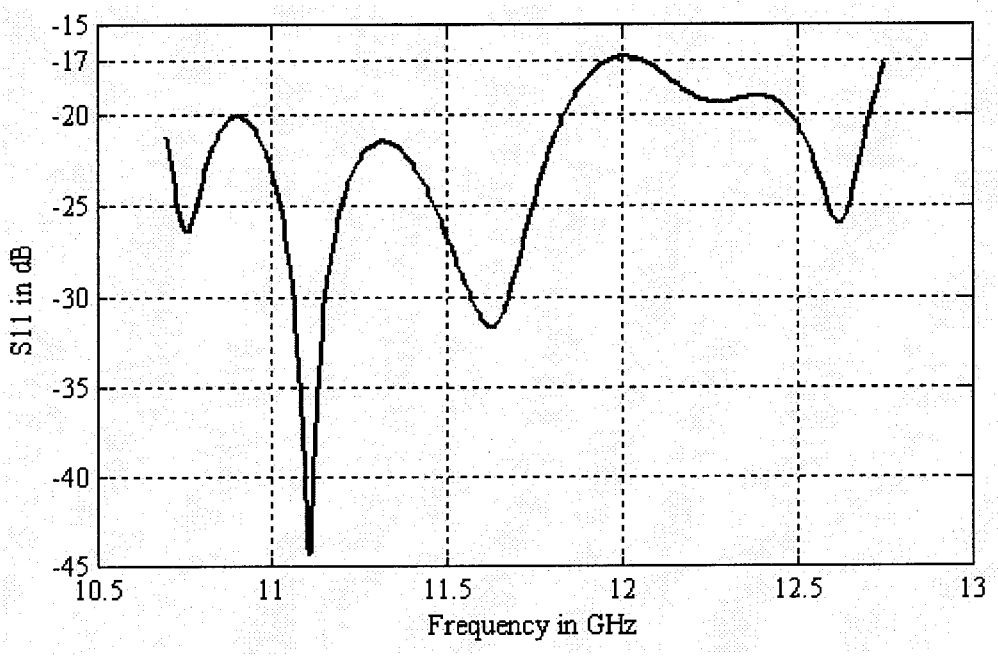

Figure 21: Feed-Multiplexer Vertical Polarization Ku-Band Return Loss - ADS®

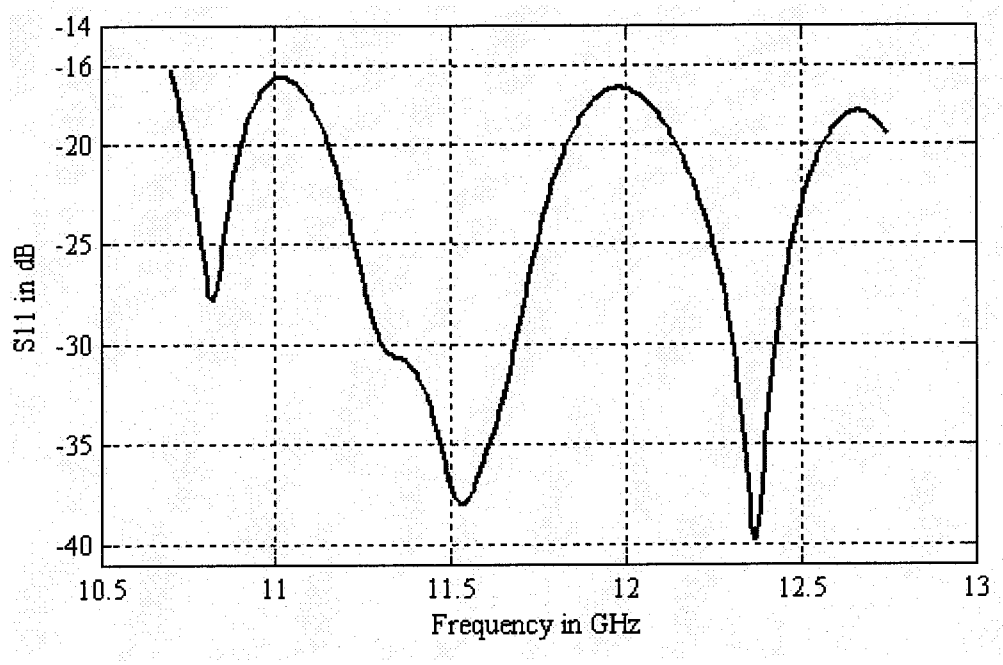

Figure 22: Feed-Multiplexer Horizontal Polarization Ku-Band Return Loss - ADS®

In Chapter 6, it was mentioned that the losses of the feed-multiplexer that attenuate the received signal detrimentally affect the signal to noise ratio of the receive chain of the SIT. As such, an indication of the dissipative losses incurred due to the use of the Ku-band probes as coupling structures and the accompanying use of rat-race combiners, would be a helpful criteria parameter for choosing this implementation within a SIT system. The system designer needs to weigh whether the losses incurred by this type of feed-multiplexer are acceptable with the specific noise performance of the LNA being used and that of the overall system application.

To obtain such an indication of the associated dissipative losses, the s-parameter files of the rat-race combiner and the rectangular waveguide coupling passages were included in back-to-back analyses of the two (vertical and horizontal polarization) receive circuits.
In effect, the microstrip circuitry in Figure 18 was untied at the feed-multiplexer outputs and mirrored to have a back-to-back symmetrical circuit. Analyses of these double circuits in ADS® were completed and the s-parameter data taken. To separate out the reflective losses (return loss) from the total insertion loss response, the total circuit return loss, at one of the two double circuit ports, was used in the power balance expression for a lossless two-port [16]:

$$|S_{11}|^2 + |S_{21}|^2 = 1 \qquad \textbf{(8-1)}$$

with

S_{11} - the total return loss

S_{21} - the insertion loss due reflection only

The insertion loss due to reflection losses only, so calculated, was subtracted from the total insertion loss of the double circuit and the resulting insertion loss value in dB, divided by two. Figures 23 and 24 show the calculated losses of the vertical and horizontal polarization circuits respectively. On average a loss of 1 dB with a possible worst case of 1.3 dB is indicated. This is not excessive for microstrip circuits and can be reduced if further development of the feed multiplexer for actual production shortens the microstrip line lengths.

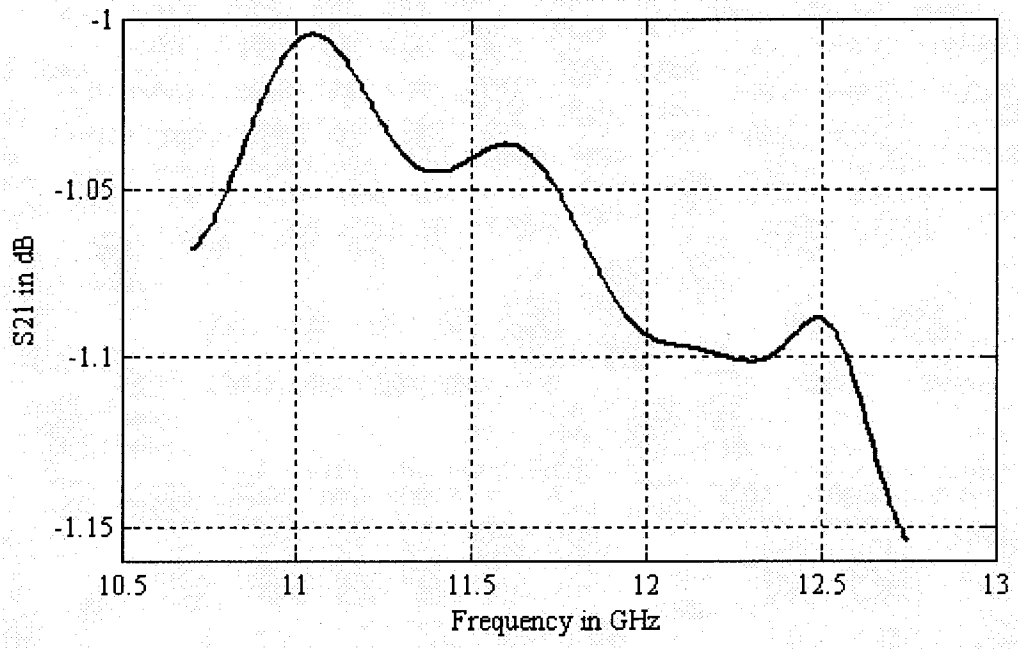

Figure 23: Vertical Polarization Ku-band Microstrip Structure Non-Reflective Insertion Loss - ADS®

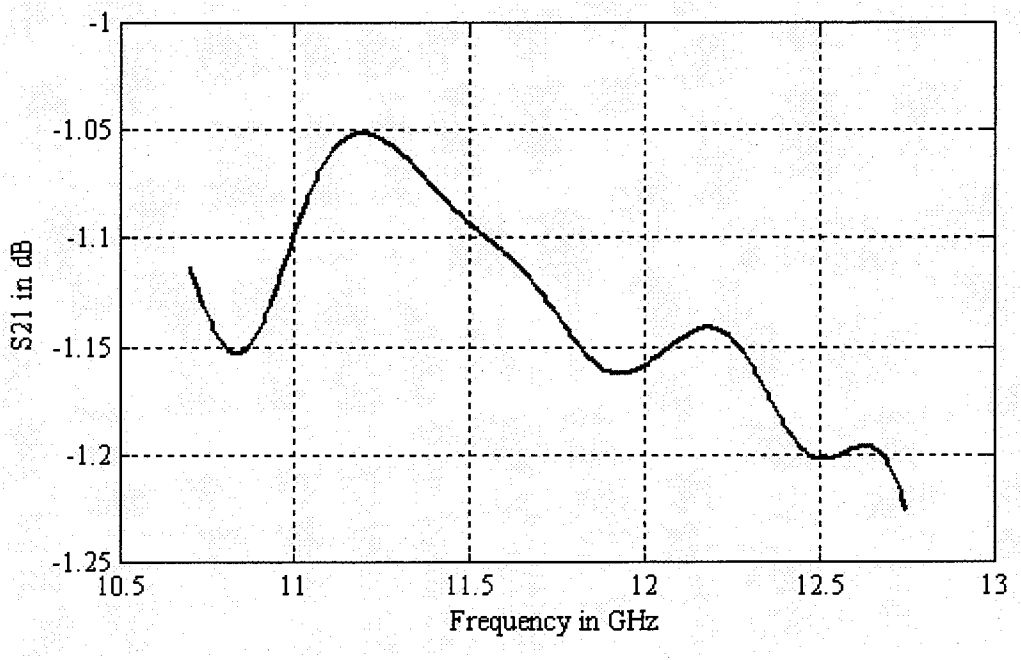

Figure 24: Horizontal Polarization Ku-band Microstrip Structure Non-Reflective Insertion Loss - ADS®

9 Ka-Band Input Structures

The design of the feed-multiplexer started in Chapter 2 with the design of the Ka-band dielectric rod antenna which determines the length and cross section diameters of the feed-multiplexer. Chapters 4 and 5 dealt with the Ku-band design of the probes and the coaxial waveguide section. It was mentioned in Chapter 4 that these structures also affect the Ka-band response. After the position and length of the Ku-band probes along with the initial length of coaxial waveguide section have been determined, the effect of these structures on both the frequency bands need to be evaluated with HFSS®. The length of the coaxial waveguide section can then be adapted to achieve the best response for both the Ka-and Ku-bands. Figure 25 shows the structures that play a role in the Ka-band input return loss response.

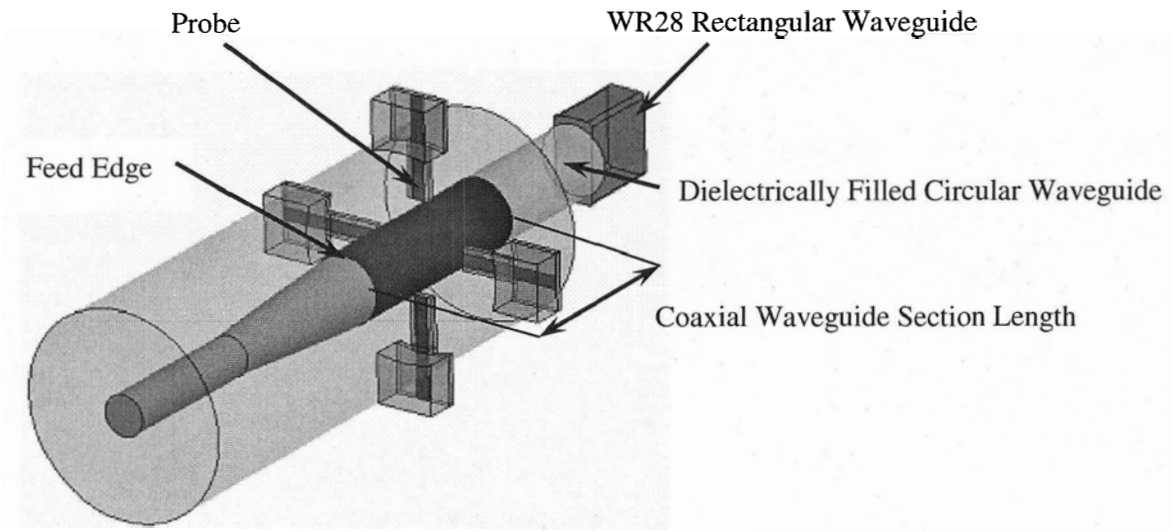

Figure 25: Structures Affecting Ka-Band Input Return Loss

In addition to the Ku-band probes and coaxial section length affecting the Ka-band return loss by interacting with the backward traveling portion of the radiated wave excited by the feed edge, as described in Chapter 2, the return loss is also affected by the discontinuity between the WR28 rectangular waveguide section and the dielectrically filled circular waveguide section. The parametric design for a good Ka-band return loss can be completed by Ka-band analysis, with HFSS®, of a quarter structure of the complete feed-multiplexer. First the WR28 waveguide section is omitted and the Ka-band return loss, as seen into the dielectrically filled circular waveguide, is optimized by the adjustment of the length of the coaxial waveguide section. Once a good response is obtained, the extra discontinuity added by the transition to WR28 waveguide can be added, with a resultant worsening of the return loss response. The response is improved by the optimization of the length of the dielectrically filled circular waveguide section between the feed-multiplexer main body and the WR28 rectangular waveguide. If the optimization of the response proves difficult, a final resort is to reduce the length of the Ka-band dielectric rod. This also means the reduction of the entire feed-multiplexer length. If improvement is obtained by this reduction in length, the radiation characteristics of the feed-multiplexer and the Ku-band return loss response need to be re-evaluated to ensure proper operation. Indeed, as mentioned in Chapter 10, the length of the dielectric rod and total feed-multiplexer needed to be optimized to obtain the best cross polar radiation response. Following this procedure a final return loss of better than 15 dB across the Ka-band (29.5 GHz to 30 GHz) was obtained, with the length of the coaxial waveguide section 18 mm, the dielectrically filled circular waveguide section length 12 mm and reductions of the dielectric rod and total feed-multiplexer lengths as stated in Chapter 10. Figure 26 shows the response obtained from HFSS®.

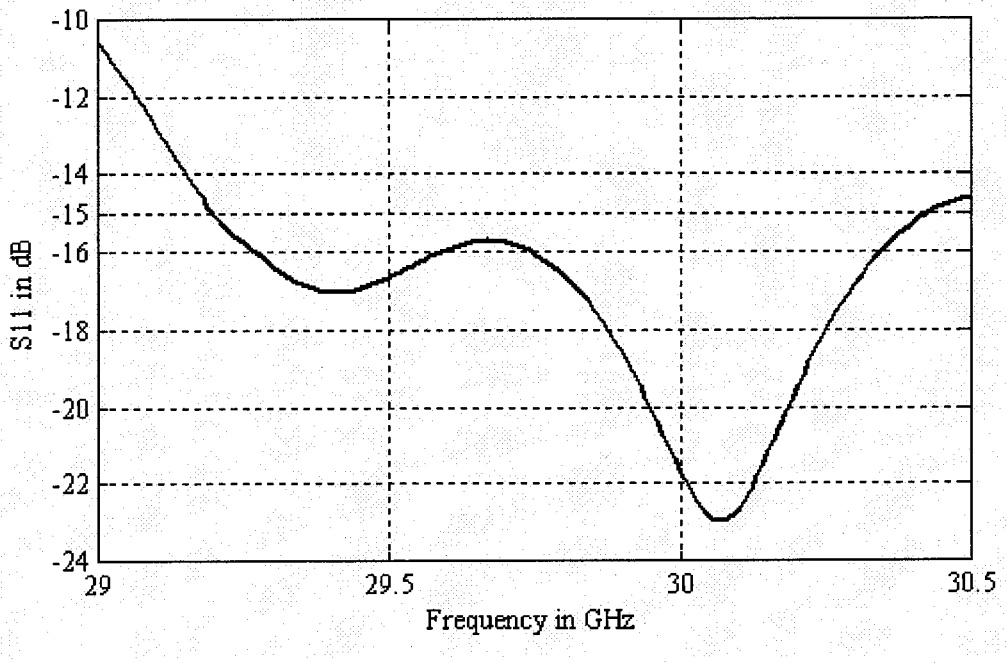

Figure 26: Ka-Band Feed-Multiplexer Input Return Loss - HFSS®

10 Radiation Characteristics

Beyond the multiplexing of the two frequency bands and the two polarizations of each band, the primary task of the feed-multiplexer is to effectively illuminate the dish reflector. Of great importance for dual band systems is the cross polar response [15], [30] of this illumination. The cross polar response of the feed-multiplexer radiation pattern plays a significant role in the cross polar response of the entire reflector dish antenna. If the cross polar response is deficient, unacceptable energy loss from one polarization will occur into the orthogonal polarization, resulting in insufficient isolation between the two channels of communication, respectively assigned to each of the polarizations. Typically, a good cross polar efficiency [15], [31] is obtained if the feed-multiplexer radiation pattern is symmetrical in the E-and H-planes [15], [32] and the E-and H-plane radiation phase centers are sufficiently co-located [15], [31].

The movement of the phase center with frequency also affects the phase efficiency [15] of the reflector antenna. Phase efficiency is a measure of the phase uniformity of the illuminating beam at the reflector antenna. Practically it is related to whether the feed-multiplexer is located with its phase center at the focal point of the reflector. Since the feed-multiplexer phase center moves with varying frequency, the integration of the feed-multiplexer with a reflector antenna requires that the feed be positioned at an optimum position to achieve the best antenna response over the frequency bands of interest. To this end, the phase center of the feed-multiplexer not only need to be co-located for the E-and H-plane patterns at a certain frequency, but also needs to be within a reasonable range of co-location over varied frequency in order for proper operation, with the reflector dish, to be possible over the frequency band of interest.

In addition to the issues mentioned above, the illumination and spillover efficiencies [15], [32] of the reflector antenna are also affected by the feed-multiplexer. These are optimized by allowing the feed-multiplexer radiation pattern main beam to have a smooth

taper across the illuminated reflector dish, such that the illumination has tapered down approximately 10 dB from the main beam peak value at the edge of the reflector. The focal distance is the distance from the center of the reflector to the focal point of the reflector. This introduces the concept of focal distance to reflector diameter ratio (f/d) [15], [32]. Implicit in the f/d ratio of a reflector antenna is the illumination half angle. This angle away from the axis of the reflector antenna at the focal point, defines the angle from the axis at which the dish edge is located [32]. Consequently, a feed-multiplexer illuminating the reflector has to be designed to have a beam that has tapered down to approximately 10 dB at an angle equal to the illumination half angle of the reflector. For an f/d of 0.6, as required in Table 2, an illumination half angle of 39.81^0 results.

10.1 Ku-Band Radiation

Figure 27 shows a cross section of the metal horn that serves as the radiation structure for the Ku-band. As mentioned in the introduction, this horn is taken from a pre-existing design, courtesy of NORSAT® Intl. Inc. . The horn is a coaxial ring corrugated horn. As the development of horns for reflector antennas unfolded, the requirement of having horns with symmetric radiation patterns with low cross polarization led to the development of corrugated horns. These horns have aperture hybrid mode fields similar to the aperture fields of a reflector dish at the dish focal point [15]. Although corrugated horns exhibit excellent performance, the corrugations are perpendicular to the flared horn metal wall. This make them difficult to manufacture and, as such, not a good choice for medium to low cost applications. Pursuant investigations into coaxial ring corrugated horns, revealed that the cylindrical hybrid mode field of a reflector dish can also be realized by these structures [15]. As can be seen in Figure 27, the corrugations of the horn are coaxial to the main waveguide of the horn. This characteristic lends itself to less demanding manufacturing processes. Casting, for instance, is a viable option for coaxial ring corrugated horns but difficult for regular corrugated horns.

The design of the horn used in this thesis was done by investigation and optimization of the structure by means of a full wave solver software package. Finally a variable prototype was constructed that had the ability to move the coaxial rings in relation to one other and the main waveguide section of the horn. This prototype was used in further optimization of the horn during measurement of the response on an antenna measuring range.

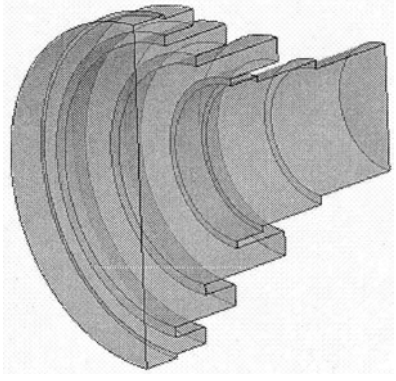

Figure 27: Cross Section of the Feed-Multiplexer Ku-Band Metal Horn, Showing the Coaxial Ring Corrugations

In order to investigate the effects of the integration of the horn into the feed-multiplexer, a series of simulations was performed by the author in HFSS®. The radiation pattern results of this investigation are shown in Figures 28 to 30. The simulations were performed at 12.75 GHz. As is customary [15], [31], the E-plane gain, H-plane gain and 45^0-plane cross polarization radiation plots are shown. Figure 28 shows the result for the coaxial corrugated horn without the dielectric rod loading the metal horn. The response in Figure 29 has the dielectric rod included, but the mode excitation was set up in HFSS® as an ideal waveguide port, i.e. the mode excitation was not done with the Ku-band probes. In Figure 30, the probes and coaxial waveguide section are included in the analysis. This represents the full proposed design. The results show that negligible variation occurs with the addition of the dielectric rod, as expected from the design considerations in Chapter 3. The addition of the coaxial section and probe excitation also do not interfere with the radiation pattern response, showing that the correct modal excitation is achieved with the use of the probes.

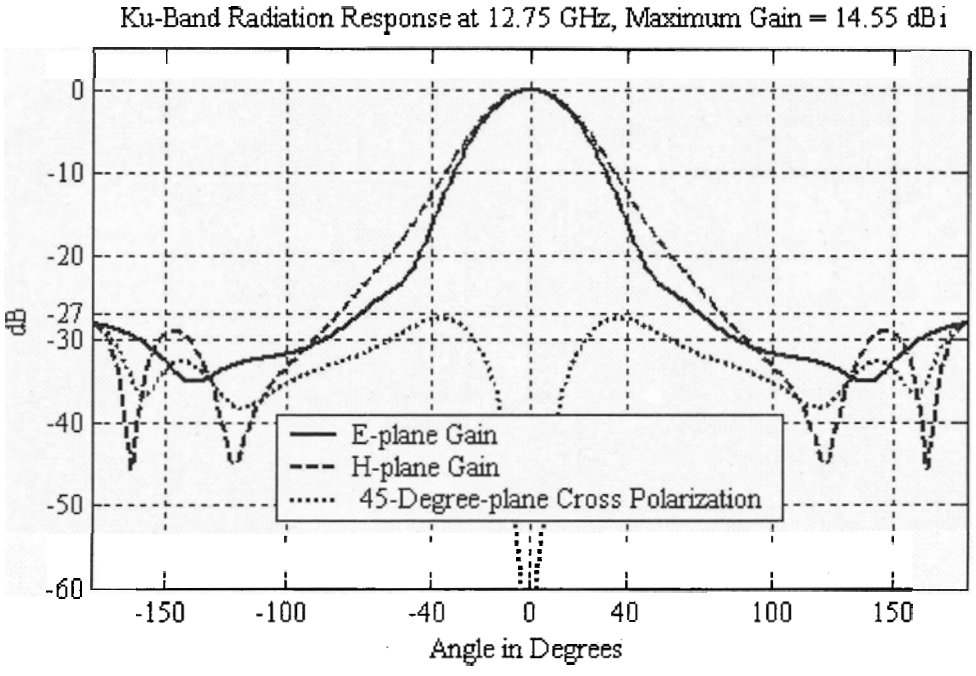

Figure 28: Radiation Patterns of the Coaxial Ring Corrugated Horn at 12.75 GHz, Without the Dielectric Rod or Probe Excitation - HFSS®

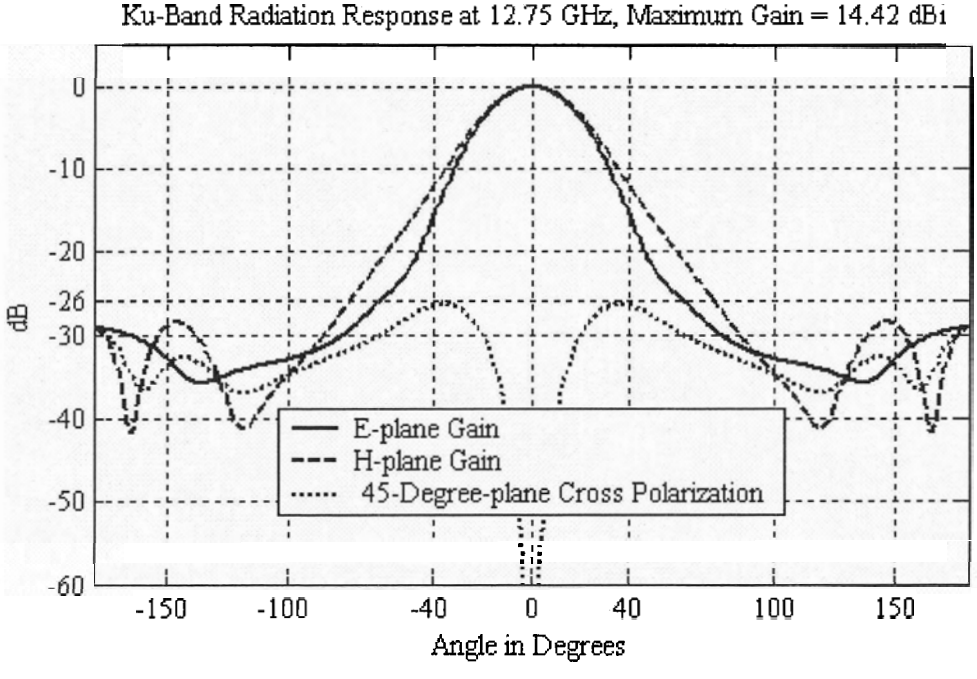

Figure 29: Radiation Patterns of the Coaxial Ring Corrugated Horn at 12.75 GHz, With the Dielectric Rod but without Probe Excitation - HFSS®

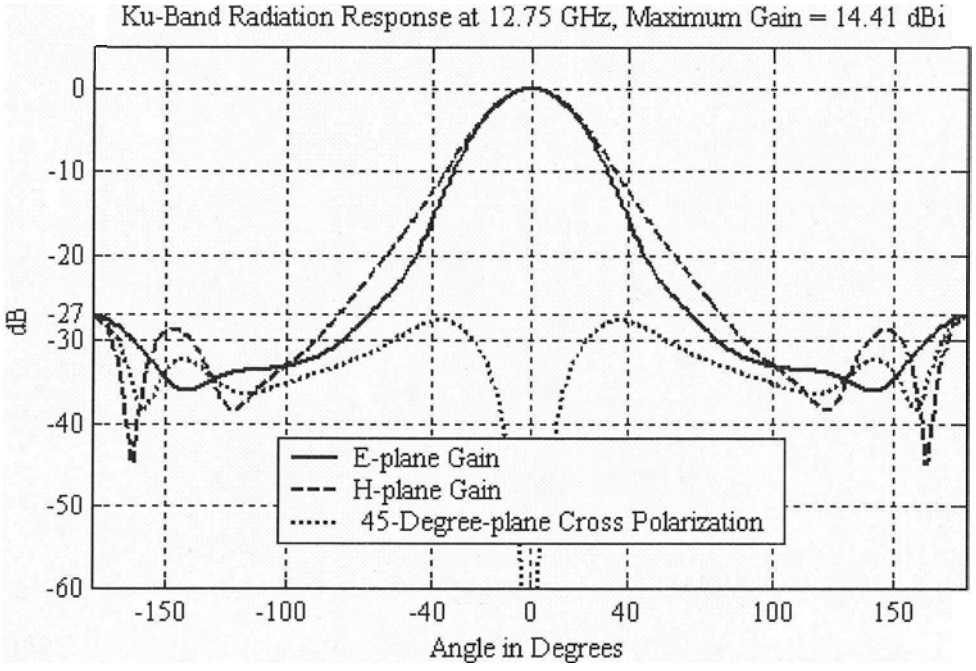

Figure 30: Radiation Patterns of the Coaxial Ring Corrugated Horn at 12.75 GHz, With both the Dielectric Rod and Probe Excitation Included - HFSS®

Figures 30 to 32 show the simulated radiation results for the feed-multiplexer at high, mid band and low frequencies of the Ku-band. Cross polar isolation of better than 27 dB is achieved. This is well within the target specification listed in Table 2. Minimum boresight gain is 12.85 dB, again compliant with Table 2. Good beam symmetry is shown for 10.7 GHz and 11.75 GHz. Although not as good as at the other two frequencies, the beam symmetry at 12.75 GHz is acceptable across the illumination angle of approximately plus and minus 40^0 (f/d =0.6). All responses exhibit a good gain pattern taper that is approximately 10 dB down at plus and minus 40^0, as is required for the use of the feed-multiplexer in a reflector antenna system with an f/d ratio of 0.6. The simulated Ku-band radiation response of the feed-multiplexer is therefore compliant with Table 2 and exhibits good stability across the relatively wide Ku-band of use.

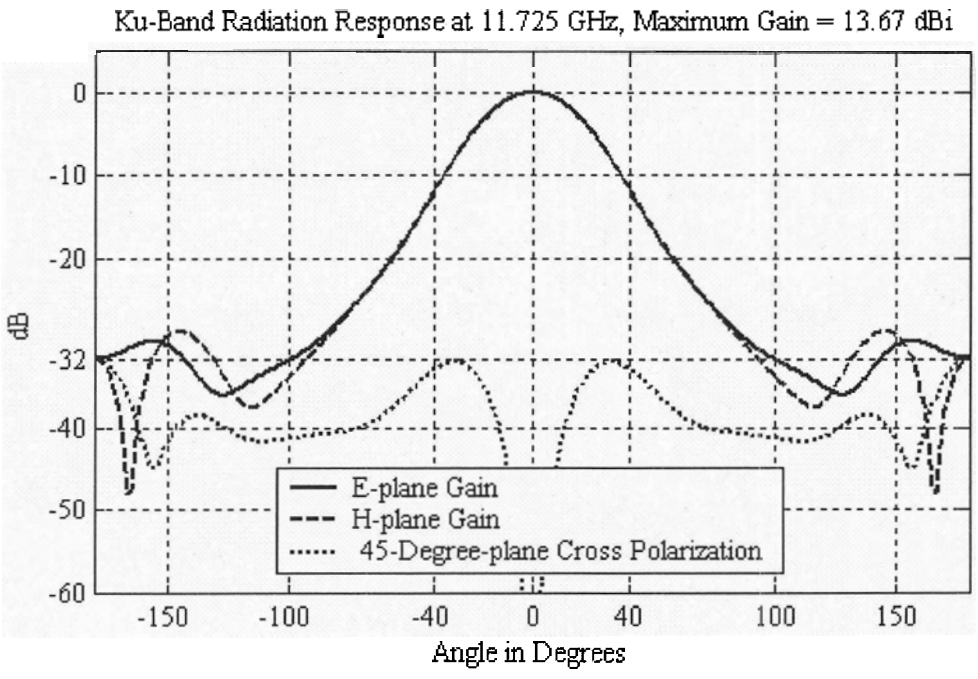

Figure 31: Radiation Patterns of the Coaxial Ring Corrugated Horn at 11.725 GHz, With both the Dielectric Rod and Probe Excitation Included - HFSS®

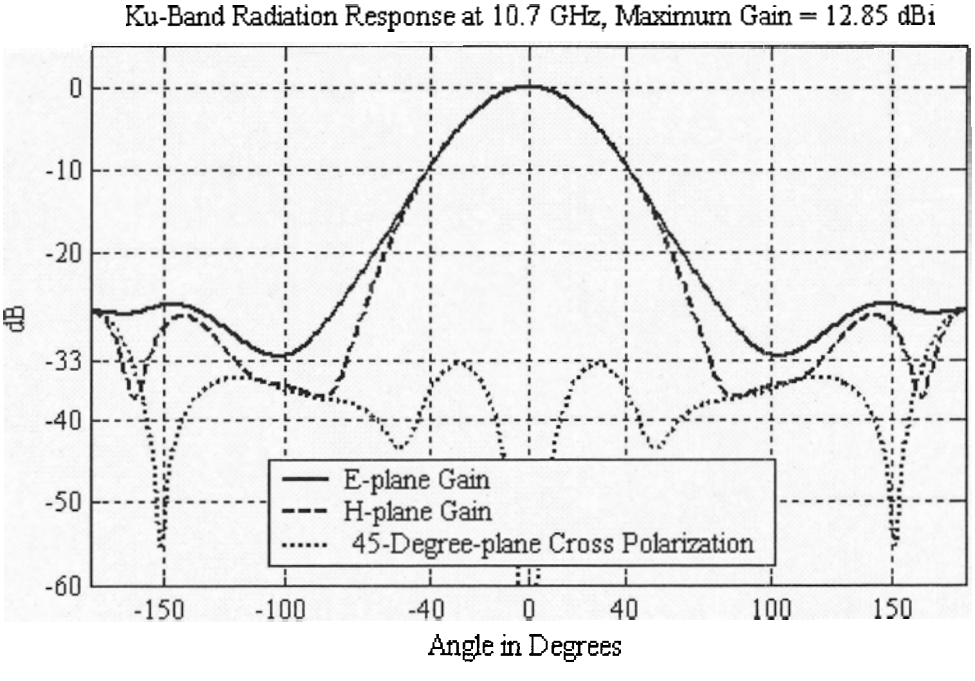

Figure 32: Radiation Patterns of the Coaxial Ring Corrugated Horn at 10.7 GHz, With both the Dielectric Rod and Probe Excitation Included - HFSS®

10.2 Ka-Band Radiation

The dielectric rod radiator is the predominant structure for the Ka-band radiation. The design of the dielectric rod was discussed, in depth, in Chapter 2. The integration of the rod into the full feed-multiplexer structure does, however, affect the Ka-band radiation characteristics. The surrounding metal horn at the aperture of the feed-multiplexer, the added backshort at the back of the Ku-band coaxial waveguide section and the addition of the Ku-band substrate carried probes, play a role in the formation of the Ka-band aperture fields and therefore affect the Ka-band radiation response. The length of the feed-multiplexer is determined by the length of the dielectric rod design in Chapter 2. Since the Ka-band radiation response is affected by the integration of the dielectric rod into the feed-multiplexer, a final optimization of the feed-multiplexer length is needed to obtain the best radiation response for the Ka-band. This was done by performing analyses of the full feed-multiplexer quarter structure in HFSS®. Finally the total feed-multiplexer length was reduced by 3 mm from the length obtained in Chapter 2 and the dielectric rod length was reduced by 5 mm, positioning the rod termination 2 mm inside the metal horn aperture.

Figures 33 to 36 show the radiation pattern results of analyses performed as part of the parametric study, performed with HFSS®, to investigate the effects of the introduction of the various feed-multiplexer structures to the original stand alone dielectric rod antenna, designed in Chapter 2. The results shown are at 30 GHz. Figure 33 shows the response of the dielectric rod as a stand alone antenna without the surrounding structures of the feed-multiplexer. Excellent beam symmetry and cross polarization is obtained, consistent with HE_{11} hybrid mode radiation of the dielectric rod. Beam taper is well formed but the 10 dB attenuation level from the 18.84 dB maximum gain is at a half angle of only 20^0.

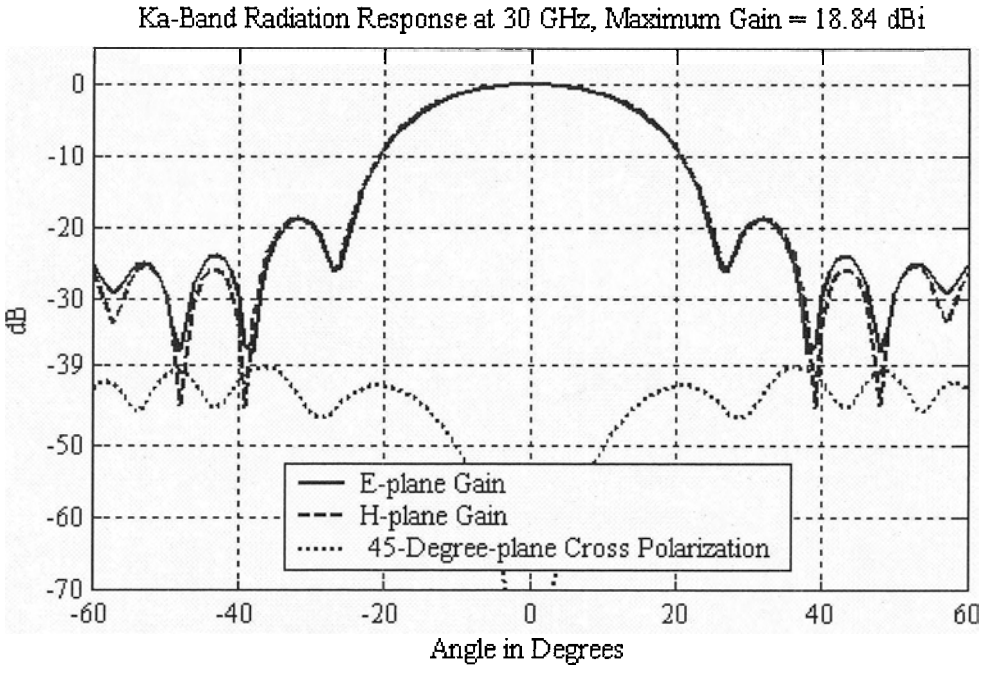

Figure 33: Radiation Patterns of the Dielectric Rod at 30 GHz, Without the Surrounding Ku-Band Metal Feed Horn Structure - HFSS®

Figure 34 shows the radiation response with the dielectric rod inserted into the metal feed-multiplexer structure, but without the Ku-band probes protruding into the structure. A widening of the beam occurs to a 10 dB taper attenuation half angle of 26^0. With the rod surrounded by the feed-multiplexer metal structure, the metal horn diameter determines the cross sectional geometry of the radiation aperture and therefore determines the beam width of not only the Ku-band radiation, but also the Ka-band radiation. Beam symmetry deteriorates but is still acceptable, especially over the 10 dB taper of the beam. Correspondingly, cross polarization deteriorates, but is still within the 20 dB specification of Table 2. Not only the introduction of the metal structure around the termination of the rod, where radiation of the HE_{11} hybrid mode occurs, worsens the beam symmetry and cross polarization. The affect of the backshort of the Ku-band coaxial waveguide section in the feed-multiplexer on the backward traveling portion of the radiated Ka-band wave, excited at the feed edge of the dielectric rod, also worsens the radiation response. As was mentioned in Chapter 2, the radiation from the dielectric rod can be viewed as the superposition of two propagating waves. I.E., the HE_{11} mode

propagating along the dielectric rod and radiating at the rod termination, and the radiated Ka-band wave generated at the feed edge of the dielectric rod. The length of the stand alone dielectric rod antenna is designed to have these two components in correct phase relation to each other for the best radiation response. Propagating inside the feed-multiplexer, the backward traveling portion of the radiated wave is reflected by the backshort of the Ku-band coaxial waveguide section and will, therefore, propagate forward in the feed-multiplexer and affect the field superposition at the rod termination and so also the final field distribution at the feed-multiplexer horn aperture. This fact is demonstrated by the result shown in Figure 35. The same structure as that for Figure 34 was analyzed, but in this case the backshort wall of the Ku-band coaxial section was assigned as an ideal wave port in HFSS®. This port absorbs the backward traveling radiated Ka-band wave and so eliminates its affect on the aperture fields. As can be seen in the figure, beam symmetry is improved and so too the cross-polarization which is better by approximately 3 dB.

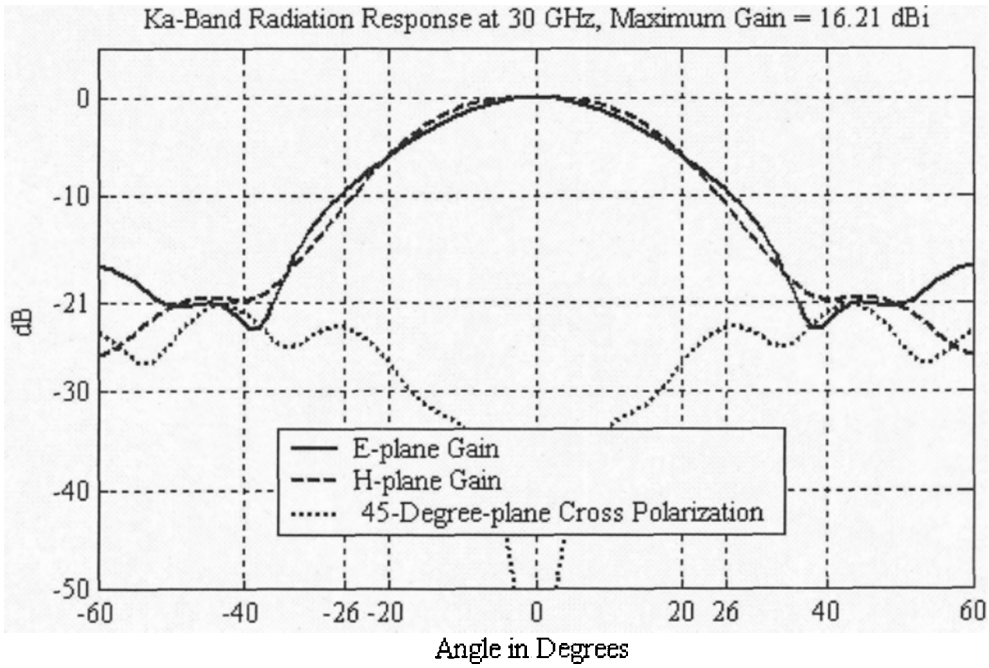

Figure 34: Radiation Patterns of the Dielectric Rod at 30 GHz, Including the Surrounding Ku-Band Metal Feed Horn Structure, but excluding the Ku-Band Probes - HFSS®

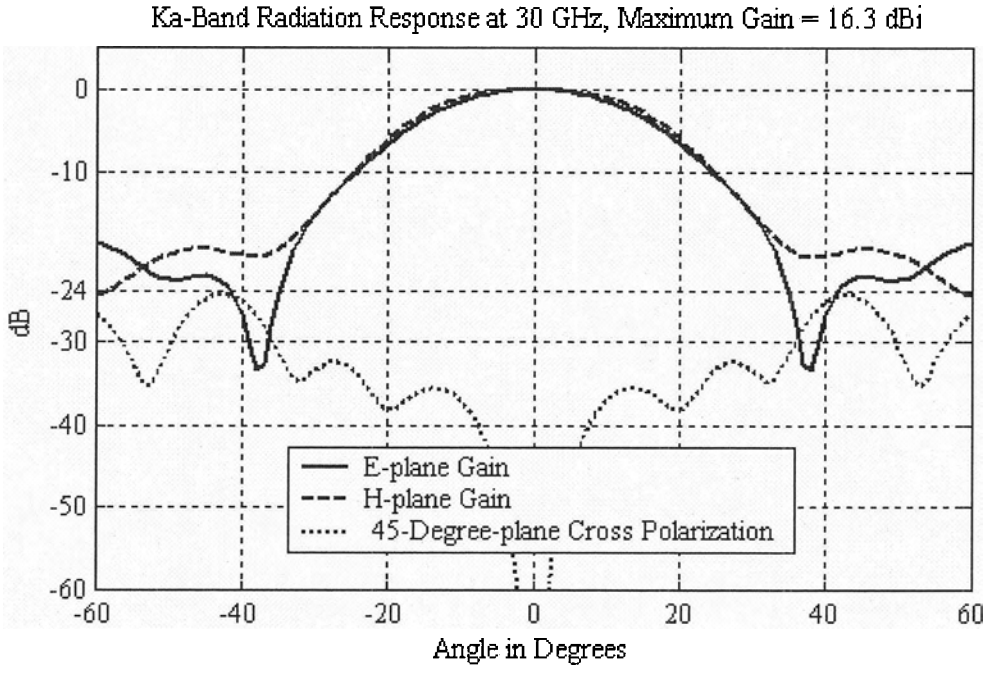

Figure 35: Radiation Patterns of the Dielectric Rod at 30 GHz (with the Coaxial Waveguide Section Backshort Assigned as a Signal Port), Including the Surrounding Ku-Band Metal Feed Horn Structure, but excluding the Ku-Band Probes - HFSS®

Results in Figure 36 has the Ku-band probes included and represents the full feed-multiplexer structure. The response is similar to that without the probes. Beam shape is affected, however, especially in the E-plane. Beam symmetry is still acceptable but the cross polarization is slightly worse and marginal compared to the 20 dB specification in Table 2. This slight deterioration can be ascribed to the interaction of the probes with the backward traveling radiated Ka-band wave as mentioned above, that affects the radiation response in a similar fashion as the interaction of the wave with the backshort of Ku-band coaxial waveguide section. What is important to note, is that the effect of the backshort of the feed-multiplexer structure is far more severe than the effect of the Ku-band probes protruding into the structure. This means that the introduction of the probes as coupling structures for the Ku-band in the feed-multiplexer does not severely deteriorate the radiation response of a feed-multiplexer utilizing a Ku-band backshort and, as such, are a valid alternative to waveguide sidewall slots for Ku-band coupling.

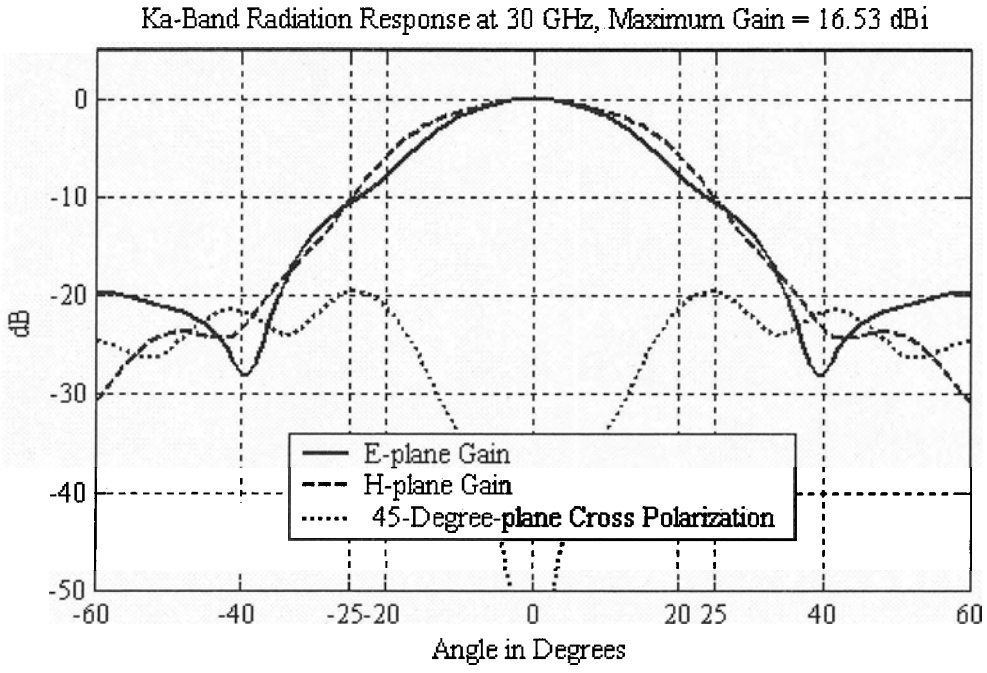

Figure 36: Ka-Band Radiation Patterns at 30 GHz, Full Structure - HFSS®

Figures 37 and 38 show the radiation response at the low and mid band frequencies of the Ka-band of operation. Beam shape is acceptable even though beam symmetry is marginal. This is offset by the fact that the cross polarization is better than at 30 GHz and convincingly within the 20 dB specification of Table 2. Across the Ka-band the 10 dB beam taper half angle is approximately 25^0 to 26^0. This corresponds to an f/d ratio of 1.025 as opposed to the required ratio of 0.6. Although this deviation from the optimum beam taper in the Ka-band will reduce the aperture efficiency of the dish antenna, the correct functioning of the dish antenna will not be affected. The difference in Ku-band and Ka-band beam widths is a direct result of the fact that the bands share the same metal horn aperture for radiation. This is a physical necessity in this type of dual band feed [11], [12], [13], [14]. For the same aperture, the beam of the higher frequency will be narrower than that of the lower frequency. Regardless, the dual band feed can still be used to good effect.

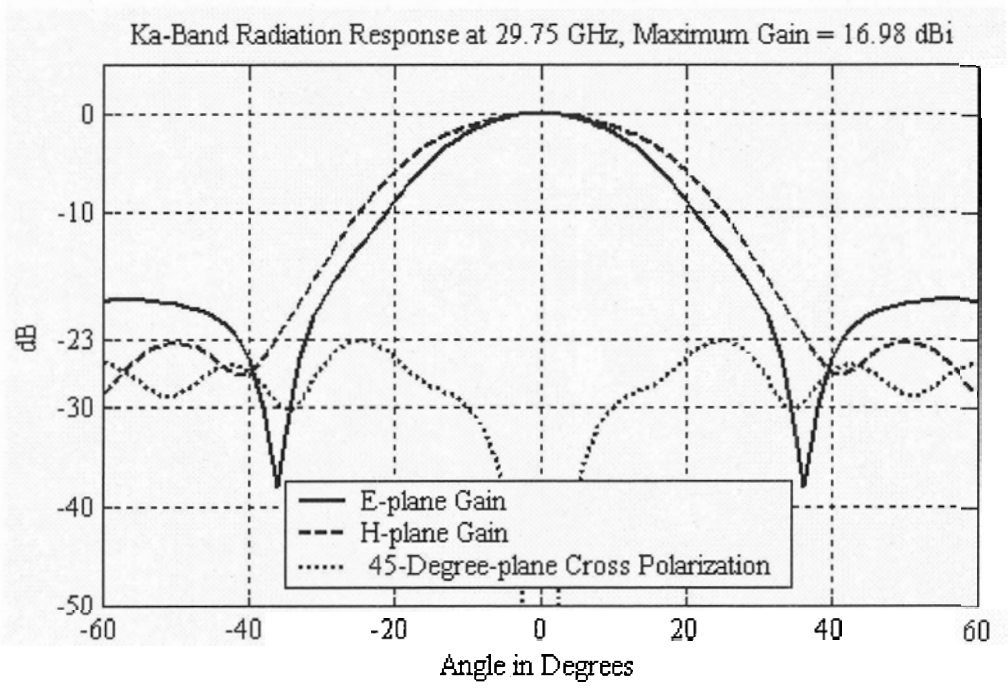

Figure 37: Ka-Band Radiation Patterns at 29.75 GHz, Full Structure - HFSS®

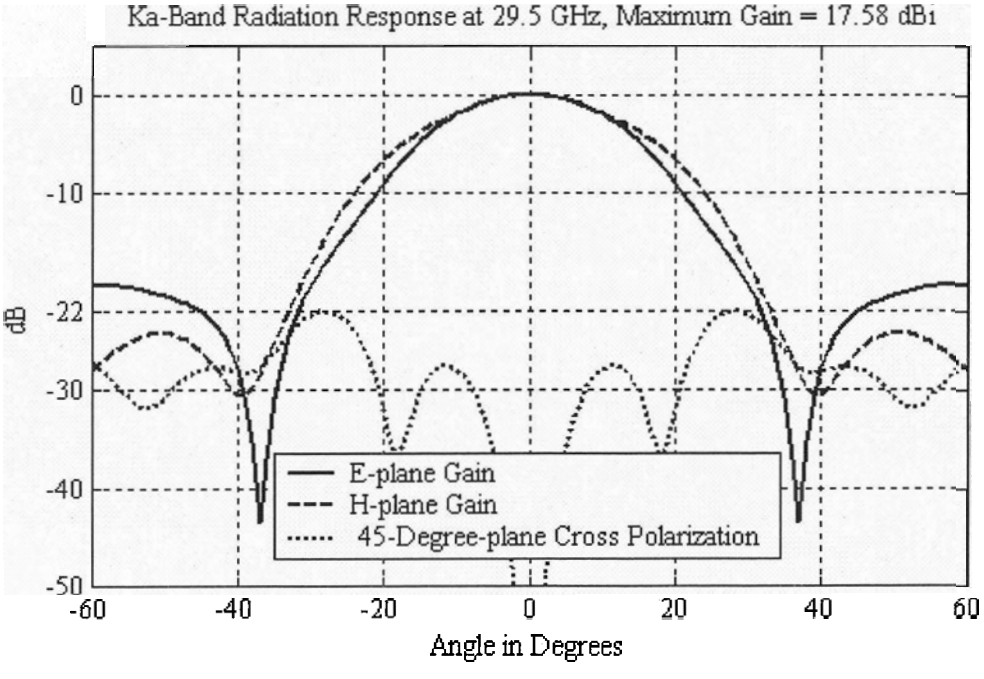

Figure 38: Ka-Band Radiation Patterns at 29.5 GHz, Full Structure - HFSS®

In both the Ka- and Ku-band the radiation pattern characteristics as predicted by the HFSS® simulations are acceptable. Unlike earlier versions of the software, the current version of HFSS® does not give the phase of the radiation field as an output. Without this phase data the phase center of the feed-multiplexer can not be investigated. The favorable radiation pattern results do indicate, though, that in both the bands the E-plane and H-plane phase centers are sufficiently co-located. Without such a co-location, proper radiation pattern results can not be obtained [15]. The only remaining unknown, in the absence of radiation field phase data, is the location of the phase center for the different frequencies and whether an optimized position can be found for which the phase variation in the radiated field, over the illumination angle at the dish reflector, will be acceptable over both the frequency bands. This can only be determined by the measurement of the radiated field pattern phase variation and/or the integration and optimization of the feed-multiplexer with a reflector dish, utilizing the measurement of the complete antenna system radiation response over frequency.

11 Prototype Manufacturing

The focus of this thesis is the use of substrate carried coupling probes as part of a dual-band, dual-polarization, feed-multiplexer implementation and specifically whether this implementation can be made to operate satisfactorily with regards to multiplexer and radiation response. The focus is on the electromagnetic design and operation of the feed-multiplexer; an exhaustive study of manufacturing possibilities, tolerance and yield issues is outside the scope of this thesis. Nevertheless, the realization of a prototype for performance verification calls for at least a brief overview of the mechanical and fabrication techniques used, especially since the realization of the probes on the same substrate board as the surrounding circuitry necessitates a cross sectional cut of the Ku-band circular waveguide to allow for the probe insertion. This implies a physical housing of the feed-multiplexer comprised of, at minimum, a two section sandwich structure.

In addition to the requirement for a sandwich structure, the use of thin copper foil to form the metal center structure of the coaxial waveguide section, requires that the copper foil be adjoined to the rest of the metal structure in such a manner as to allow ohmic conduction, in order for the coaxial waveguide section to function properly. If soldering is to be used to make this connection, the metal immediately surrounding the copper foil at the backshort of the coaxial waveguide section needs to be made of a compatible metal. These two issues were the major factors imposed by the design on the physical implementation.

Figure 39 shows a front and back view of the complete prototype. The Ku-band horn is attached to a rectangular main housing body, which is shown with the two coaxial connectors for the two Ku-band polarization circuits, as well as with the Ka-band WR28 rotation plate at the back of the main housing body, for changing the Ka-band polarization. The main body housing comprises three sandwiched sections. The main section that carries the substrate boards is shown in Figure 40. The remaining two

sections are shown in Figure 41. On the left is the top-plate that forms the front lid of the main body housing to which the Ku-band horn is attached. As can be seen in the figure, the top-plate also has a square protrusion that forms the probe channels and completes the Ku-band circular waveguide by direct metal attachment to the adjoining base-plate section. Similarly, the back-plate has a protrusion that adjoins the base-plate and forms the backshort of the coaxial waveguide section in the feed-multiplexer. The back-plate is shown with the dielectric rod inserted, as it is the back-plate that supports the dielectric rod. The protrusion of the back-plate is made, for the prototype, out of copper in order to ensure proper soldering contact between the backshort metal of the coaxial waveguide section and the copper foil wrapped around the dielectric rod, to form the center structure of the coaxial waveguide section. The critical issue, with the use of a sandwich structure and the copper foil, is proper ohmic contact between the various metal sections of the feed-multiplexer. Without this, the current distributions of the waveguide sections involved may be disturbed and so detrimentally affect the operation of the feed-multiplexer. The favorable measured results obtained, as set out in Chapter 12, show however, that correct operation was realized with the manufactured prototype.

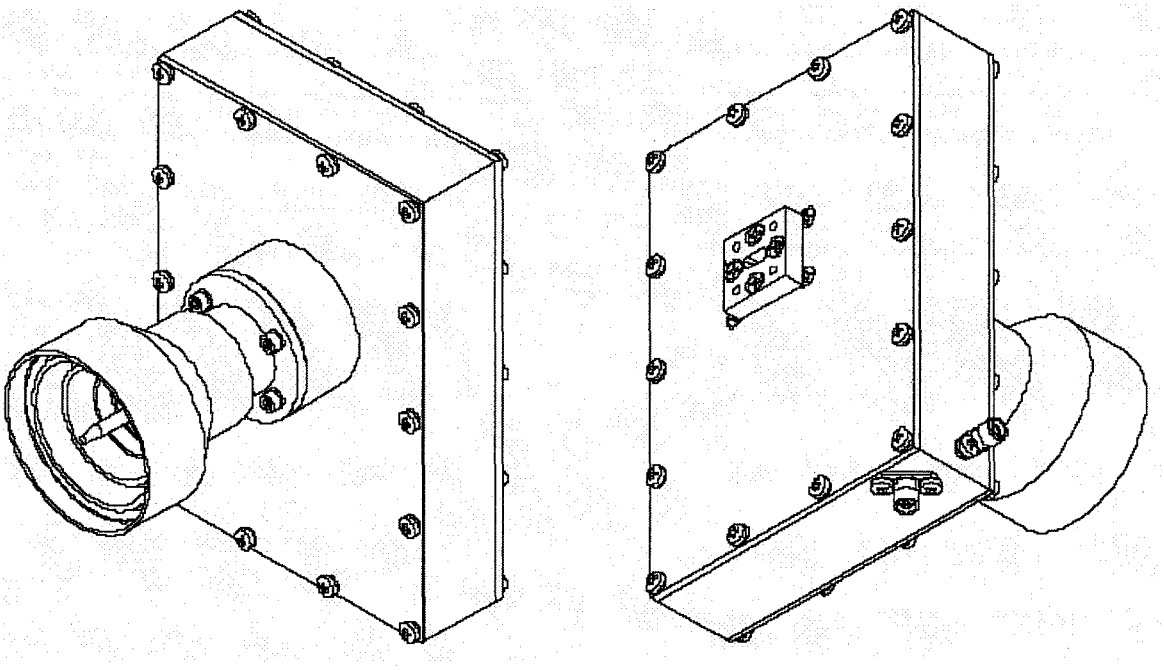

Figure 39: Front and Back View of the Complete Feed-Multiplexer Prototype

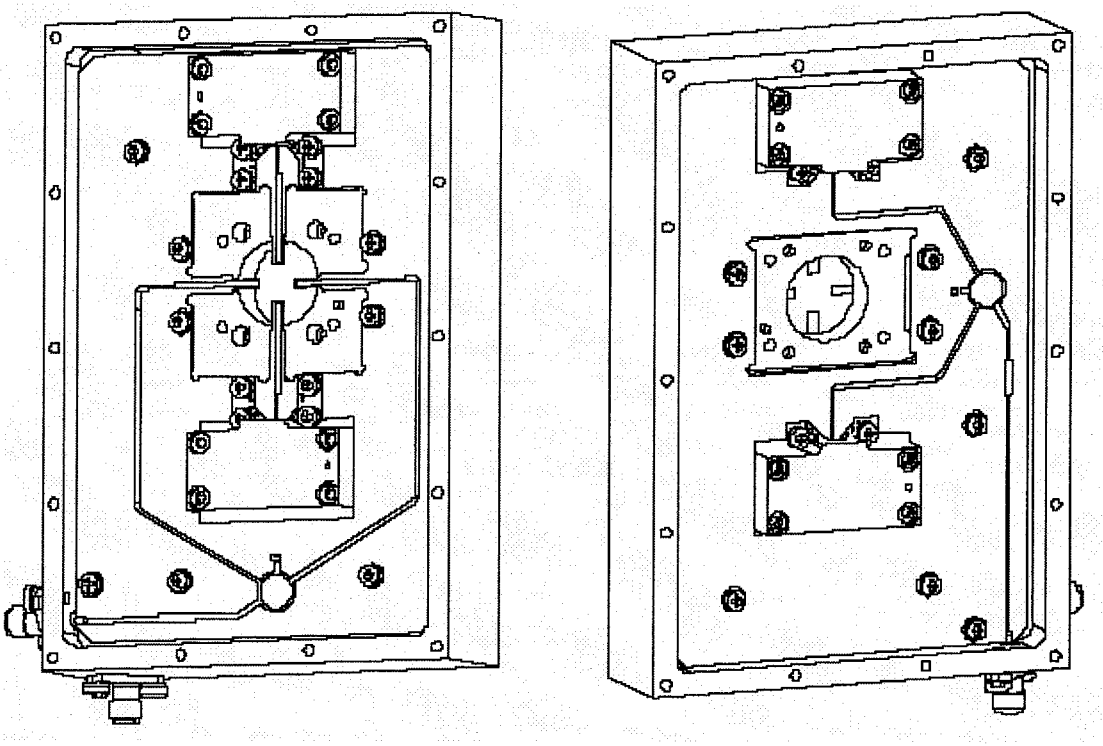

Figure 40: Front and Back of the Base-Plate with Substrate Boards and Connectors.

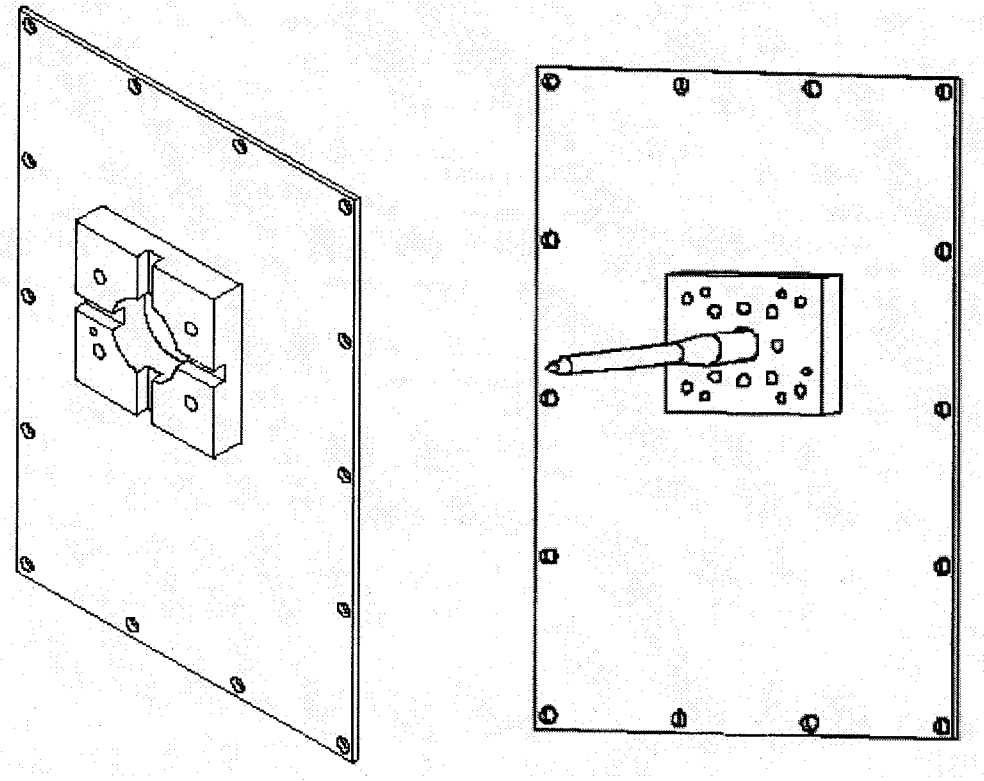

Figure 41: Top-Plate (Left) and Back-Plate Sections.

Manufacturing tolerances were specified at (+/- 0.003") or (+/- 0.0762 mm), which from experience with the various parametric studies of the feed-multiplexer, is satisfactory. One exception to this tolerance specification is the length of the coaxial waveguide section, since, for the prototype, this section is formed by manual application of the copper tape to the dielectric rod. A greater variance may consequently occur than with the machined parts of the feed-multiplexer. To investigate the possible change in response, analysis was performed with HFSS® on the design structure with the coaxial center metal shortened by 1 mm. Figures 42 and 43 show the resultant return loss response for the two Ku-band polarization channels. Although changed from the responses in Figures 21 and 22, leaving the parameter un-optimized, both responses are still acceptable. Figure 44 shows the resultant radiation response at 12.75 GHz. The predicted cross polarization is worse than that of Figure 30, but the response is still acceptable.

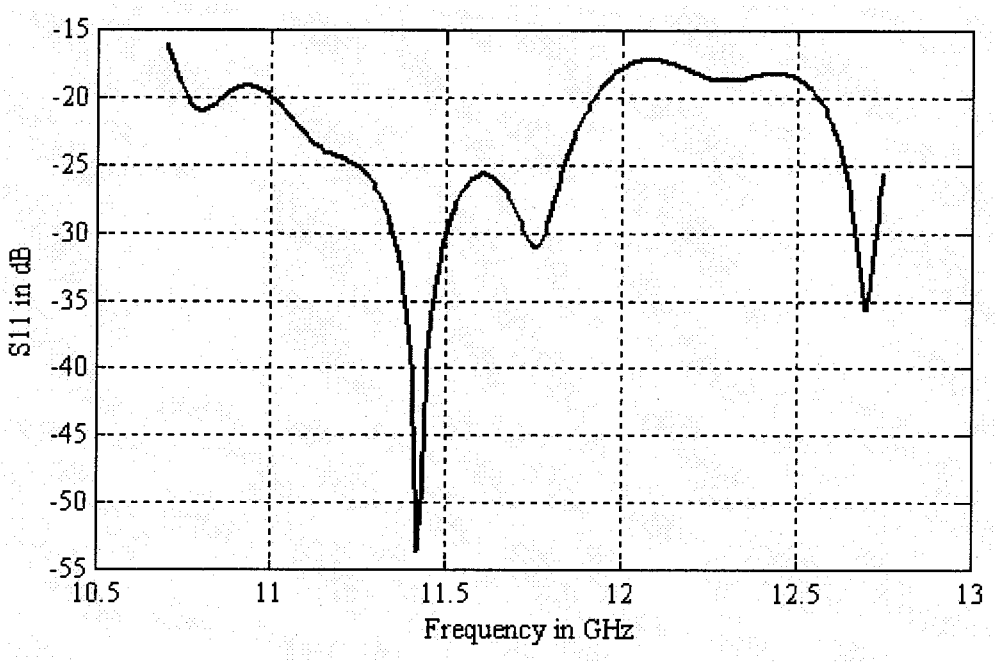

Figure 42: Vertical Polarization Ku-Band Return Loss with the Coaxial Waveguide Section Shortened by 1 mm - ADS®.

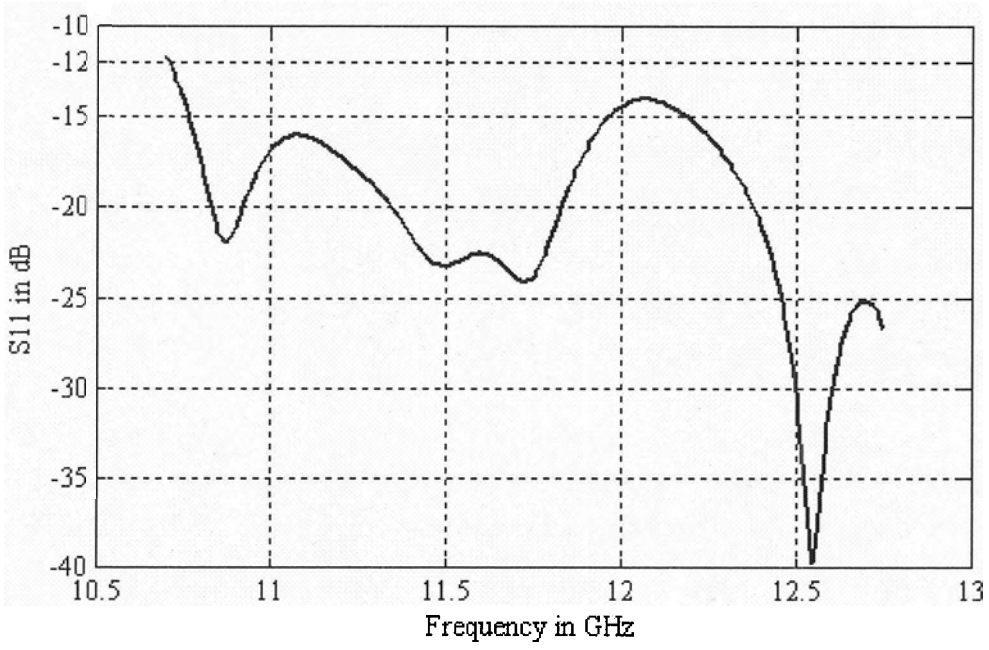

Figure 43: Horizontal Polarization Ku-Band Return Loss with the Coaxial Waveguide Section Shortened by 1 mm - ADS®.

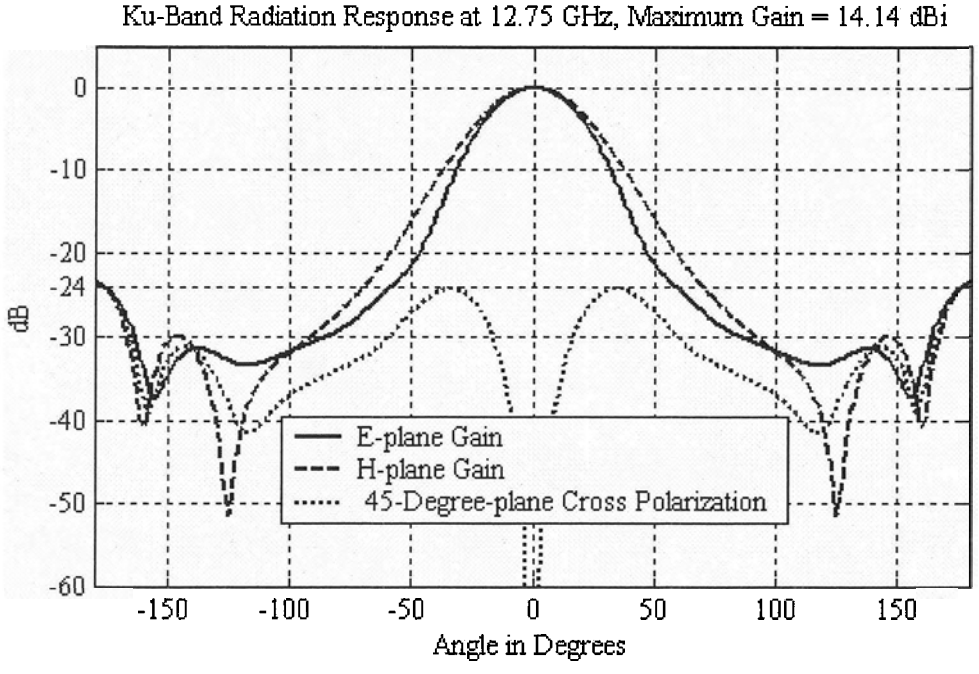

Figure 44: Feed-Multiplexer Radiation Response at 12.75 GHz with the Coaxial Waveguide Section Shortened by 1 mm - HFSS®.

Figure 45 shows the resultant Ka-band return loss response. The response has worsened compared to that in Figure 26, but it is still acceptable across the band. Figure 46 shows the radiation response with the shortened coaxial waveguide section at 30 GHz. The cross polarization is improved over that of Figure 36 and so is the accompanying pattern symmetry. It follows from these analyses that the design tolerance for variation in the coaxial waveguide section length is robust enough to withstand at least 1 mm of error in the assembly.

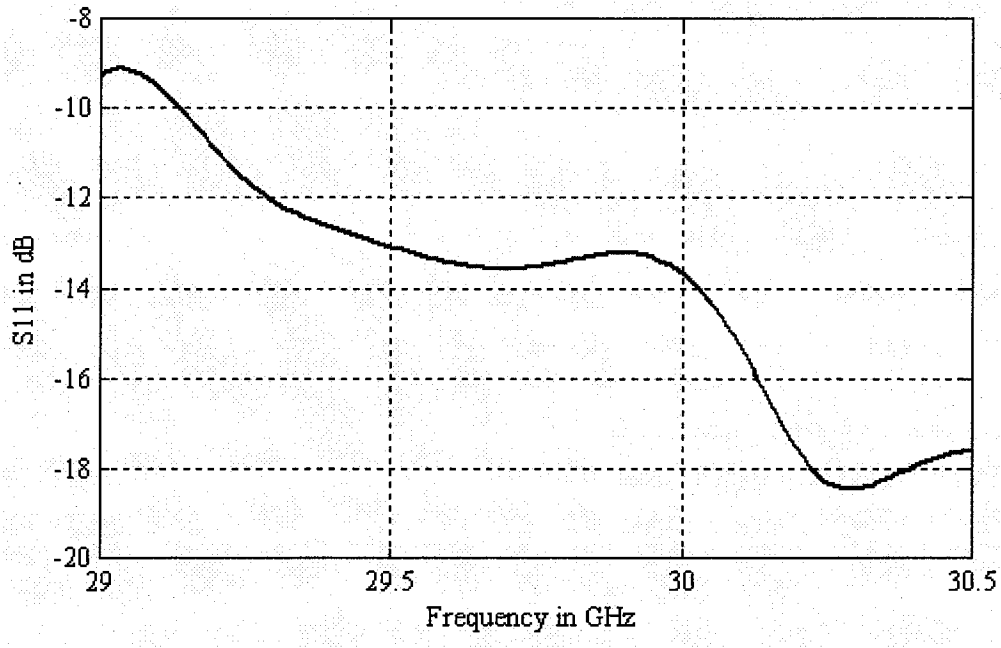

Figure 45: Ka-Band Return Loss with the Coaxial Waveguide Section Shortened by 1 mm - HFSS®.

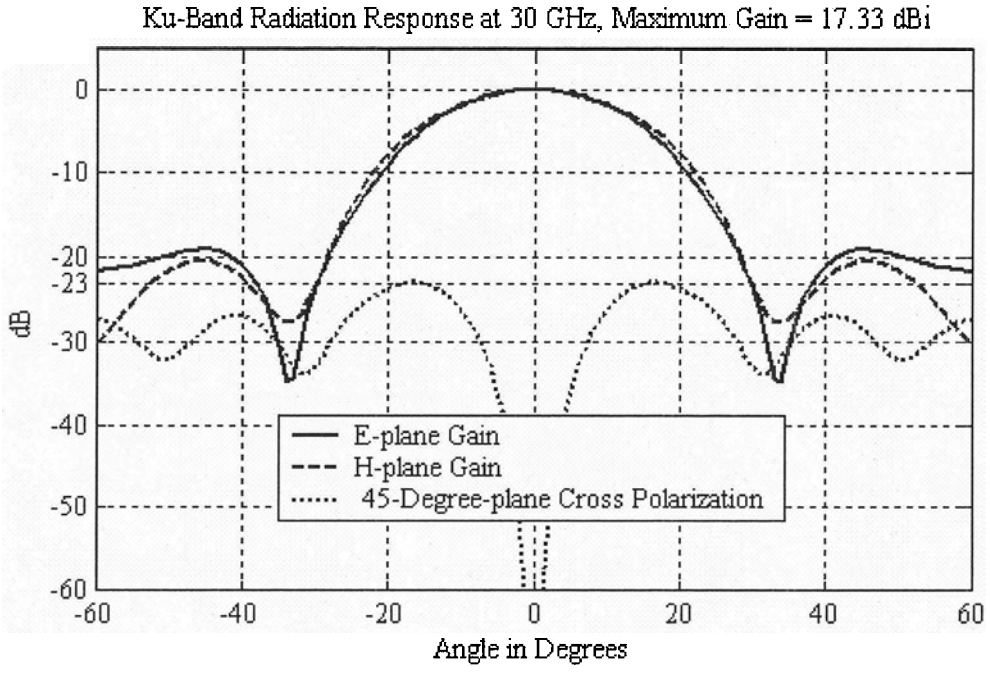

Figure 46: Feed-Multiplexer Radiation Response at 30 GHz with the Coaxial Waveguide Section Shortened by 1 mm - HFSS®.

12 Measured Results

The measured results for the feed-multiplexer prototype, manufactured as set out in Chapter 11, are presented in this chapter. The Ku-and Ka-Band S-parameter results are presented as well as the Ku-band radiation patterns. The S-parameter results were obtained by measurement on a VNA (vector network analyzer) [33]. An Anritsu 37397C VNA was used. For this VNA the measurement uncertainty at the frequencies and power levels measured, is specified as being approximately 0.8 dB for reflection measurements and 0.2 dB for transmission measurements. The Ku-band radiation pattern measurements were done in an anechoic chamber. Facilities for the measurement of the Ka-band radiation patterns were not available. Figures 47 and 48 show front and side views of the manufactured prototype that was measured. A Canadian quarter coin is included for size comparison.

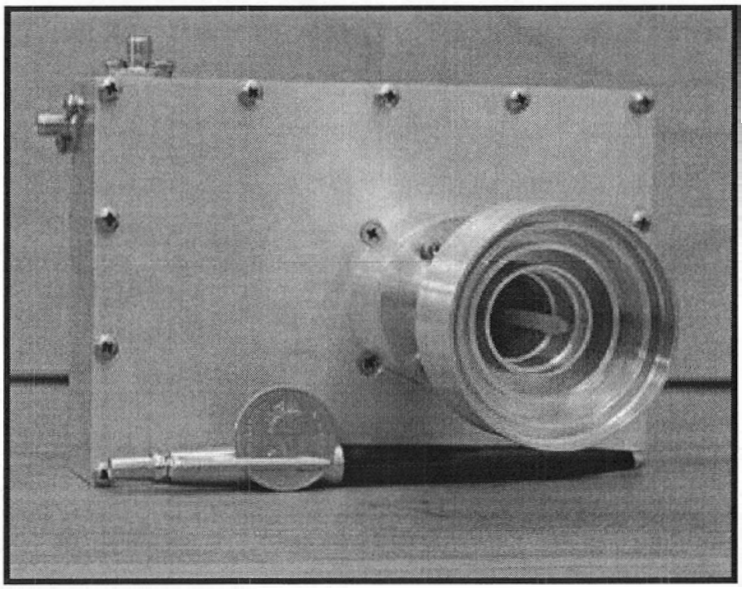

Figure 47: Front View of the Feed-Multiplexer Prototype.

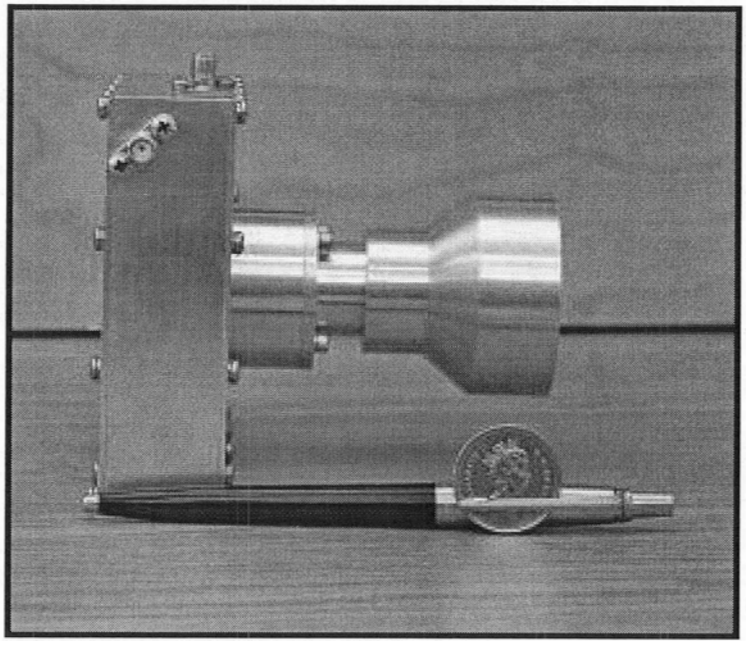

Figure 48: Side View of the Feed-Multiplexer Prototype.

12.1 Ku-Band S-Parameter Results

Figures 49 and 50 show the return loss response for the vertical and horizontal polarization ports of the feed-multiplexer. Figure 18 in Chapter 8 shows the location of these ports. Both the simulated responses obtained in Chapter 8 (Figures 21 and 22) and the measured responses are shown. Since the prototype feed-multiplexer had SMA type coaxial connectors on the respective ports, in order to interface with the test cables of the VNA, the effects of these connectors on the measured response had to be de-embedded [25] to see the response that would load surrounding microstrip circuitry in an integrated component. This was done by simulating the microstrip to coaxial connector transition in HFSS® and using the resulting S-parameters of the transition to compute the Z-parameter equivalent T-circuit [16] of the transition. The Z-parameter T-circuit was de-embedded from the total measured load (calculated from the measured S_{11} value) of the applicable port in order to obtain the required response.

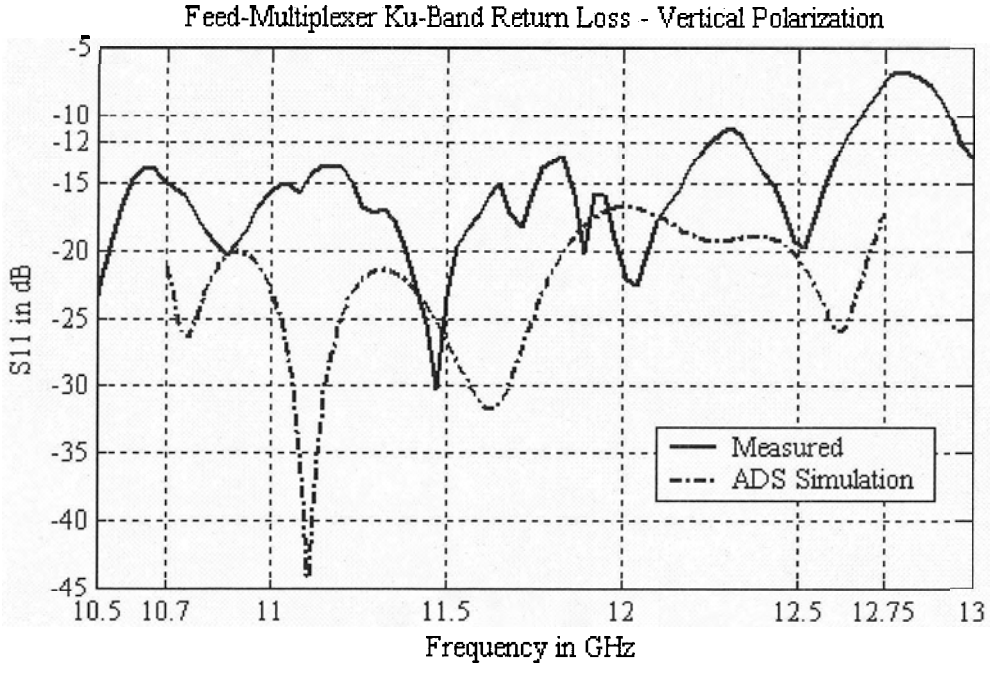

Figure 49: Ku-Band Vertical Polarization Port, Measured and Simulated Return Loss Response.

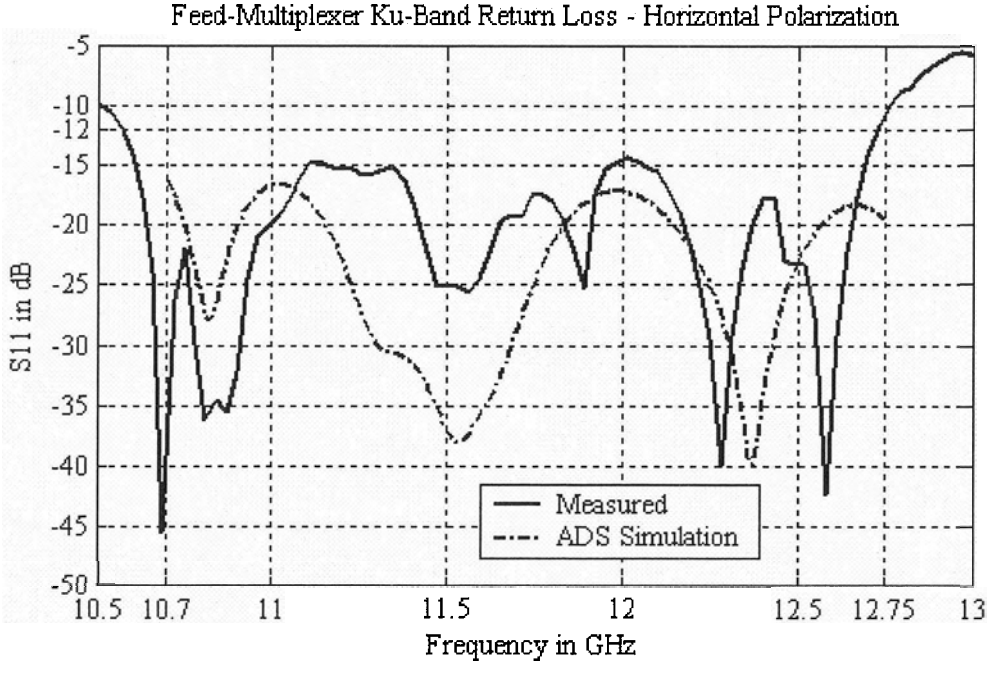

Figure 50: Ku-Band Horizontal Polarization Port, Measured and Simulated Return Loss Response.

Relatively good agreement between the measured and simulated response was achieved. Deviation from exact agreement can be attributed to the fact that the exact full structure could not be simulated in HFSS® and this necessitated a two stage simulation with the S-parameter results from HFSS® imported as a data element in the equivalent circuit model ADS® software. This means that the simulated response for the feed-multiplexer in HFSS® was used as an ideal case response without the effects of the loading of the rest of the circuitry on the multiplexer. The response of the actual measured component will include the effects of the loading. Furthermore, the effects of the full feed-multiplexer component housing cavity on the microstrip circuitry could not be simulated and may have contributed to a change in response. However, for the purposes of designing for a certain maximum threshold to the response the agreement is sufficient. The horizontal polarization shows a very good response across almost the entire band of operation, with a measured return loss well below the specified 12 dB of Table 2. The vertical polarization response is worse with violations of the specification between 12 GHz and 12.75GHz. Possible reasons for the poorer response in the vertical polarization are slight deviations in manufacturing as well as the fact that the actual physical soldered connection between the microstrip and coaxial connector of the horizontal polarization port may agree better with the modeled transition used for the de-embedding of the response than the physical connection for the vertical polarization port.

Figure 51 shows the measured isolation between the two polarization ports as measured and without any de-embedding of the coaxial connectors. Since the return loss response of the coaxial connector to microstrip transition model had a response of better than 13 dB, the effect of the connectors on the isolation can be considered negligible, especially with the isolation better than 37 dB. This is well within the specified 20 dB of Table 2.

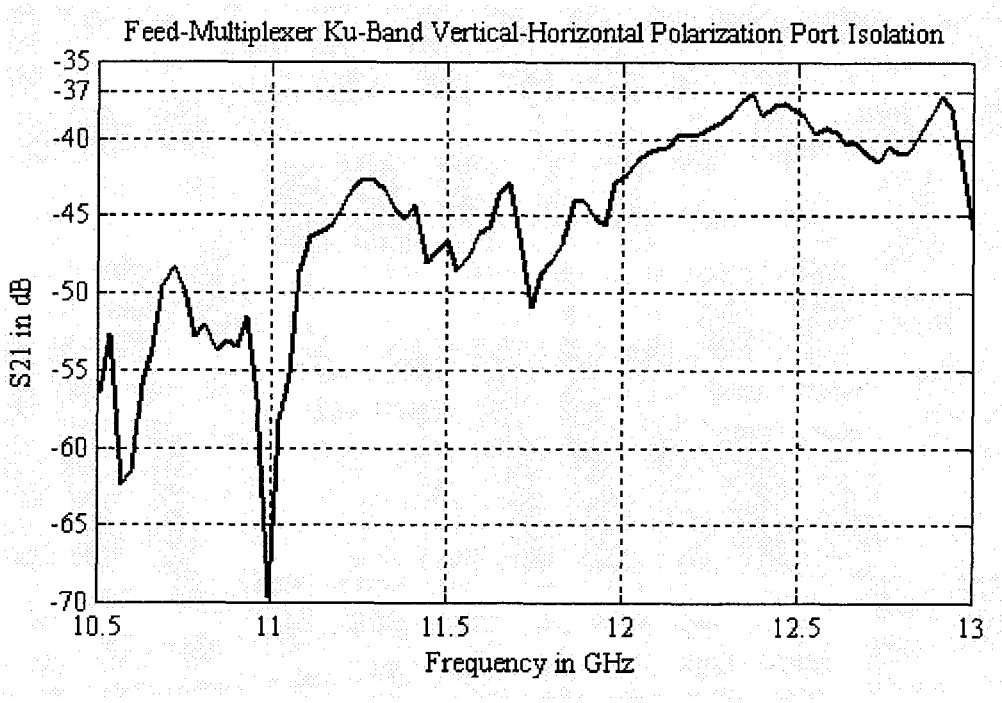

Figure 51: Ku-Band Vertical to Horizontal Polarization Port Isolation.

12.2 Ka-Band S-Parameter Results

Figure 52 shows the measured and simulated (see also Chapter 9, Figure 26) return loss response for the Ka-band port formed by the WR28 waveguide in Figure 2. The polarization selection for the Ka-band is done by the rotation of the WR28 waveguide section as mentioned in Chapter 1. The HFSS® simulation was performed on the symmetrical waveguide sections of the feed only, without the inclusion of the external Ku-band structures, and thus the simulated responses for the two polarizations are the same and represented by only one graph. The measured results, which include the entire feed-multiplexer structure, show that the loading of the external Ku-band structures did not affect the return loss of the two Ka-band polarizations differently. The measurement of the return loss response was done by the use of coaxial line to waveguide transitions connected to the test cable of the VNA. An LRL (line-reflect-line) [25] calibration procedure was used to include these transitions in the calibration. In so doing, the

response measured is the exact response at the WR28 waveguide input to the feed-multiplexer, and no further de-embedding is required.

An acceptable return loss for both polarizations to serve proof of concept was achieved, even though the specified 14 dB return loss of Table 2 was not attained. The response resembles more closely that of Figure 45 in Chapter 11, where the effect of tolerance on the coaxial waveguide section length of the feed-multiplexer is investigated. The length of this section was confirmed by measurement to be 18 mm as designed and simulated. The exact length and variations on the dielectric rod taper was more difficult to measure however, and a slight deviation in the starting position and dimensions of the taper may have contributed to the deviation in response. Nonetheless, a functional Ka-band multiplexing structure was realized that could be improved with further development-for-manufacturing work.

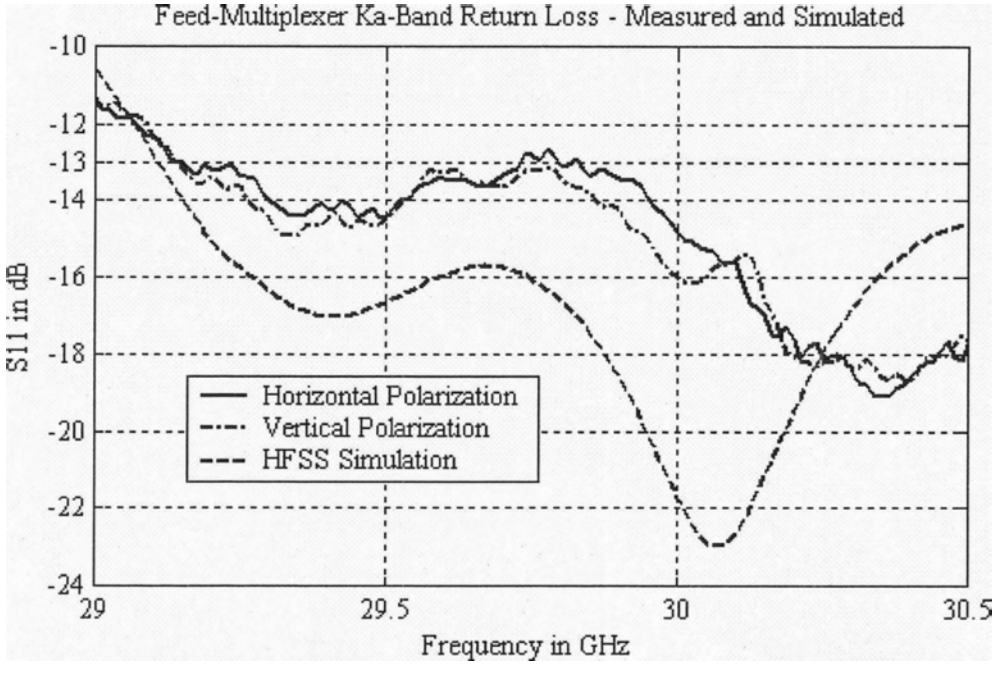

Figure 52: Ka-Band Measured and Simulated Return Loss response.

Figures 53 and 54 show the measured isolation between the Ka-band input port and the respective Ku-band ports. The measurements were done by removing the WR28 waveguide to coaxial connector transition from one of the two VNA test cables and connecting the remaining coaxial connector to the SMA connector of the applicable Ku-band port. As such, the LRL calibration had to be disturbed. Furthermore, the isolative effect of the SMA connector at Ka-band is included in the measurement. As a result the measurements are not absolutely accurate and can only serve as an indication of the isolation. Table 2 specifies an isolation of 20 dB or greater. This is sufficiently exceeded in the results of all the possible polarization combinations to surpass the uncertainty of the calibration disturbance and SMA connector effects. The one exception is the isolation between the vertically launched Ka-band and vertical polarization Ku-band port. This is to be expected since the co-polarized Ka-band signal in the feed-multiplexer will couple most strongly to the co-aligned probes of the vertical polarization Ku-band circuitry. The co-polarization isolation in the horizontal case (Figure 54) is better by about 15 dB due to the fact that the Ku-band structure includes the waveguide coupling passages which add to the Ka-band isolation. This is also evident in the fact that the cross-polarized isolation of the vertically launched Ka-band and horizontal Ku-band port (Figure 53) is much better than that of the horizontally launched Ka-band and vertical Ku-band port (Figure 54) since the former includes the coupling passages in the Ku-band structures. The worst case isolation achieved is better than 23 dB and within the specification of Table 2, but considering the uncertainty introduced by the calibration disturbance and SMA connector, it would be wise to introduce extra filtering in the microstrip circuitry to improve the Ka-band isolation. How much more isolation and whether it is to be targeted across the band or for only a certain section will depend on the frequency plan of the system used with the feed-multiplexer.

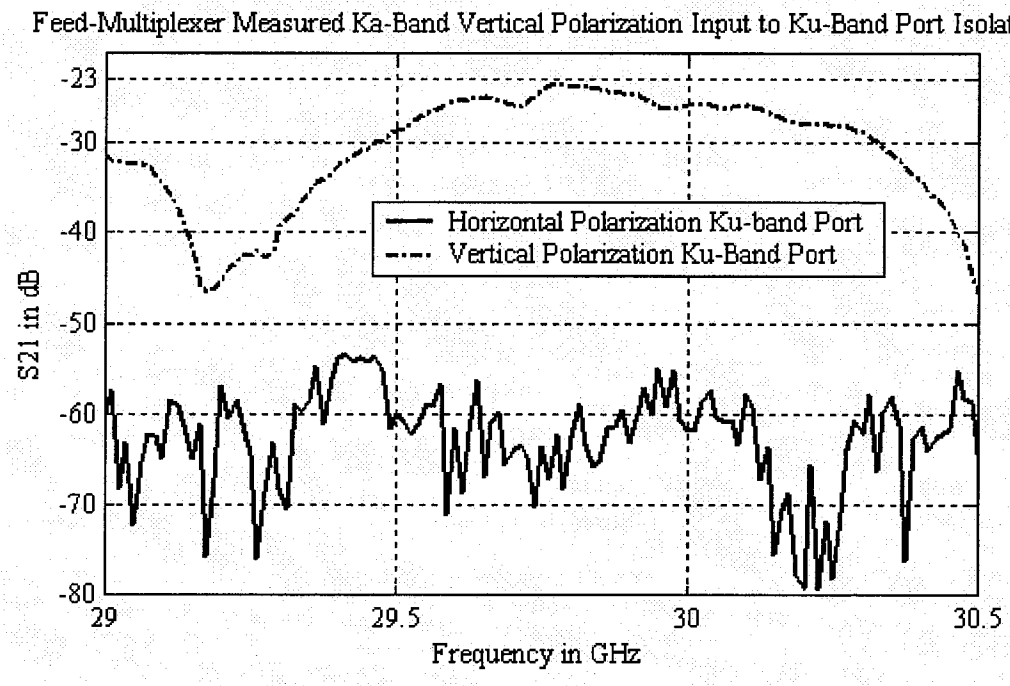

Figure 53: Ka-Band Vertical Polarization to Ku-Band Port Isolation.

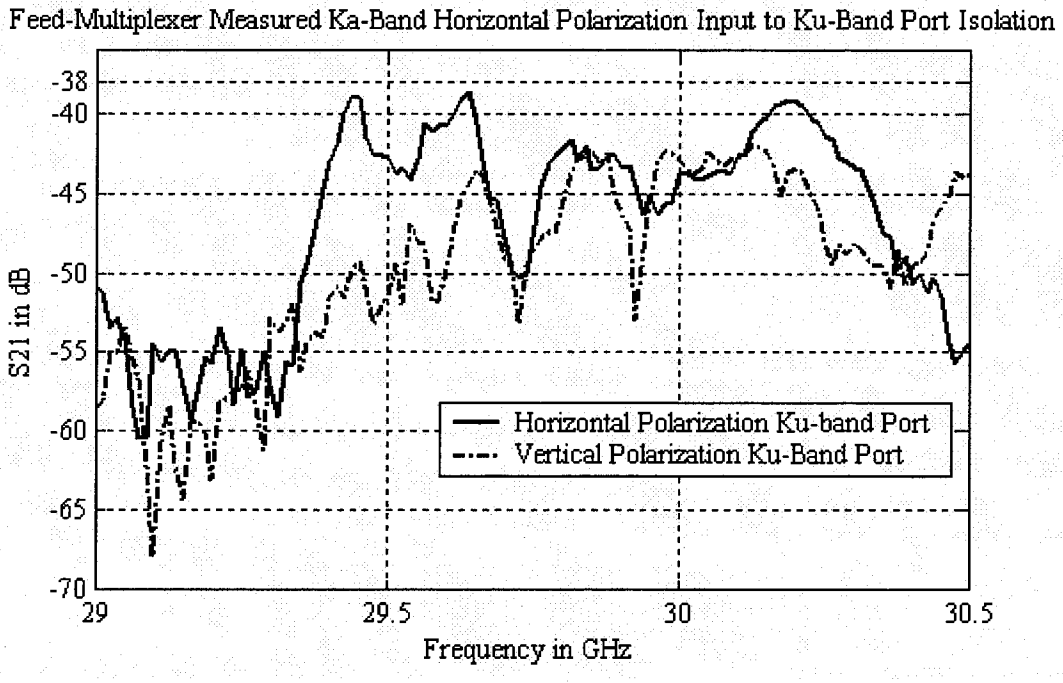

Figure 54: Ka-Band Horizontal Polarization to Ku-Band Port Isolation.

12.3 Ku-Band Radiation Results

Figures 55 to 57 show the measured Ku-band radiation patterns. Due to the fact that an amplifier was not available to improve the signal strength, the measured power levels were low. As a consequence the co-polar patterns become more noisy as the measurement frequency increases and the actual cross-polarization response falls below the noise level. The measurements for the cross-polarization therefore indicate worst case maxima, all of which are well below the 20 dB specification of Table 2. Very good pattern shape agreement of the measured co-polar radiation patterns with the simulated patterns (Figures 30 to 31) over the +/- 40^0 illumination angle was achieved. Absolute gain measurements could not be performed.

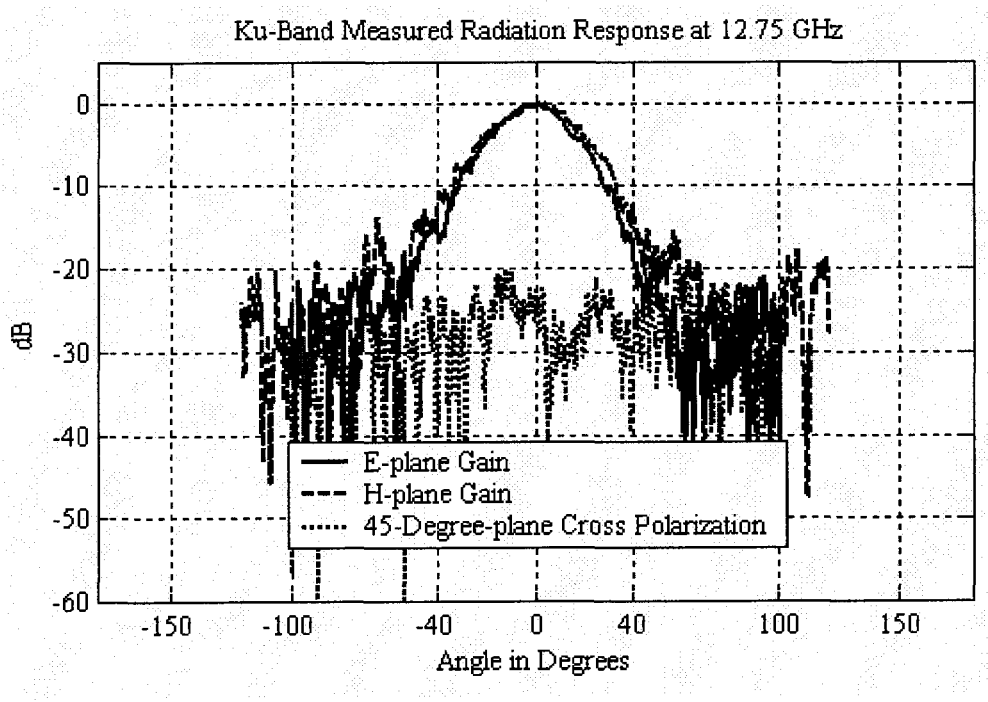

Figure 55: Measured Ku-Band Radiation Patterns at 12.75 GHz.

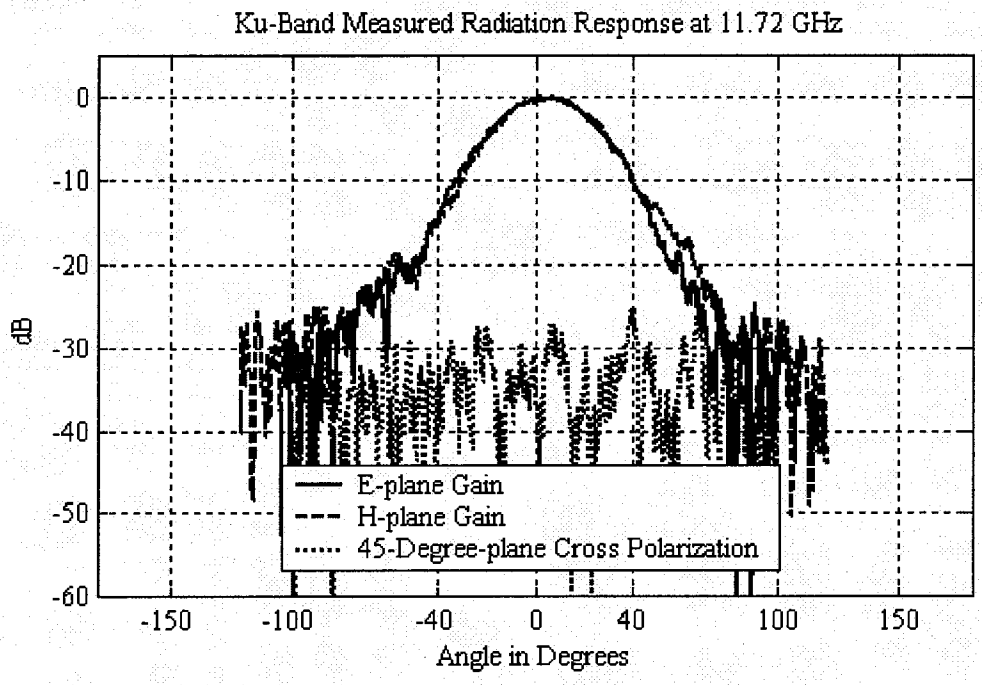

Figure 56: Measured Ku-Band Radiation Patterns at 11.72 GHz.

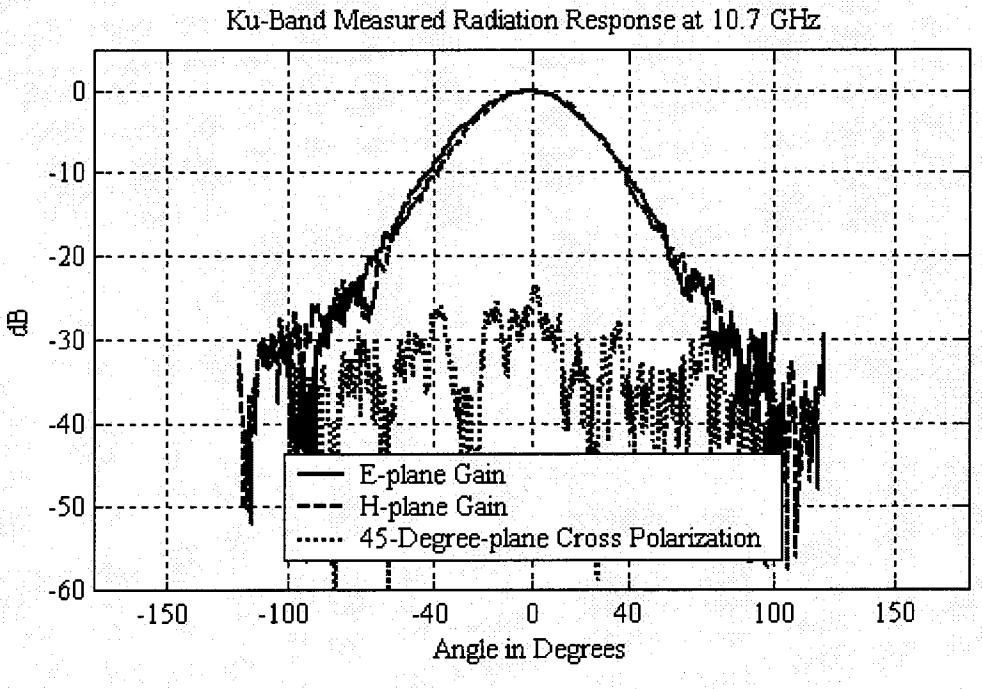

Figure 57: Measured Ku-Band Radiation Patterns at 10.7 GHz.

13 Conclusion

The objective of this thesis was to achieve proof of concept and proper operation of a dual-band and dual-polarization feed multiplexer for Ku/Ka-band operation that employs substrate carried probes as the coupling structures of the Ku-band. The thesis documented the design of this structure and the various related design considerations.

Initial design and optimization of the feed-multiplexer was successfully completed, including simulations with the HFSS® and ADS® software packages that predicted a functional design.

A prototype of the feed-multiplexer was manufactured and the issues related to manufacturing documented. This prototype was measured and a satisfactory response was obtained.

In summary, the Ku-band results performed well for both the return loss response and isolation between the two polarizations. Only the vertical polarization return loss exceeded specification towards the higher end of the band. Agreement between measured and simulated responses are reasonably good, but differences should be accounted for in future development iterations. Measured radiation pattern results showed very good agreement with simulated results and were compliant with design specifications.

Ka-band results were equally encouraging with the return loss exceeding the specification by only 1 dB. Agreement with the simulated response is sufficient for design purposes. Ka-Ku-band isolation performed well except for the co-polar case that does not include the Ku-band waveguide coupling passages. Extra filtering within the microstrip circuitry will have to be employed to improve the response, depending on the dictates of the system employing the feed-multiplexer. Ka-band radiation patterns could not be measured due to unavailable facilities, but the S-parameter results and good agreement

between simulated and measured Ku-band radiation patterns support confidence in the Ka-band radiation performance as simulated.

With the design procedure documented in this thesis the foundation is laid for future ready-to-market development work. This development should focus on a study of manufacturing techniques to realize the feed-multiplexer integration with surrounding system components in view of desired cost targets. This should include an in-depth study of the expected tolerances associated with the manufacturing techniques and the resultant effects on feed-multiplexer performance.

In conclusion, proof of concept was achieved along with satisfactory first iteration development results. A functional structure was realized by the research of the thesis that adds a design solution option to the existing repertoire of dual-band dual-polarization feed-multiplexers in literature. This solution enables possible savings in cost and space by increasing the viability of greater component integration and could aid the cost-effective deployment of consumer market, two-way, communication satellite access.

14 References

[1] "Croation Vodatel and SES ASTRA Introduce Broadband Internet and Video On-Demand Services", press release of SES-ASTRA 10 January 2005, www.ses-astra.com/press-info/news/press-releases/05/20050110.shtml.

[2] "About EMS SatNet", Company Information for EMS Satellite Networks, www.emssatnet.com/companyinfo.asp.

[3] "Broadband Satellite Communications", presentation of DC-SAT.NET LTD., www.dc-sat.net, http://dc-sat.net/pdfs/DC%20Broadband%20Satellite%20Communications.pdf.

[4] "Satellite Internet Services", Broadband Products and Services from SES-ASTRA, www.ses-astra.com/products/broadband/sis.shtml.

[5] Astra Return Channel System ARCS SIT, Schedule L-Outdoor Unit Specification, Doc.No. ARCS.25C.CT-A001-3.0, 13 December 1998.

[6] ETSI EN 301 359 V1.1.1 (1999-04), " Satellite Earth Stations and Systems (SES); Satellite Interactive Terminals (SIT) using satellites in geostationary orbit operating in the 11 GHz to 12 GHz (space-to-earth) and 29.5 GHz to 30.0 GHz (earth-to-space) frequency bands.

[7] L.J. Ippolito Jr., "Radiowave Propagation in Satellite Communications", Van Nostrand Reinhold Company Inc., New York 1986.

[8] J.N. Slater and L.A. Trinogga, " Satellite Broadcasting Systems Planning and Design", Ellis Horwood Ltd., Chichester 1985.

[9] S. Prentiss, " Satellite Communications"2nd edition, TAB Books Inc., Blue Ridge Summit 1987.

[10] R.W. Jackson, "A Planar Orthomode Transducer", IEEE Microwave and Wireless Components Letters, vol. 11, no. 12, pp. 483-485, December 2001.

[11] H. Kumazawa, M. Koyama and Y. Kataoka, "Wide-Band Communication Satellite Antenna Using a Multifrequency Primary Horn", IEEE Transactions on Antennas and Propagation, volume AP-23, no.3, pp. 404-407, May 1975.

[12] M.S. Narasimhan and M.S. Sheshadri, "Propagation and Radiation Characteristics of Dielectric Loaded Corrugated Dual-Frequency Circular Waveguide Horn Feeds", IEEE Transactions on Antennas and Propagation, volume AP-27, no.6, pp. 858-860, November 1984.

[13] J.C. Lee, "A Compact Q-/K-Band Dual Frequency Feed Horn", IEEE Transactions on Antennas and Propagation, volume AP-32, no.10, pp. 1108-1111, October 1984.

[14] G.L. James, P.R. Clark and K. J. Greene, " Diplexing Feed Assemblies for Application to Dual-Reflector Antennas", IEEE Transactions on Antennas and Propagation, volume 51, no.5, pp. 1024-1029, May 2003.

[15] A.D. Olver, P.J.B Clarricoats, A.A. Kishk and L. Shafai, "Microwave Horns and Feeds", The Institution of Electrical Engineers and IEEE Press, New York 1994.

[16] D.M. Pozar, "Microwave Engineering", Chapters, John Wiley and Sons, Inc., 1998.

[17] R.C. Johnson and H. Jasik, "Antenna Engineering Handbook", 2nd edition, Chapter 12, F.J Zucker, McGraw-Hill, 1984.

[18] Richard C. Booton, "Computational Methods for Electromagnetics and Microwaves", John Wiley and Sons, Inc., 1992.

[19] D. Kajfez and P. Guillon, "Dielectric Resonators", Chapter 3, Artech House, Inc., 1986.

[20] J.D. Kraus, "Antennas", 2nd edition, pp. 685-687, McGraw-Hill Inc., 1988.

[21] W.H. Press, B.P. Flannery, S.A.Teukolsky, W.T. Vetterling, " Numerical Recipes-The art of scientific computing", Cambridge University Press, 1986.

[22] J. Uher, J. Bornemann and U. Rosenberg, "Waveguide Components for Antenna Feed Systems. Theory and CAD", Artech House Inc., Norwood 1993.

[23] R.K. Hoffman, " Handbook of Microwave Integrated Circuits", Artech House Inc., Norwood MA. 1987.

[24] B.C. Wadell, "Transmission Line Design Handbook", Artech House Inc., Boston 1991.

[25] Jamal S. Izadian and Shahin M. Izadian, Microwave Transition Design. Artech House Inc., Boston, 1988.

[26] Yi-Chi Shih, Thuy-Nhung Ton and Long Q. Bui, "Waveguide-to-Microstrip Transitions for Millimeter-Wave Applications", IEEE MTT-S Digest, pp.473-475, May 1988.

[27] Yoke-Choy Leong and S. Weinreb, "Full-Band Waveguide-to-Microstrip Probe Transitions", IEEE MTT-S Digest, pp.1435-1438, June 1999.

[28] T.T. Ha, "Solid-State Microwave Amplifier Design", John Wiley and Sons, New York 1981.

[29] K.C. Gupta, Ramesh Garg, Inder Bahl and Prakash Bhartia, " Microstrip Lines and Slotlines",2nd edition, Artech House Inc., Boston 1996.

[30] A.C. Ludwig, "The Definition of Cross Polarization", IEEE Transactions on Antennas and Propagation, AP-21, pp. 116-119, 1973.

[31] P.J.B. Clarricoats and A.D. Olver, "Corrugated Horns for Microwave Antennas", Peter Peregrinus Ltd., 1984.

[32] C.A. Balanis, "Antenna Theory Analysis and Design", 2nd edition. John Wiley and Sons, Inc., 1997.

[33] Thomas S Laverghetta, "Microwave Measurements and Techniques", 6th printing, Artech House Inc., Dedham Ma., 1985.

[34] R.E. Collin, "Field Theory of Guided Waves", 2nd edition, IEEE Press, New York, 1991.

[35] P.J.B Clarricoats and B.C. Taylor, " Evanescent and Propagating Modes of Dielectric-loaded Circular Waveguide", Proc. IEE, vol. 111, no. 12, December 1964.

Appendix I: Ka-Band Numerical Evaluation Code

%KaBetaCalcFin4.m

```
%This file calculates the x values corresponding to the HE1N modes for a
%circular dielectric rod in free space
%Singular value decomposition is performed on the dispersion equation matrix
%Where the minimum singular value is zero corresponds to where the determinant of the
%matrix is zero, and hence, where detF=0 is satisfied
%Minimum singular values vs. the radial wavenumber in the rod region
%are plotted and the dominant mode propagation
%constant is calculated

function z = KaBetaCalcFin4(ar,er1,freq,N)

%define the required accuracy (allowable difference of minimum singular value from 0)
acctarget=1e-7;

ar=ar; %rod radius
er1=er1; %rod dielectric constant
u0=4*pi*1e-7;
e0=8.854e-12;
ediel=e0*er1;
freq=freq;
omega=2*pi*freq;
```

```
cvac=2.9979e8;
lamda=cvac/freq;
k0=(2*pi)/lamda;

%specify the evaluation range for x
xstart=0.01;
xintN=600;
xpnt=xintN+1;
xstop=k0*ar*sqrt(er1-1);% maximum value for x to have y real
offset=0.001; %offset from xstop
xint=(xstop-offset-xstart)/xintN;
kc1int=xint/ar;
kcount=1;
x=xstart;

%evaluate the minimum singular values over the x-values
while x < xstop

% call evaluation subroutine
minSm=HE1NminSing(ar,er1,freq,x/ar);

%write the values to a matrix
minSmat(kcount,1)=minSm;
xmat(kcount,1)=x;
kcount=kcount+1;
x=x+xint;

end

%calculate the radial wavenumbers in the rod region
kc1mat=xmat./ar;
```

```
%plot the minimum singular values over the radial wavenumbers
plot(kc1mat,minSmat,'LineWidth',1.6)
xlabel('Radial wavenumber in dielectric region (kc1)')
ylabel('Minimum singular values')
title('Minimum singular values vs. kc1');

%search for the zeros
Smatsize=size(minSmat);
searchstop=Smatsize(1,1)-1; %offset of 1 due to points for slope calculation
 sgnk=1;

 %evaluate the slope from each point, to the point after and the point
 %before
for searchcnt=2:searchstop

   slpk1=minSmat(searchcnt,1)-minSmat(searchcnt-1,1);
   slpk2=minSmat(searchcnt+1,1)-minSmat(searchcnt,1);
   sgn1=slpk1/abs(slpk1);
   sgn2=slpk2/abs(slpk2);

%a negative followed by a positive slope indicates a possible zero
%write these points and the minimum singular values there to matrices
   if ((sgn1 < 0) & (sgn2 > 0))

     rtsmat(sgnk,1)=kc1mat(searchcnt,1);
     rtsSmat(sgnk,1)=minSmat(searchcnt,1);
     rtsminSmatindex(sgnk,1)=searchcnt;%tag the position in  minSmat matrix
     sgnk=sgnk+1;

   end
end
```

```
   rtsmat  % 1N mode radial wavenumbers
   rtsSmat % Min Singular values at the 1N mode values
   rtsminSmatindex% array index at the values
   rt1N=rtsmat(N,1)% radial wavenumber at the specified N mode
   rtS1N=rtsSmat(N,1)% Min Singular value at the specified N mode
   rtminSindex=rtsminSmatindex(N,1)% array index for the chosen value
   x1N=rt1N*ar;
   Beta1N=(sqrt(((k0*ar)^2)*er1-x1N^2))/ar% Beta at the chosen value
%*****************************************************************
%refine the search for the specified N mode x value
% Perform a Golden-Section routine line search
rtslow=kc1mat(rtminSindex-1,1);%Range Of Uncertainty start
rtshi=kc1mat(rtminSindex+1,1);% ROU stop
ROUtarget=1e-4;% acceptable ROU for adequate accuracy

%call search routine
rt1NACC=GoldKc1HE1Nsearch(rtslow,rtshi,ROUtarget,ar,er1,freq)

%calculate Beta at accurate x value
x1NACC=rt1NACC*ar;
  Beta1NACC=(sqrt(((k0*ar)^2)*er1-x1NACC^2))/ar
    z=Beta1NACC;

%*****************************END*********************************
```

%HE1NminSing.m

```
% This file evaluates the minimum singular value for the HE1N mode at the
% specified kc1 value.
%the file is called by other routines to perform the evaluation.

function z = HE1NminSing(ar,er1,freq,kc1)

%define the variables for the dispersion function

ar=ar;  %input
er1=er1; %input
u0=4*pi*1e-7;
e0=8.854e-12;
ediel=e0*er1;
freq=freq;%input
omega=2*pi*freq;
cvac=2.9979e8;
lamda=cvac/freq;
k0=(2*pi)/lamda;
x=kc1*ar;
y=sqrt(((k0*ar)^2)*(er1-1)-x^2);
Beta=(sqrt(((k0*ar)^2)*er1-x^2))/ar;

%define the substitute variables i.t.o. the bessel functions

J1=besselj(1,x);
J1d= -besselj(2,x) + (x^-1)*besselj(1,x);
K1=besselk(1,y);
K1d=-besselk(2,y) + (y^-1)*besselk(1,y);

%calculate the singular values
```

```
Row1=[J1 0 -K1 0];
Row2=[0 J1 0 -K1];
Row3=[Beta*ar*J1/(x^2) omega*u0*ar*J1d/x  Beta*ar*K1/(y^2)  omega*u0*ar*K1d/y];
Row4=[omega*ediel*ar*J1d/x  Beta*ar*J1/(x^2)  omega*e0*ar*K1d/y
Beta*ar*K1/(y^2)];
A=[Row1;Row2;Row3;Row4];
[Um,Sm,Vm]=svd(A);
diagSm=diag(Sm);
minSm=min(diagSm);
z=minSm;

%*****************************END*******************************
```

%GoldKc1HE1Nsearch.m

```
% This file performs a line search using the Golden-Section search method given the
% start interval points, desired ROU (Range of Uncertainty) and evaluation function that
%is the called routine HE1NminSing.m

function  z=GoldKc1search(xlow,xupper,accuracy,ar,er1,freq)

func='HE1NminSing';
xL1=xlow;
xU1=xupper;
Istart=xU1-xL1;
Istop=accuracy; %ROU acceptable
KG=1.618034;

%calculate the start interval values

I2=Istart/KG;
xa1=xU1-I2;
xb1=xL1+I2;
fa1=eval([func '(ar,er1,freq,xa1);']);
fb1=eval([func '(ar,er1,freq,xb1);']);
k=1;
Ikplus1=I2;
xaK=xa1;
xbK=xb1;
faK=fa1;
fbK=fb1;
xLK=xL1;
xUK=xU1;
Ik=Istart;
k=1;
```

```
Istopplus1=Istop/KG;

%Perform the iterative ROU reduction search

while Ik > Istopplus1

   if xaK > xbK
      break
   end

   Ikplus2=Ikplus1/KG;

   if faK >= fbK
      xLplus1=xaK;
      xUplus1=xUK;
      xaplus1=xbK;
      xbplus1=xLplus1+Ikplus2;
      faplus1=fbK;
      fbplus1=eval([func '(ar,er1,freq,xbplus1);']);

   else
     xLplus1=xLK;
      xUplus1=xbK;
      xaplus1=xUplus1-Ikplus2;
      xbplus1=xaK;
      fbplus1=faK;
      faplus1=eval([func '(ar,er1,freq,xaplus1);']);
   end

faK=faplus1;
fbK=fbplus1;
```

```
xaK=xaplus1;
xbK=xbplus1;
xLK=xLplus1;
xUK=xUplus1;
Ikplus1=Ikplus2;
Ik=xUK-xLK;
k=k+1;
end

%compute results

if faK >fbK
xval=(xbK+xUK)/2;
end

if faK < fbK
xval=(xLK+xaK)/2;
end

 if faK == fbK
xval=(xaK+xbK)/2;
end

ROUstop=xUK-xLK
k
z=xval;
minSstop=eval([func '(ar,er1,freq,xval);']);

%*****************************END*********************************
```

%RodE2Plot1d.m

```
%This file calculates and plots the E field components in the air region outside a
%dielectric rod at a certain frequency with a certain radius ar,for the HE11 mode.
% phi and z dependence is ignored by setting the functions/factors for these =1
%this means calculated values will always be at the phi for maximum field for each
%component

%define the variables for the dispersion function

ar=1.80e-3; %input
er1=2.55;  %input
Beta=642.3763 %from previous calculation
freq=29.50e9;  %input
omega=2*pi*freq;
cvac=2.9979e8;
u0=4*pi*1e-7;
lamda=cvac/freq;
k0=(2*pi)/lamda
rstart=ar;
rint=600;
rpnt=rint+1;
rstop=10*ar;
kr2=sqrt(Beta^2-k0^2);

%compute the excitation coefficients,note they are constant for a certain
%freq,er,and radius of rod hence they stay constant over the plot vs. radial distance

coeff=const1Fe(Beta,ar,freq,er1);
coeff=coeff(:);
C=coeff(3,1);
D=coeff(4,1);
```

```
%define the values of r to plot over.
r=rstart:(rstop-rstart)/rint:rstop;
r=r(:);

%set up the Bessel function variables
arg2=kr2*r;
arg2Bound=kr2*ar;
K1=besselk(1,arg2);
K1bound=besselk(1,arg2Bound);
dK1=-besselk(2,arg2) + (arg2.^-1).*besselk(1,arg2);
dK1bound=-besselk(2,arg2Bound) + (arg2Bound.^-1).*besselk(1,arg2Bound);

%define Ez2norm function
Ez2=C*K1;
Ez2normbot=C*K1bound;
Ez2N=Ez2./Ez2normbot;
dBEz2N=20*(log10(Ez2N));

% define the Ephi2norm function
Ephi2Ntop=Beta*C*(r.^-1).*K1 + omega*u0*kr2*D*dK1;
Ephi2Nbot=Beta*C*(r.^-1).*K1bound + omega*u0*kr2*D*dK1bound;
Ephi2N=Ephi2Ntop./Ephi2Nbot;
dBEphi2N=20*(log10(Ephi2N));

% define the Er2norm function
Er2Ntop=Beta*kr2*C*dK1 + omega*u0*D*(r.^-1).*K1;
Er2Nbot=Beta*kr2*C*dK1bound + omega*u0*D*(r.^-1).*K1bound;
Er2N=Er2Ntop./Er2Nbot;
dBEr2N=20*(log10(Er2N));
```

```
% plot E over r
rmm=r*1000;
plot(rmm,dBEphi2N,'k-.',rmm,dBEr2N,'b-',rmm,dBEz2N,'r--','LineWidth',1.6);
set(gca,'fontname','Times New Roman','fontsize',10)
grid on
legend('E_{\phi}','E_{\rho}','E_{z}')
xlabel('Radius from dielectric rod center in mm')
ylabel('Normalized E_{\phi},E_{\rho} and E_{z} in dB')
axis([ 1.8   15  -50  0]);

%*******************************END*********************************
```

```
% const1Fe.m
%This file computes the field excitation amplitude constants of a dielectric rod in air
%given that constant A is chosen as =1 and the modal Beta is known

function z=const1Fe(Betarod,rodrad,freq,epsR)

%Input the operating Beta, rod radius, frequency and dielectric constant

Beta=Betarod;
ar=rodrad;
f=freq;
er1=epsR;

%Other constants
c0=2.9979e8;
lamda0=c0/f;
k0=2*pi/lamda0;
u0=4*pi*10^-7;
e0=8.854e-12;
etadiel=sqrt(u0/(er1*e0));
kdiel=k0*sqrt(er1);
kr1=sqrt((kdiel^2)-Beta^2);
x=kr1*ar;
y=sqrt(((k0*ar)^2)*(er1-1)-x^2);

%Define the Bessel function coefficients

J1=besselj(1,x);
J1d= -besselj(2,x) + (x.^-1).*besselj(1,x);
K1=besselk(1,y);
K1d= -besselk(2,y) + (y.^-1).*besselk(1,y);
```

```
% Define the required functions

F2=J1d./x + K1d.*J1./(y.*K1);
F3=Beta.*J1.*((x.^-2) + (y.^-2))/(k0*sqrt(er1));

%Calculate the constants
A=1; %chosen
C=J1*A/K1;
B=(-1/etadiel)*(F3/F2)*A;
D=B*(J1/K1);
z=[ A B C D]';

%*****************************END*******************************
```

Appendix II: Ku-Band Numerical Evaluation Code

%cutoffevalFIN.m

```
%This file calculates the cut-off frequencies for a circular waveguide of radius br, loaded
%by a dielectric rod of radius ar. The br values are varied over a specified range while
%the ar value is specified as a fixed value in calling routine KuCutOffCalcFin1Call.m

%specify the range for br
rstart=6e-3;
rstop=12e-3;
rstep=1e-3;

%evaluate the cut-off frequencies
count=1;
for rad=rstart:rstep:rstop

   lab(count,1)=KuCutOffCalcFin1Call(1.8e-3,rad,2.55,6.5e9,14e9,1);
   radmat(count,1)=rad*1000;
   count=count+1;

end

result=[radmat lab]

%**************************************END**************************
```

```
%KuCutOffCalcFin1Call.m
%This file calculates the cut-off frequencies corresponding to the TE1N modes for a
%circular waveguide of radius br, loaded by a dielectric rod of radius ar.
%Singular value decomposition is performed on the dispersion equation matrix.
%Where the minimum singular value is zero, corresponds to where the determinant of the
%matrix is zero, and hence, where detF=0 is satisfied.
%A Golden-Section search routine is used to refine the accuracy of the calculated value.
%The cut-off frequency of the specified TE1N mode is given as output.

function z = KuCutOffCalcFin1Call(ar,br,er1,freqstart,freqstop,N)

%define the required accuracy (allowable difference of minimum singular value from 0)
acctarget=1e-7;

ar=ar;    %rod radius
br=br;    %circular waveguide radius
er1=er1; %rod dielectric constant
u0=4*pi*1e-7;
e0=8.854e-12;
cvac=2.9979e8;

%specify the evaluation freq. range
fstart=freqstart;
fstop=freqstop;
fint=0.01e9;
kcount=1;
freq=fstart;

%evaluate the minimum singular values over the frequencies

while freq < fstop
```

```
% call evaluation subroutine
minSm=TE1NminSing(ar,br,er1,freq);

%write the values to a matrix
minSmat(kcount,1)=minSm;
freqmat(kcount,1)=freq;
kcount=kcount+1;
freq=freq+fint;

end

freqmatGHz=freqmat./(1e9);

%search for the zero's
Smatsize=size(minSmat);
searchstop=Smatsize(1,1)-1; %offset of 1 due to points for slope calculation
 sgnk=1;
 %evaluate the slope from each point, to the point after and the point
 %before
for searchcnt=2:searchstop

   slpk1=minSmat(searchcnt,1)-minSmat(searchcnt-1,1);
   slpk2=minSmat(searchcnt+1,1)-minSmat(searchcnt,1);
   sgn1=slpk1/abs(slpk1);
   sgn2=slpk2/abs(slpk2);

%a negative followed by a positive slope indicates a possible zero
%write these points and the minimum singular values there to matrices
   if ((sgn1 < 0) & (sgn2 > 0))
```

```
      rtsmat(sgnk,1)=freqmat(searchcnt,1);
      rtsSmat(sgnk,1)=minSmat(searchcnt,1);
      rtsminSmatindex(sgnk,1)=searchcnt;%tag the position in  minSmat matrix
      sgnk=sgnk+1;

   end
end

   rtsmat;  % 1N mode cut off frequency
   rtsSmat; % Min Singular values at the 1N mode values
   rtsminSmatindex;% array index at the values
   rt1N=rtsmat(N,1);% cut off frequency at the specified N mode
   rtS1N=rtsSmat(N,1);% Min Singular value at the specified N mode
   rtminSindex=rtsminSmatindex(N,1);% array index for the chosen value

   Freqcut=rt1N;

%*********************************************************************
%refine the search for the specified N mode cut-off value
% Perform a Golden-Section line search
rtslow=freqmat(rtminSindex-1,1);%Range Of Uncertainty(ROU) start
rtshi=freqmat(rtminSindex+1,1);% ROU stop
ROUtarget=1e-4;% acceptable ROU for adequate accuracy

%call search routine
rt1NACC=GoldTE1Ncutoffsearch(rtslow,rtshi,acctarget,ar,br,er1);
CutOff=rt1NACC;
z=CutOff/(1e9);
%*********************************END*****************************
```

%TE1NminSing.m

```
% This file evaluates the minimum singular value for the TE1N mode.
%The file is called by other routines to perform the evaluation.

function z = TE1NminSing(ar,br,er1,freq)

%define the variables for the dispersion function

ar=ar;  %input
br=br;  %input
er1=er1; %input
u0=4*pi*1e-7;
e0=8.854e-12;
freq=freq;%input
omega=2*pi*freq;
cvac=2.9979e8;
lamda=cvac/freq;
k0=(2*pi)/lamda;
Beta=0;
kc1=sqrt(k0*k0*er1-Beta*Beta);%for cut off Beta=0;
kc2=sqrt(k0*k0-Beta*Beta);

%define the substitute variables i.t.o. the bessel functions
r1ar=kc1*ar;
r2ar=kc2*ar;
J1r1ar=besselj(1,r1ar);
J1r2ar=besselj(1,r2ar);
Y1r2ar=bessely(1,r2ar);
J1dr1ar= -besselj(2,r1ar) + (r1ar^-1)*besselj(1,r1ar);
J1dr2ar= -besselj(2,r2ar) + (r2ar^-1)*besselj(1,r2ar);
Y1dr2ar= -bessely(2,r2ar) + (r2ar^-1)*bessely(1,r2ar);
```

```
r2br=kc2*br;
J1dr2br= -besselj(2,r2br) + (r2br^-1)*besselj(1,r2br);
Y1dr2br= -bessely(2,r2br) + (r2br^-1)*bessely(1,r2br);

%calculate the roots by use of Singular values

kc1sqr=kc1*kc1;
kc2sqr=kc2*kc2;
Row1=[J1dr1ar/kc1  -J1dr2ar/kc2  -Y1dr2ar/kc2];
Row2=[J1r1ar -J1r2ar -Y1r2ar ];
Row3=[0  J1dr2br  Y1dr2br];
A=[Row1;Row2;Row3];
[Um,Sm,Vm]=svd(A);
diagSm=diag(Sm);
minSm=min(diagSm);
z=minSm;

%**********************************END**************************
```